Generation, Ascent and Eruption of Magma on the Moon: New Insights Into Source Depths, Magma Supply, Intrusions and Effusive/Explosive Eruptions (Part 1: Theory)

Lionel Wilson [1,2] and James W. Head[2]

[1]Lancaster Environment Centre, Lancaster University,
Lancaster LA1 4YQ, UK

[2]Department of Earth, Environmental and Planetary Sciences
Brown University, Providence, RI 02912 USA.

Submitted to *Icarus* Special issue on Lunar Reconnaissance Orbiter:
August 5, 2015
Revised Version Submitted: November 17, 2015

Abstract:

We model the ascent and eruption of lunar mare basalt magmas with new data on crustal thickness and density (GRAIL), magma properties, and surface topography, morphology and structure (Lunar Reconnaissance Orbiter). GRAIL recently measured the broad spatial variation of the bulk density structure of the crust of the Moon. Comparing this with the densities of lunar basaltic and picritic magmas shows that essentially all lunar magmas were negatively buoyant everywhere within the lunar crust. Thus positive excess pressures must have been present in melts at or below the crust-mantle interface to enable them to erupt. The source of such excess pressures is clear: melt in any region experiencing partial melting or containing accumulated melt, behaves as though an excess pressure is present at the top of the melt column if the melt is positively buoyant relative to the host rocks and forms a continuously interconnected network. The latter means that, in partial melt regions, probably at least a few percent melting must have taken place. Petrologic evidence suggests that both mare basalts and picritic glasses may have been derived from polybaric melting of source rocks in regions extending vertically for at least a few tens of km. This is not surprising: the vertical extent of a region containing inter-connected partial melt produced by pressure-release melting is approximately inversely proportional to the acceleration due to gravity. Translating the ~25 km vertical extent of melting in a rising mantle diapir on Earth to the Moon then implies that melting could have taken place over a vertical extent of up to 150 km. If convection were absent, melting could have occurred throughout any region in which heat from radioisotope decay was accumulating; in the extreme this could have been most of the mantle.

The maximum excess pressure that can be reached in a magma body depends on its environment. If melt percolates upward from a partial melt zone and accumulates as a magma reservoir, either at the density trap at the base of the crust or at the rheological trap at the base of the elastic lithosphere, the excess pressure at the top of the magma body will exert an elastic stress on the overlying rocks. This will eventually cause them to fail in tension when the excess pressure has risen to close to twice the tensile strength of the host rocks, perhaps up to ~10 MPa, allowing a dike to propagate upward from this point. If partial melting occurs in a large region deep in the mantle, however, connections between melt pockets and veins may not occur until a finite amount, probably a few percent, of melting has occurred. When interconnection does occur, the excess pressure at the top of the partial melt zone will rise abruptly to a high value, again initiating a brittle fracture, i.e. a dike. That sudden excess pressure is proportional to the vertical extent of the melt zone, the difference in density between the host rocks and the melt, and the acceleration due to gravity, and could readily be ~100 MPa, vastly greater than the value needed to initiate a dike. We therefore explored excess pressures in the range ~10 to ~100 MPa.

If eruptions take place through dikes extending upward from the base of the crust, the mantle magma pressure at the point where the dike is initiated must exceed the pressure due to the weight of the magmatic liquid column. This means that on the nearside the excess pressure must be at least ~19 ± 9 MPa and on the farside must be ~29 ± 15 MPa. If the top of the magma body feeding an erupting dike is a little way below the base of the crust, slightly smaller excess pressures are needed because the magma is positively buoyant in the part of the dike within the upper mantle. Even the smallest of these excess pressures is greater than the ~10 MPa likely maximum value in a magma reservoir at the base of the crust or elastic lithosphere, but the values are easily met by the excess pressures in extensive partial melt zones deeper within the mantle. Thus magma accumulations at the base of the crust would have been able to intrude dikes part-way through the crust, but not able to feed eruptions to the surface; in order to be

erupted, magma must have been extracted from deeper mantle sources, consistent with petrologic evidence.

Buoyant dikes growing upward from deep mantle sources of partial melt can disconnect from their source regions and travel though the mantle as isolated bodies of melt that encounter and penetrate the crust-mantle density boundary. They adjust their lengths and internal pressure excesses so that the stress intensity at the lower tip is zero. The potential total vertical extent of the resulting melt body depends on the vertical extent of the source region from which it grew. For small source extents, the upper tip of the resulting dike crossing the crust-mantle boundary cannot reach the surface anywhere on the Moon and therefore can only form a dike intrusion; for larger source extents, the dike can reach the surface and erupt on the nearside but still cannot reach the surface on the farside; for even larger source extents, eruptions could occur on both the nearside and the farside. The paucity of farside eruptions therefore implies a restricted range of vertical extents of partial melt source region sizes, between ~16 to ~36 km. When eruptions can occur, the available pressure in excess of what is needed to support a static magma column to the surface gives the pressure gradient driving magma flow. The resulting typical turbulent magma rise speeds are ~10 to a few tens of m s^{-1}, dike widths are of order 100 m, and eruption rates from 1-10 km long fissure vents are of order 10^5 to 10^6 m^3 s^{-1}.

Volume fluxes in lunar eruptions derived from lava flow thicknesses and surface slopes or rille lengths and depths are found to be of order 10^5 to 10^6 m^3 s^{-1} for volume-limited lava flows and >10^4 to 10^5 m^3 s^{-1} for sinuous rilles, with dikes widths of ~50 m. The lower end of the volume flux range for sinuous rilles corresponds to magma rise speeds approaching the limit set by the fact that excessive cooling would occur during flow up a 30 km long dike kept open by a very low excess pressure. These eruptions were thus probably fed by partial melt zones deep in the mantle. Longer eruption durations, rather than any subtle topographic slope effects, appear to be the key to the ability of these flows to erode sinuous rille channels.

We conclude that: (1) Essentially all lunar magmas were negatively buoyant everywhere within the crust; (2) Positive excess pressures of at least 20-30 MPa must have been present in mantle melts at or below the crust-mantle interface to drive magmas to the surface; (3) Such pressures are easily produced in zones of partial melting by pressure-release during mantle convection or simple heat accumulation from radioisotopes; (4) Magma volume fluxes available from dikes forming at the tops of partial melt zones are consistent with the 10^5 to 10^6 m^3 s^{-1} volume fluxes implied by earlier analyses of surface flows; (5) Eruptions producing thermally-eroded sinuous rille channels involved somewhat smaller volume fluxes of magma where the supply rate may be limited by the rate of extraction of melt percolating through partial melt zones.

1. Introduction

The role of the generation, ascent and eruption of magma in shaping the surface of the Earth has long been studied, and the major environments of emplacement and extrusion (lithospheric plate boundaries, intraplate volcanic centers, and Large Igneous Provinces) are well known. Prior to the advent of the Space Age in 1957, the Moon was the first laboratory beyond Earth in which fundamental questions about the generation, ascent and eruption of magma could be considered in an independent and different planetary environment (e.g., unknown origin, uncertain interior structure, smaller size, different gravity, lack of an atmosphere, etc.). Was the Moon accreted hot or cold? How did the lunar nearside and farside compare? Were interior heating and extrusive volcanism important? What was the origin of the tens of thousands of craters: volcanic (interior) or impact (exterior)? How did the resurfacing history of the Moon compare with that of the Earth? The advent of the Space Age (with the first lunar mission, Luna 1, in 1959) immediately led to an era of exploration missions that rapidly addressed these questions using orbital remote sensing, human and robotic surface exploration, deployment of geophysical instruments and analysis of returned samples (see background and reviews in Fielder, 1961; Baldwin, 1963; Toksoz et al., 1974 and Wilhelms, 1987).

In the first twenty five years of the Space Age, a wide variety of morphologic features and deposits representing a range of volcanic eruption styles was identified and documented on the Moon, mostly in and associated with the lunar maria (e.g., Schultz, 1976a; Guest and Murray, 1976; Head, 1976). By 1981, analysis of these data and returned samples led to an initial understanding of the basic principles of the generation, ascent and eruption of magma on the Moon, and how they compared with those of the Earth (Wilson and Head, 1981). Indeed, a synthesis was compiled comparing the processes of basaltic volcanism on the Earth, Moon and the terrestrial planets (BVSP, 1981), and the emerging picture of lunar evolution was used as a planetary frame of reference (e.g., Taylor, 1982).

On the basis of the diversity and abundance of data about volcanism on the Moon, and the clear distinction between magmatic styles on the Earth and one-plate planets like the Moon (Solomon, 1978), the Moon has become a reference body for the understanding of crustal formation and evolution, magmatism (plutonism and volcanism), and the thermal evolution of one-plate planetary bodies. We now know that lunar mare basalt deposits cover ~17% of the lunar surface, occur preferentially on the nearside and in topographic lows, and have a total volume estimated at 1×10^7 km^3 (Head and Wilson, 1992a). Returned samples and remote sensing studies show that mare volcanism began prior to the end of heavy impact cratering (the period of cryptomare formation; Whitten et al., 2015a,b), in pre-Nectarian times (Wilhelms, 1987), and continued possibly into the Copernican Period (Hiesinger et al., 2011), a total duration approaching 3.5–4 Ga. Stratigraphic analyses (e.g., Hiesinger et al., 2011) show that the volcanic flux was not constant, but peaked in early lunar history, during the Imbrian Period (which spans the period 3.85-3.2 Ga) (Head and Wilson, 1992a). Average lunar volcanic output rate during this peak period, ~10^{-2} km^3/a, was very low relative to the present global terrestrial volcanic output rate (comparable to the present local output rates for individual volcanoes such as Vesuvius, Italy, and Kilauea, Hawai'i) (Head and Wilson, 1992a). On the other hand, volcanic landforms indicate that peak fluxes were often extremely different from average fluxes. Some eruptions associated with sinuous rilles (e.g., Hurwitz et al., 2012, 2013) were of large volume and are estimated to have lasted on the order of a year and emplaced 10^3 km^3 of lava, representing the equivalent in one year of about 100,000 years of the average flux (Head and Wilson, 1992a). Due primarily to the low frequency of dike intrusions into a single specific area of the crust, shallow magma reservoirs were uncommon (Head and Wilson, 1991); those observed are related to intrusions of sills into low-density breccia zones below impact craters (e.g., Schultz, 1976b; Jozwiak, 2012, 2015).

The asymmetry of mare deposits between the nearside and farside appears to be due largely to differences in crustal thickness (Head and Wilson, 1992a; Whitten et al., 2011). Magma ascending from the mantle or from a buoyancy trap at the base of the crust should preferentially extrude to the surface on the nearside, but should generally stall and cool in dike intrusions in the farside crust, extruding only in the deepest basins. Dikes that establish pathways to the surface on the nearside should have very large volumes, comparable to the volumes associated with many observed flows (Schaber, 1973; Moore and Schaber, 1975; Bugiolacchi and Guest, 2008) and sinuous rille eruptions (e.g., Hurwitz et al., 2012, 2013).

As the Moon thermally evolves and loses heat dominantly by conduction (Solomon and Head, 1982; Spohn et al., 2001; Ziethe et al., 2009), the interplay between thermal contraction and differentiation leads to net cooling and ultimate contraction of the outer portions of the Moon, resulting in a regional horizontal compressive stress acting on the lunar crust (Solomon and Head, 1982). In addition, overall cooling leads to deepening of sources requiring the production of ever-larger volumes of magma in order to reach the surface. Crustal stresses became large enough with time so that few intruded dikes could open to the surface, causing eruptive activity to be severely diminished in the Eratosthenian, and to cease in the Copernican Period. Lunar mare deposits provide an example of the transition from primary crusts to secondary crusts (Taylor, 1989) relevant to the ascent and eruption of magma and they illustrate the significance of several factors in the evolution of secondary crusts, such as crustal density, variations in crustal thickness (Wieczorek and Phillips, 1998; Wieczorek and Zuber, 2001; Hikida and Wieczorek, 2007; Wieczorek et al., 2013), presence of impact basins, state and magnitude of stress in the lithosphere, and general thermal evolution. These factors are also responsible for the extremely low lunar volcanic flux, compared with Earth, even during periods of peak extrusion (Head and Wilson, 1992a).

In parallel with the documentation of surface volcanic features and deposits, numerous analyses have treated the petrology and geochemistry of the generation of mare basalts (e.g., summary in Shearer et al., 2006) and the physical processes associated with their ascent and eruption (e.g., Wilson and Head, 1981; Head and Wilson, 1992a,b; Head and Wilson, 1994; Wilson and Head, 2003a). In particular, it has been shown that the main path for the ascent and eruption of magma from mantle source regions is through magma-filled cracks, i.e. dikes (Head and Wilson, 1992a). Lacking, however, has been an up-to-date treatment of the generation, ascent and eruption of magma that includes the full assessment of dike initiation in the deep mantle, volatile sources and effects, and the behavior of dikes that penetrate to the shallow subsurface, but do not penetrate fully to the surface to form significant effusive eruptions.

In this paper we present such an updated treatment of the generation, ascent and eruption of magma using: 1) new data on lunar crustal thickness and structure from the Gravity Recovery and Interior Laboratory (GRAIL) mission (Zuber et al., 2013), 2) new data on lunar rock and melt density (Kiefer et al., 2012), 3) updated treatments of the generation of magma and the initiation and propagation of magma-filled cracks (dikes) (Weinberg and Regenauer-Lieb, 2010; Bouilhol et al., 2011; Havlin et al., 2013), 4) new data on the production of volatiles during magma ascent and eruption (Wilson and Head, 2003a; Rutherford and Papale, 2009; Saal et al., 2008; Wetzel et al., 2015), 5) the global topography of the Moon from new altimetry (Lunar Orbiter Laser Altimeter, LOLA; Zuber et al., 2010; Smith et al., 2010), and 6) detailed characterization of lunar volcanic features and deposits using new imaging (Lunar Reconnaissance Orbiter Camera, LROC; Robinson et al., 2010), altimetry (Lunar Orbiter Laser Altimeter, LOLA; Zuber et al., 2010; Smith et al., 2010), and spectral reflectance (Moon Mineralogy Mapper, M3; Pieters et al., 2009) data. We begin with an updated assessment of lunar crustal structure, and then provide a new assessment of the modes of dike initiation and propagation from magma sources. Using this framework, we document the theoretical basis for the ascent, intrusion and eruption of magma, including deep and near-surface processes of gas release. Finally, we summarize the main themes, findings and predictions about the generation, ascent and eruption of magma on the Moon and conclude with a discussion of the major factors that are important in explaining the spectrum of lunar volcanic structures and deposits and how they differ from those on Earth and other planets. In a separate analysis (Head and Wilson, 2015), we compare this theoretical treatment and its predictions with the variety and context of observed volcanic features, structures and deposits in order to test the predictions and refine the principles of ascent and eruption and to provide an interpretative framework for the major characteristics of mare basalt and related volcanism on the Moon. We also treat there the wide (up to 40 km) linear dike-like features that are interpreted to have been emplaced much earlier in lunar history than lunar mare basalts (Andrews-Hanna et al., 2013) and the intrusion of early lunar pre-mare Mg-suite magmas (Shearer et al., 2006).

2. The influence of the structure of the Moon on volcanism

The early thermal evolution of the Moon's interior has been modelled (Solomon and Head, 1980; Hess and Parmentier, 1995, 2001; Spohn et al., 2001; Wieczorek et al., 2006; Shearer et al., 2006; Ziethe et al., 2009) assuming conductive cooling through the crust (the volume of mare lavas is too small a fraction of the total crustal volume for advective heat transfer to be an important contributor) and heating from a convecting rather than a conducting mantle (the option that maximises upward heat flow). All such models imply that the elastic lithosphere must have been 100-150 km thick during the main period of mare volcanism, mostly in the interval 3.9 to 3 Ga before present, with minor activity as recent as ~1 Ga ago (Hiesinger et al., 2000, 2011), whereas the thickness of the crust would have already become fixed by solidification of an initial magma ocean to lie in the present-day range of ~30-50 km (Wieczorek et al., 2013). Thus plumes in a convecting mantle would have encountered a rheological boundary (Figure 1a) well below the base of the compositionally-defined lunar crust (Hess, 2000). It is therefore clear on theoretical rock-mechanical grounds (e.g. Pollard, 1988; Rubin, 1993) that magma transport at all depths shallower than this rheological boundary, not only through the shallow crust of the Moon but also though the upper mantle, must have taken place by flow through dikes held open by elastic stresses in rocks that behaved in a brittle fashion.

Other mechanisms of magma transport must have operated in the deeper interior (Hess, 1991). The main alternative to flow though brittle fractures is porous flow along grain boundaries in regions of partial pressure-release melting accompanied by compaction of the matrix (Richter and McKenzie, 1984; Bouilhol et al., 2011). Insertion of plausible values for the parameters involved into the equations governing this process (Shearer et al., 2006) yields melt transport speeds within an order of magnitude of 1 m per year, in stark contrast to the likely rise speeds of magmas in brittle dikes which, under lunar conditions, are likely to be of order 3 m s^{-1} (Wilson and Head, 1981). A hybrid state must exist in the upper part of a region of partial melting where concentration of melt enlarges some small veins at the expense of others leading to rapid melt migration in a small number of large veins (Sleep, 1988). Indeed, a complex heirarchy of veins with a wide range of sizes may develop (Brown, 2004; Maaløe, 2005) encouraging melt percolation (Schmeling, 2006) until ductile fracture mechanisms allow a brittle fracture to nucleate (Weinberg and Regenauer-Lieb, 2010). These mechanisms are encouraged by the creation of local non-hydrostatic pressures as a result of the volume increase that most silicate minerals undergo on melting, but this process was probably not important on the Moon. This is because such excess pressures are important only if the melting rate is so fast (as was the case in early-forming asteroids heated by decay of short-lived ^{26}Al), that plastic flow of the mantle surrounding the partial melt zone could not occur fast enough to relax the developing stresses (Wilson et al., 2008). An integrated model of the change from melt percolation to dike initiation in the lunar interior is developed by Havlin et al. (2013).

Mantle convection provides an obvious mechanism to cause melting by pressure release. However, it is not guaranteed that mantle convection was possible at all times in lunar volcanic history (Stevenson, 2003) and an alternative is melt formation by accumulation of radiogenic heat in finite regions due to the concentration of radioactives driven by gravitational overturn and negative diapirism of density-stratified cumulates (Delano, 1990; Wagner and Grove, 1997). Melt migration and upward concentration by porous flow is possible within such regions, but models involving this mechanism (Hess, 1991) generally place the melt sources even further below the elastic lithosphere. The frequency of mare lava eruptions (one large-volume eruption every 10^6 years – Head and Wilson, 1992a) implies that the time scale for the accumulation of a sufficient volume of magma to trigger an eruption is commonly much shorter than the Ga time scales of large-scale crustal deformation driven by global cooling. The boundary within a planet between elastic and plastic responses to applied stresses is strain-rate- as well as temperature-dependent, and so the rheological boundary for magma percolation should be deeper than the base of the elastic lithosphere as usually defined. This emphasizes the requirement for magma transfer in dike-like conduits in at least the upper part of the mantle. Perhaps the most compelling evidence of the need for such pathways (Wilson and Head, 2003a) is the petrologic implication that the picritic melts forming the orange, green and black pyroclasts found at the Apollo 15 and 17 sites were transported to the surface from sources at depths of 250-600 km on time scales of hours to days (Spera, 1992) without significant chemical interaction with the rocks through which they passed. This is a similar argument to that proposed for kimberlite eruptions on Earth (Wilson and Head, 2007a). The experimental verification (Beck et al., 2006) that relatively porous dunite channels should develop quickly over a large range of depths in the lunar mantle during a protracted melt-extraction episode provides an attractive explanation for the connection between deep inter-grain porous flow and shallower transport in dikes formed by brittle fracture.

Ideas on the relative importance of magma buoyancy and magma source pressure in lunar eruptions have evolved considerably with improvements in values for the density and thickness of the lunar crust (Wieczorek et al., 2013) and for the densities of the erupted magmas (Wieczorek et al., 2001; Shearer et al., 2006; Kiefer et al., 2012). Current estimated values of key parameters having a bearing on the physics of lunar volcanism can be summarized as follows. The lunar crust varies in total thickness, probably being on average ~30 km thick on the Earth-facing hemisphere and ~50 km thick on the far side (Fig. 3 of Wieczorek et al., 2013). This thickness for the near side crust may be a slight over-estimate due to the neglect of the mare lava fill in the analysis of the GRAIL mission data. The average crustal density, ρ_c, is ~2550 kg m^{-3} and the bulk density of the mantle, ρ_m, is inferred to lie between 3150 and 3370 kg m^{-3} (Wieczorek et al., 2013). Finally, the liquidus densities, ρ_l, of mare basalts and picritic magmas have been calculated by Wieczorek et al. (2001) and Shearer et al. (2006) to span the ranges 2775 to 3025 and 2825 to 3150 kg m^{-3}, respectively. Kiefer et al. (2012) measured the densities of some returned lunar basalt samples in the range 3010 to 3270 kg m^{-3}, which would correspond to ~2980 to 3240 kg m^{-3} at liquidus temperatures. Thus with no exceptions mare basalts were negatively buoyant in the crust of the Moon. For subsequent modeling we take the density of the mantle to be the average of the estimated range, 3260 kg m^{-3}, and based on the various estimates we assume the density of erupting basalts to be either 2900 or 3010 kg m^{-3}.

The earliest estimates of the density structure of the Moon led to the suggestion that an excess pressure was required in the magma source region to enable melts to erupt at the surface, irrespective of whether those melts traveled directly from source to surface in a single event (Solomon, 1975; Wilson and Head, 1981) or were temporarily stored in a reservoir at some intermediate depth (Head and Wilson, 1992a,b). The new data confirm that such excess pressures are important. Their presence is understandable, because the melt in any region experiencing partial melting or containing accumulated melt will behave as though an excess pressure is present at the top of the melt column provided that the melt is positively buoyant relative to the host rocks and forms a continuously connected network. The value of this effective excess pressure is the product of the finite vertical extent of the region, the difference in density between the host rocks and the melt, and the acceleration due to gravity at the relevant depth. Petrologic evidence suggests that both mare basalts and picritic glasses may have been derived from polybaric melting of source rocks in regions extending vertically for at least a few tens of km (Shearer et al., 2006). This is not surprising: the vertical extent of an inter-connected partial melt region is expected to be approximately inversely proportional to the acceleration due to gravity (Turcotte and Schubert, 2002) and hence should be ~6 times larger on the Moon than on the Earth if no other factors intervene. Deciding what vertical extent of partial melting on Earth to use in such scaling is not trivial. Almost all melt production on Earth is associated with plate tectonics and the melting region is subject to horizontal shearing. Maaløe (2005) suggested that the vertical extent of melting in an unsheared rising mantle diapir on Earth could be as small as ~2 km; in contrast, estimates of the depths over which partial melting takes place under Hawai'i are ~25-40 km (Farnetani et al., 2010). We adopt the lower end of this range as being most likely to be relevant, and so melting in lunar diapirs might be expected to extend over a vertical distance of up to ~($6 \times 25 =$) 150 km. The excess pressure due to a typical ~300 kg m^{-3} density difference between magma and host mantle would then be 1.62 m $s^{-2} \times$ 150 km $\times$ 300 kg m^{-3} = ~73 MPa. We therefore include the possibility of excess magma source pressures up to ~100 MPa in our modeling. These values apply whether the magma source is a partial melt zone deep in the mantle or the melt at the top of a diapiric body stalled at a rheological trap at or beneath the base of the elastic lithosphere.

Excess pressures would also be present in bodies of melt trapped in magma reservoirs at the compositional discontinuity at the base of the crust or at other neutral buoyancy levels within the crustal lithosphere if these exist. In this latter case these excess pressures would be limited because they would only increase by the addition of more magma until the elastic deformation of the host rocks caused their fracture toughness to be exceeded somewhere, at which point a dike (or sill) would begin to propagate. As a result, excess pressures in these crustal magma bodies would probably be no more than twice the tensile strength of the host rocks (Tait et al., 1989), perhaps up to ~10 MPa, an order of magnitude smaller than those in deep partial melt zones. We use the above concepts and numerical values in subsequent analyses.

3. Modes of dike initiation and development from magma sources

3.A General considerations

Dikes are initiated when the rocks overlying a melt body fracture in a brittle mode. As suggested above, in the mantle this may be the result of the excessive strain rate imposed on mantle rocks above a diapir rising to a rheological boundary where the decreasing temperature of the host rocks forces them to cease to respond in a plastic manner. In shallower bodies of melt already accumulated in elastic host rocks, fracture is likely to be the result of tensile failure of the host rocks as the pressure in the already-accumulated magma increases, either as a result of the arrival of more magma from depth or because the volume of the already-accumulated magma increases as chemical or thermal evolution occurs. Cooling of magma and crystallization of dense minerals causes a reduction of volume and a pressure decrease (Carslaw and Jaeger, 1947), but the attendant chemical changes may in principle force volatile exsolution and hence a volume and pressure increase. While significant for many magmas on Earth, this is not likely to be an important process for lunar magmas due to their low contents of dissolved volatile species and the fact that their commonest volatile, CO, was produced in a chemical reaction requiring absolute pressures less than ~40 MPa (Sato, 1976, 1979; Fogel and Rutherford, 1995; Nicholis and Rutherford, 2006, 2009; Wetzel et al., 2015).

The geometry of a growing dike that develops from an initial fracture will be dictated by the excess pressure, if any, in the magma source region, the stress regime in the host rocks, and the relative densities of the magma and host rocks (Pollard, 1988). The density of the host rocks will in general be a function of depth below the surface as described in Section 2. The density of the magma (neglecting the small effects of pressure-dependent compressibility) will be a function of the way volatiles (if available) are released from, and accumulate in, the magmatic liquid, and will vary with position and time along the growing dike until the upper dike tip either reaches the surface or ceases to propagate (Wilson and Head, 2003a). Treatments allowing predictions of dike propagation conditions exist for only limited ranges of circumstances and focus on two scenarios: the rise of magma that is everywhere positively buoyant relative to the host rocks and has no excess source pressure (Spera, 1980; Spence et al., 1987; Lister, 1990a, 1990b, 1991; Lister and Kerr, 1991; Mériaux and Jaupart, 1998; Dahm, 2000a, 2000b; Menand and Tait, 2002; Rivalta and Dahm, 2006; Chen et al., 2007; Roper and Lister, 2007), and the mainly lateral spreading of magma in dikes centered on a level of neutral buoyancy, again with no excess source pressure (Lister, 1990b; Lister and Kerr, 1991). Roper and Lister (2005) proposed a model of upward dike propagation including source pressure, but again only for positively buoyant magmas. Chen et al. (2011) and Taisne et al. (2011) discuss the arrest of buoyant dikes propagating upward from shallow and deep sources, respectively, when they encounter a neutral buoyancy level. Taisne et al. (2011) also address the limitations on dike propagation distance due to changes in dike shape, and Maccaferri et al. (2011) discuss sill formation linked to host rock density and stress changes.

Early attempts to use the static dike models of Weertman (1971) to approximate all types of propagating dikes (Head and Wilson, 1992a; Wilson and Head, 2001) were legitimately criticized (Shearer et al., 2006) on the grounds that they ignored the dynamic aspects of dike propagation. In particular, in the magma in a propagating dike there must be a pressure gradient driving magma motion against wall friction (Lister, 1990a). The pressure at the base of a dike connected to a large-volume magma reservoir is essentially fixed by the pressure at the top of the reservoir, and so the pressure at the propagating upper tip must decrease to a low value to maximize the magma flow rate. Lister and Kerr (1991) and Rubin (1993) inferred that this minimum value should be the pressure at which the most soluble magmatic volatile present (commonly water in magmas on Earth) is just saturated, and that the uppermost part of a dike will consist of an elongate cavity containing pure gas at this saturation pressure. Wilson and Head (2003a) pointed out that in addition there must be a zone of magmatic foam beneath the gas-filled tip cavity. We enlarge on this model for propagating dikes feeding the opening stages of lunar eruptions below.

Unless the magma in it suffers excessive cooling during transport, a dike containing magma that is everywhere buoyant in its host rocks would inevitably reach the surface and erupt until the supply of magma ceases. However, if the magma is not positively buoyant at all depths, and the dike is relying to some extent on an excess pressure in the magma source to aid its growth, the upper tip of the dike may cease to propagate for a number of reasons in addition to thermal limitations. The stress intensity at the dike tip may no longer be able to fracture the overlying rocks; or the combination of source pressure and magma-host-rock density contrast may not be able to support the magma column any closer to the surface. In principle, another option that could apply to both positively and negatively buoyant magma is that all of the available magma might be removed from the source region. However, this would require the rocks surrounding the source region to deform on a time scale, and by an amount, consistent with the flow speeds of magmas in dikes (commonly within a factor of 10 of ~3 m s^{-1} on the Moon and Earth - Wilson and Head, 1981) and the duration of the eruption. The deformation speed of the mantle rocks surrounding a deep mantle source are likely to be similar to those inferred for mantle convection, within 2 orders of magnitude of ~0.1 m a^{-1} (Crowley and O'Connell, 2012) on Earth and presumably nearly an order of magnitude less on the Moon because of the smaller acceleration due to gravity. This contrast by a factor of order at least 10^8 suggests that only a very small fraction of the total available magma can be extracted quickly from a deep mantle reservoir. Extraction would be aided if there were an excess pressure in the melt as a result of elastic stresses in the host rocks, but even in the case of very shallow magma reservoirs, where the host rocks behave entirely elastically, Blake (1981) showed that only ~0.1% of the reservoir is likely to be erupted before the excess internal pressure is relaxed. Numerous individual mare lavas flows with volumes up to ~200 km^3 are observed (Head, 1976). Mare lava ponds have a wide range of sizes from 15 to 1045 km^3, with mean pond volumes of 190 km^3 in the Smythii basin, 270 km^3 in the Marginis basin, 240 km^3 in Mare Orientale and 860 km^3 in the South Pole-Aitkin basin (Yingst and Head, 1997, 1998; Whitten et al., 2011). We infer that if they behaved elastically, the source regions feeding these eruptions must have had total volumes (assuming they contained ~0.1% by volume melt) of order 10^5 to 10^6 km^3. These volumes would, for example, be consistent with spherical bodies of diameters ~60 to 125 km or flattened ellipsoids of greater horizontal extent. It is difficult to imagine spherical magma bodies of this size being present at the base of a 30-50 km thick crust without producing surface consequences, but diapiric bodies of this size might well be present deeper in the mantle. An option for a shallow source might be crustal underplating forming an areally extensive sill, but a 10 km thick example of such a sill would need to have a diameter of ~350 to 1100 km.

The relative values of crust, mantle and magma densities for the Moon quoted in Section 2 imply that essentially all lunar magmas are negatively buoyant everywhere in the crust. Dikes containing these magmas that originate from diapirs that have stalled at rheological boundaries in the mantle will rise as far as the level of neutral buoyancy at the crust-mantle interface; as long as the least principle stress is horizontal they will then spread out both vertically and laterally. In some cases the upper tips of such dikes can reach the surface, provided that the positive buoyancy in the part of the dike in the mantle is great enough. However, in other cases the upper tip must remain below the surface. This is a circumstance commonly encountered in the lateral rift zones of shield volcanoes on Earth. A model of the growth of such a system is given by Lister (1990b) and Lister and Kerr (1991) and a model of the final configuration is given by Rubin and Pollard (1987). The model of Lister (1990b) and Lister and Kerr (1991) assumes that the growing dike intrusion is fed from a point source at the level of neutral buoyancy, the source having no excess pressure, whereas in fact such a dike will always bring with it an internal excess pressure acquired in its deep mantle source zone, ensuring that there is a positive pressure, in excess of the local lithostatic load, at the neutral buoyancy depth. This excess pressure is not included in Lister and Kerr's (1991) dynamic model, which led Wieczorek et al. (2001) to conclude, we infer incorrectly, that lateral intrusions at neutral buoyancy depths can never reach the surface. The option of including such an excess pressure is part of the Rubin and Pollard (1987) static model describing the final configuration of such a dike, and we use this treatment to model the final geometry of intruded dikes that do not erupt at the surface and to estimate the eruption conditions in such dikes that do breach the surface. Dikes able to intrude the crust or erupt are likely to have been the norm during the first quarter of lunar history when interior heating and global expansion induced extensional stresses in the crust (Solomon and Head, 1980), and, indeed, this period overlaps the main era of mare volcanism (Hiesinger et al., 2003). In cases where the least principle stress is not horizontal, most likely during the latter three-quarters of lunar history when global cooling induced compressive stresses in the crust (Solomon and Head, 1980), mantle dikes encountering the density discontinuity at the crust-mantle boundary are more likely to have initiated sills underplating the crust. The possibility exists that some of these magma bodies evolved chemically in ways that subsequently allowed them to inject rare high-silica dikes into and through the crust (e.g., Wilson and Head, 2003b).

A final but critical issue concerns dikes that grow from the tops of diapiric bodies deep in the mantle. These dikes can in principle grow upward to a great length, albeit slowly because they are being fed by melt migrating through the unmelted mineral fabric of the diapir. However, if a dike becomes too vertically extensive under these slow-growth conditions (Figure 1b), the overall stress distribution can cause the dike to pinch off from its source while the upper tip is still extending (Weertman, 1971; Muller and Muller, 1980; Crawford and Stevenson, 1988). The slow growth rate means that this stage of the dike's development can be adequately treated by the static stress models of Weertman (1971). After disconnecting from its source, the dike migrates as a discrete body of fixed volume, with the host rocks fracturing and opening above and closing behind the dike. This process leads to a limitation on the maximum volume of melt that can be transferred upward from the deep mantle in a single dike-forming event. This volume limitation would not necessarily apply to a dike reaching the surface or near-surface from a shallower diapir to which it was still connected.

The above considerations suggest that we need to address the following scenarios for the Moon (Figure 1): (a) dikes growing from magma sources so deep that the dike pinches off from the top of the magma source before the upper tip of the dike is arrested by any of the mechanisms discussed above, and (b) dikes growing from magma sources sufficiently shallow that a continuous dike pathway can exist between the top of the magma source region and the upper tip of the dike, irrespective of how far the dike is able to penetrate into the crust and whether or not it reaches the surface. The first of these scenarios is a guide to the major issues involved.

3.B Stability and sizes of dikes growing from deep mantle sources

Consider a dike that has grown upward to a length L from a diapiric magma body of vertical extent E_d. The stress intensity at the upper tip of the dike, K_u, is given by

$$K_u = (\pi L)^{1/2} [P_d + (g \Delta\rho L)/\pi] \quad (1),$$

where $\Delta\rho$ is the density difference between host mantle and magma, (ρ_m - ρ_l), and P_d is the driving pressure at the dike inlet, given by

$$P_d = g\ \Delta\rho\ E_d \qquad (2).$$

Given the earlier arguments, it seems reasonable to assume that the diapiric body is undergoing partial melting over a vertical distance of at least E_d = 10 km; in that case, with ρ_m = 3260 kg m^{-3} and ρ_l = 2900 kg m^{-3}, so that $\Delta\rho$ = 360 kg m^{-3}, and g = 1.62 m s^{-2}, P_d will be 5.8 MPa. The requirement for fracturing to occur at the upper dike tip, allowing it to grow, is that K_u must be greater than the fracture toughness of the host rocks, K_{crit}. Values of K_{crit} measured in laboratory-scale samples are ~3 MPa m$^{1/2}$, and for crustal-scale masses of volcanic rocks values have been estimated at ~100 MPa m$^{1/2}$ (Rubin, 1995). With P_d = 5.8 MPa, K_u would exceed K_{crit} if L were ~ 11.5 cm for the lower fracture toughness value and ~93 m for the higher value. Given that we are assuming that partial melt occupies a region extending vertically for at least 10 km, having interconnected melt veins ready to form an embryonic dike with a vertical extent of even the larger of these values does not seem likely to be a problem.

The stress intensity at the lower dike tip is K_l given by

$$K_l = (\pi\ L)^{1/2}\ [P_d - (g\ \Delta\rho\ L)/\pi] \qquad (3).$$

Initially the vertical dike length L is small and the term $[(g\ \Delta\rho\ L)/\pi]$ is much less than P_d, so that the stress intensities at both ends are similar and equal to $[(\pi\ L)^{1/2}\ P_d]$. As the dike grows, i.e. L increases, K_u constantly increases because both P_d and $[(g\ \Delta\rho\ L)/\pi]$ in equation (1) are positive. In contrast, the negative second term in equation (3) causes K_l to go through a maximum and eventually decrease, reaching zero when L reaches a critical value L_m such that $P_d = (g\ \Delta\rho\ L)/\pi$, i.e.,

$$L_m = (\pi\ P_d)/(g\ \Delta\rho) \qquad (4a),$$

We note here that equations (1) and (3) above differ from the equivalent formulae given by Muller and Muller (1980) by a factor of 2 in the second term on the right-hand side; we have made this change as the only way of reconciling expression (4a) with the more detailed analysis given by Weertman (1971). Figure 2 shows an example of how K_u and K_l vary with L, again for P_d = 5.8 MPa: K_u increases continuously as L increases, whereas K_l increases at first to a maximum of 705 MPa m$^{1/2}$ when L = 10.5 km and then decreases to zero at $L = L_m$ = 31.4 km. The fact that K_l reaches zero means that the stress acting on the lower tip of the dike causes its width to go to zero. At this point the dike, containing positively buoyant magma throughout its length as long as its top has not reached the crust-mantle interface, decouples from the diapiric source region and migrates upward as a discrete entity (Figure 1b). Rocks ahead of it fracture and dilate to provide a path and close back together behind it. In practice a small amount of magma is likely to be left on the walls of the closing crack, so that the volume of the dike is steadily depleted, but this is likely to be a small effect for dikes of the sizes relevant here. If we substitute for P_d from equation (2) into equation (4a), we find

$$L_m = \pi\ E_d \qquad (4b).$$

Thus the maximum vertical extent of a stable dike is slightly more than three times the vertical extent of the diapiric body that feeds it. Furthermore, L_m is independent of the density difference between magma and mantle host rocks, as long as there is a difference. If E_d is 10 km, as in the above example, L_m is ~31 km, and if E_d were as large as 100 km, L_m would be 314 km. But even in that case, it would still not be possible for a continuous dike pathway to exist between a deep mantle source region, at a depth of ~500 km, and the surface. Note that these results depend only on the criterion that the stress intensity at the pinch-off point is zero, and are completely independent of the fracture toughness assumed for the host rocks.

Large dikes that have decoupled from their source regions will have complex shapes because the need to do work against wall friction requires a pressure gradient to drive magma flow, and we do not model these shapes in detail during the passage of the dikes through the mantle. However, we can estimate the mean dike widths and initial volumes of magma in dikes of this kind as they decouple from the source by noting that their slow growth up to this point suggests that they will have the "penny" shape often cited as likely for static dikes, in which the horizontal extent is equal to the vertical length, L_m, and the mean thickness, W, can be obtained by numerically integrating Weertman's (1971) equation (20) and is well-approximated by

$$W = (\pi/6)\ [(1 - \nu)/\mu]\ L_m\ P_d \qquad (5).$$

where ν is the Poisson's ratio and μ is the shear modulus of the host rocks. Adopting $\nu = 0.25$ and $\mu = 4$ GPa (Bieniawski, 1984; Rubin, 1990) gives conservative estimates of W. The volume, V, of magma in the dike is then given by $[(\pi/4)\ L_m^2\ W]$, i.e.

$$V = (\pi^2/24)\ [(1 - \nu)/\mu]\ L_m^3\ P_d \qquad (6).$$

Using the above relationships, Table 1 shows the implied dike-base driving pressures, vertical lengths and volumes of dikes produced from diapiric partial melt zones of a range of vertical extents. For later reference the table also contains the driving pressure at the dike center, P_0, which is greater than P_d by an amount $(g\ \Delta\rho\ 0.5\ L_m)$. Using equations (2) and (4b),

$$P_0 = [1 + (\pi/2)]\ (g\ \Delta\rho\ E_d) = [1 + (\pi/2)]\ P_d \qquad (7).$$

Two implications can be drawn from Table 1. First, unless source regions are many tens of km in vertical extent, the volumes of magma available to reach shallow depths in a single extraction episode are a few thousand km^3. Only a fraction of this is likely to be erupted at the surface - we return to this issue later. These magma volumes are large enough that the limitations on isolated dike propagation due to changing shape discussed by Taisne et al. (2011) do not apply. Second, the widths of the propagating isolated dikes are so large that magma motion within them is likely to be turbulent and thus not controlled explicitly by the magma viscosity. If, as generally assumed, the pressure in the upper tip of a propagating dike decreases to a low value to induce the pressure gradient, dP/dz, driving the magma motion, the pressure gradient must be of order (P_d / L_m), and equation (4a) shows that this will be $(g\ \Delta\rho)/\pi$, ~185 Pa m^{-1}, in all cases. The turbulent flow speed U of magma in a dike of width W under a pressure gradient dP/dz is given by

$$U = [(W\, dP/dz)/(f\, \rho_l)]^{1/2} \quad (8)$$

where f is a friction factor close to 0.02. For the range of values of W in Table 1, U spans the range from ~4 m s^{-1} to ~70 m s^{-1}. At an intermediate speed of 30 m s^{-1}, a propagating isolated dike would require only 4.6 hours to reach the surface from a depth of 500 km, a speed of ~100 km/hour.

3.C Isolated dikes encountering the crust-mantle interface density trap

As mentioned earlier, the volumes of all but the very smallest dikes shown in Table 1 are large enough that we do not need to consider the details of their evolving shapes while they are rising through the mantle, a general issue addressed by Taisne et al. (2011). Instead we focus next on what happens when an isolated dike reaches the base of the crust. As long as the least principle stress is horizontal, the dike penetrates the crust and, as long as it does not erupt, stabilizes with its center at or very close to the crust-mantle density discontinuity. This geometry was modeled by Rubin and Pollard (1987). The criteria for stability are that the stress intensity at the tips of the dike should be equal to the fracture toughness of the host rock. In the present case the more important end of the dike is the upper tip because the lower tip is located in rocks that have already fractured to allow passage of the dike. There is an added requirement, that the driving pressure should adjust until the thickness of the dike is such that the volume of magma that it contains is equal to the volume of magma that was in the dike when it left the mantle source zone. The equations specifying the stress intensities at the upper and lower dike tips, K_{top} and K_{base}, respectively, and the new mean dike thickness, W_n, are:

$$K_{top} = P_n\, (A_u\, A_l)^{1/4} - g\, [(\pi^{-1} + 4^{-1})\, (\rho_l - \rho_c)\, A_u^{3/2} + (\pi^{-1} - 4^{-1})\, (\rho_m - \rho_l)\, A_l^{3/2}] \quad (9),$$

$$K_{base} = P_n\, (A_u\, A_l)^{1/4} - g\, [(\pi^{-1} - 4^{-1})\, (\rho_l - \rho_c)\, A_u^{3/2} + (\pi^{-1} + 4^{-1})\, (\rho_m - \rho_l)\, A_l^{3/2}] \quad (10),$$

$$W_n = [(1 - \nu)/\mu]\, \{0.5\, \pi\, P_n\, (A_u\, A_l)^{1/2} - 0.33\, g\, [(\rho_l - \rho_c)\, A_u^2 + (\rho_m - \rho_l)\, A_l^2]\} \quad (11),$$

where P_n is the new driving pressure at the crust-mantle boundary and A_u and A_l are the extensions of the dike above and below that boundary, respectively. Setting $K_{base} = 0$,

$$P_n\, (A_u\, A_l)^{1/4} = g\, [(\pi^{-1} - 4^{-1})\, (\rho_l - \rho_c)\, A_u^{3/2} + (\pi^{-1} + 4^{-1})\, (\rho_m - \rho_l)\, A_l^{3/2}] \quad (12).$$

Inserting this expression for $P_n\, (A_u\, A_l)^{1/4}$ into (9), and setting $K_{top} = K_{crit}$,

$$K_{crit} = 0.5\, g\, [(\rho_m - \rho_l)\, A_l^{3/2} - (\rho_l - \rho_c)\, A_u^{3/2}] \quad (13),$$

which gives a relationship between A_u and A_l:

$$A_l^{3/2} = \{[K_{crit}\, (0.5\, g)] + (\rho_l - \rho_c)\, A_u^{3/2}\}/\, (\rho_m - \rho_l) \quad (14).$$

These equations can be solved with the following steps: (i) an estimate is made of A_u; (ii) equation (14) is used to find the corresponding value of A_l; (iii) the values of A_u and A_l are inserted into equation (12) to find P_n; (iv) the values of A_u, A_l and P_n are inserted into equation (11) to find W_n; (v) the magma volume implied by these values, V_n, approximated by ($\pi\, A_u\, A_l$

W_n), is calculated and compared with the original volume leaving the mantle source, V, given by equation (6); (vi) the estimate of A_u in step (i) is varied until the two volumes are equal. This process is readily implemented in a spreadsheet.

Table 2 shows the results using K_{crit} = 100 MPa m$^{1/2}$. Part (a) of the table assumes a magma density, ρ_l, of 2900 kg m^{-3} and part (b) assumes ρ_l = 3010 kg m^{-3}. The values of E_d, L_m, W, V and P_0 are repeated from Table 1 for comparison with the values of the dike lengths above and below the crust-mantle interface, A_u and A_l, the mean dike width, W_n, and the driving pressure at the dike center, P_n, after it has intruded the crust. For ρ_l = 2900 kg m^{-3}, the trend is for both the mean width of the dike and its driving pressure to decrease, by ~30% and slightly more than a factor of 2, respectively. The total vertical length of the dike, $A_d = (A_u + A_l)$, increases by ~15%. For ρ_l = 3010 kg m^{-3}, both the mean width of the dike and its driving pressure decrease, by ~17% and ~52%, respectively, and the total vertical length of the dike, ($A_u + A_l$), increases by ~11%. These results are not strongly dependent on the value assumed for K_{crit}. Reducing the value by an order of magnitude to 10 MPa m$^{1/2}$ to be more consistent with values determined in laboratory experiments only change the values of dike length, width and driving pressure in the part of the table that we shall show to be of most importance by at most 5%.

Table 2 is of critical importance in understanding why eruptions are concentrated on the nearside of the Moon. The upper group of values in italics in both parts of Table 2 are solutions for which A_u is less than 30 km, meaning that the upper tips of dikes do not reach the surface on either the near- or farsides of the Moon. These conditions do not lead to eruptions but instead represent intrusions. The tops of these intrusions are generally at shallower depths on the nearside, with depths ranging up to ~13 km, than on the farside, where depths range up to ~43 km. The lower group of values in italics in both parts of the table represent solutions for which A_u is greater than 50 km, meaning that upper dike tips could reach the surface on the farside, so that eruptions would have readily occurred on both the near- and farsides of the Moon. These solutions are not in agreement with the observation that farside eruptions are very rare. The non-italic values in the center of each table are solutions where eruptions can occur on the nearside but not on the farside, as observed. We infer that these represent the actual conditions during the main period of mare volcanism. They imply that the vertical extents of the mantle diapiric source regions that produced the erupted magmas lay in the restricted range of 17 to 27 km for a basalt density of 2900 kg m^{-3} and 22 to 36 km for a basalt density of 3010 kg m^{-3}. If we include dikes that intruded the crust but did not erupt, the implication is that to allow intrusions anywhere on the Moon, but to allow eruptions on the nearside while at the same time forbidding eruptions on the farside of the Moon, mantle diapiric sources could have had any vertical extents up to a limiting value of ~32 ± ~5 km.

3.D Erupted volumes and eruption rates from isolated dikes breaching the surface

The values of parameters in Table 2 can be used to make estimates of the expected volumes of magma erupted when the tops of dikes stalled at the crust-mantle boundary reached the surface and caused a fissure vent to become active. Once the surface was breached, the conditions in the dike changed in several ways. The excess internal pressure was relaxed as magma spilled onto the surface, and the eruption continued until an equilibrium was reached between the horizontal stress state in the crust and the negative buoyancy, relative to the crust, of the magma in the dike. Recall that dikes capable of reaching the surface were intruded during the period of lunar history when internal heating had led to expansion of the interior and the production of a net tensional deviator, relative to hydrostatic stresses, in the crust. Solomon and Head (1980, their Fig. 20) estimated that this tensional deviator, T, was present in the interval between 3.8 and 3.0 Ga ago and reached a maximum value of ~20 MPa near the middle of this time interval. The tensional deviator replaced the internal excess pressure as the stress holding the intruded dike open, the upper part of the dike occupied the full thickness of the crust, C, and the extent of the part of the dike in the mantle shrank to a new final value, A_{lf}, such that the stress intensity at the lower dike tip was exactly zero. By analogy with equation (10) this requires

$$K_{base} = 0 = T\,(C\,A_{lf})^{1/4} - g\,[(\pi^{-1} - 4^{-1})\,(\rho_l - \rho_c)\,C^{3/2} + (\pi^{-1} + 4^{-1})\,(\rho_m - \rho_l)\,A_{lf}^{3/2}] \qquad (15),$$

which allows A_{lf} to be found for any given values of T and C. The mean width of the final intrusion, by analogy with equation (11) is W_f where

$$W_f = [(1 - \nu)/\mu]\ \{0.5\,\pi\,T\,(C\,A_{lf})^{1/2} - 0.33\,g\,[(\rho_l - \rho_c)\,C^2 + (\rho_m - \rho_l)\,A_{lf}^{2}]\} \qquad (16),$$

Setting C = 30 km for the nearside crust, Figure 3 shows how A_{lf} varies with T and Figure 4 shows how W_f varies with T, in each case for magma densities 2900 and 3010 kg m^{-3}. Figure 4 implies that if T is less than some limiting value, ~6.2 MPa for ρ_l = 2900 kg m^{-3} and ~7.1 MPa for ρ_l = 3010 kg m^{-3}, no stable residual dike can exist, and so all of the magma in the potential intrusion is forced out onto the surface as lava. To establish the actual volumes involved we need to know the horizontal extent of the residual dike. In keeping with the concept used earlier of the rising dike having had a penny-like shape, the horizontal length is assumed to be still approximated by the total vertical height before the surface was reached, $A_d = (A_u + A_l)$. The volume of the residual dike is therefore $V_f = [(C + A_{lf})\ W_f\ A_d]$, and the volume of magma erupted, V_e, is the difference between the original volume of the dike in the mantle, V given by equation (6), and the residue in the intrusion, V_f. Figures 5(a) and (b) show how V_e varies with T for magma densities of 2900 and 3010 kg m^{-3}, respectively. In each case the graphs are labeled with the range of values of E_d, the mantle source zone extent, that allows eruptions on the nearside but not the farside. As expected, for large values of T much of the magma remains in the residual intrusion and does not erupt, but for values of T less than the limiting values implied by Figure 4, essentially all of the magma erupts. The range of erupted volumes extends from the order of tens of km^3 up to more than 750 km^3 for a magma density of 2900 kg m^{-3} and to more than 1600 km^3 for a magma density of 3010 kg m^{-3}. These values are entirely consistent with the range of lava flow and lava pond volumes reported in Section 3.A.

Estimating the erupted volume fluxes during the eruptions produced by these dikes is also not easy without a much more elaborate model than that presented here. However, an estimate of the eruption rate soon after the surface is first breached can be found by evaluating the pressure at the base of the magma column in the dike, subtracting the static weight of the magma in the dike, and noting that the difference, if positive, is the pressure differential available to drive magma upward against fluid friction with the dike walls. Dividing this by the vertical extent of the dike gives the pressure gradient that can be used to give the magma rise speed in the dike. The pressure at the base of the magma column in the dike is P_b where

$$P_b = \rho_c\,g\,C + \rho_m\,g\,A_l \qquad (17).$$

The pressure due to the weight of the magma is P_w where

$$P_w = \rho_l\, g\, (C + A_l) \qquad (18).$$

The pressure difference driving the magma upward is dP = (P_b - P_w), and the length of the magma column is (C + A_l), so the pressure gradient driving magma motion, dP/dz, is

$$dP/dz = g\, \{[A_l\, (\rho_m - \rho_l) - C\, (\rho_l - \rho_c)]/(C + A_l)\} \qquad (19).$$

We cannot decide *a priori* if the motion of the magma in the dike is laminar or turbulent and so adopt the procedure shown to work by Wilson and Head (1981): we calculate the speed using both assumptions, i.e.,

$$U_{lam} = (W_n^2\, dP/dz)/(6\, \eta) \qquad (20),$$

$$U_{turb} = [(W_n\, dP/dz)/(f\, \rho_l)]^{1/2} \qquad (21),$$

and adopt whichever is the smaller speed. In these equations η is the magma viscosity, taken as 1 Pa s, and f is a dimensionless wall friction factor close to 0.02. Finally, the volume flux of magma being erupted from a fissure vent of horizontal extent L_e is F_e given by

$$F_e = \mathrm{MIN}(U_{lam}, U_{turb})\, W_n\, L_e \qquad (22).$$

Theoretically, there is no reason to think that the length, L_e, of the surface fissure from which magma erupts will be the same as the entire subsurface horizontal extent of the dike, A_d. Penny-shaped dikes are by definition convex-upward where they approach the surface. If the shape were preserved, half of the magma in the dike would have to be erupted before L_e became as large as A_d. Most of the pressure gradient driving the eruption would have been relaxed by this time and a much shorter fissure would be able to accommodate the magma volume flux. There are very few well-preserved examples of volcanic vents on the Moon, many vents being drowned in the late stages of eruptions (*Head*, 1976; *Head and Wilson*, 1992a; *Head and Wilson*, 2015). Perhaps the most useful evidence comes from the sizes of the source depressions feeding sinuous rilles. These depressions are interpreted to be the results of thermal erosion at the bases of lava ponds fed by explosive eruptions (Wilson and Head, 1980; Head and Wilson, 1980). A survey of the asymmetries of 15 elongate sinuous rille source depressions (Head and Wilson, 1981 and unpublished data) suggests that the fissure vents that fed them had lengths that ranged from 200 to 7000 m, with a median value of 1600 m. Adopting this value for L_e, Figure 7 shows the inferred magma rise speeds, U_e, all of which are found to be turbulent, and the corresponding erupted volume fluxes, F_e. For a magma density of 2900 kg m^{-3}, erupted volume fluxes lie in the range 10^5 to 10^6 m^3 s^{-1}; for a magma density of 2900 kg m^{-3}, the volume fluxes are all of order 10^6 m^3 s^{-1}. We show later that volume fluxes of order 10^5 m^3 s^{-1} are implied in the formation of sinuous rilles, and that fluxes of order 10^6 m^3 s^{-1} are required to form the longest mare lava flows.

Note the smaller range of values of Ue and Fe for the higher density magma in both parts of Figure 7. This dikes in which this magma rises are capable of reaching the surface, but it is so dense that its positive buoyancy in the mantle cannot compensate completely for its negative buoyancy in the crust. In practice, such a situation would lead to volatile exsolution in the magma in the upper part of the dike and the formation of a gas pocket overlying a column of foam, effectively reducing the magma density and making it possible for an eruption to begin; we discuss these dynamic effects in more detail shortly. The rate at which magma was expelled from the bulk of the dike would be a function of the rate at which the crustal host rocks relaxed in response to the changing stress conditions. It seems likely, based on the trend of the values of U_e and F_e in the rest of the figure, that eruptions from these dikes would have taken place at volume fluxes in the range 10^4 to 10^5 m^3 s^{-1}.

3.E Eruptions and intrusions when dikes are connected to their melt source zones.

Our previous treatments of dikes erupting at the surface (Wilson and Head, 1981; Head and Wilson, 1992a) assumed that they were still connected to their magma source zones, a condition which we have seen above is not possible for magma sources deep in the mantle. However, for shallower mantle sources such a scenario is still possible, but imposes restrictions on the possible depths and sizes of magma sources. The model of the Moon's thermal development proposed by Solomon and Head (1980, their Fig. 21) suggests that partial melting at depths less than ~250 km was confined to the first ~500 Ma of lunar history, and that melting at greater depths was not possible in this period. The models of Spohn et al. (2001) and Ziethe et al. (2009) allow for melting at depths between~200 km and ~600 km during this period. Figure 6 shows a scenario in which early mare basalts are generated by partial melting within a finite region in the upper mantle of vertical extent E. The level at which the stresses combine to initiate a dike is at a depth Z below the surface. The positive buoyancy of the magma in the mantle diapir leads to an excess pressure at the dike inlet, and this pressure is available to support the column of magma in the dike. If the excess pressure is great enough, the column of magma can be supported all the way to the surface and an eruption can occur. If the pressure is not great enough, the dike will stall with its top at some depth H below the surface (Figure 6). In that case, the balance of stresses is

$$g\,\rho_l\,(E + Z - H) = g\,\rho_c\,C + g\,\rho_m\,(E + Z - C) \qquad (23a).$$

so that

$$H = [C\,(\rho_m - \rho_c) - (Z + E)\,(\rho_m - \rho_l)]\,/\,\rho_l \qquad (23b).$$

If H given by this expression is negative, a column of magma could in principle extend above the lunar surface. In practice, the excess pressure represented by the weight of this magma, ($g\,H\,\rho_l$), is used to drive the magma motion against wall friction up the eruption pathway of length Z. The equivalent pressure gradient is then given by

$$\mathrm{d}P/\mathrm{d}z = (g/Z)\,[(Z + E)\,(\rho_m - \rho_l) - C\,(\rho_m - \rho_c)] \qquad (24).$$

The mean thickness W_{av} of the dike is again calculated using the model of Rubin and Pollard (1987). The thickness found is a realistic estimate of the intrusion thickness if no eruption occurs and is an estimate of the initial thickness, subject to later relaxation, when an eruption does occur. In that case the initial magma rise speed U_i is again found as the smaller of the values given by equations (20) and (21) and the initial volume flux, V_i, from a 1600 m-long fissure is given. Note that we do not specify any non-hydrostatic stress in the crust because we are considering volcanism occurring at a time before large extensional or compressive stresses are likely to have built up in the lunar crust due to thermal effects (Solomon and Head, 1980). Also, we tacitly assume that the magma source region contains a great enough volume of magma to fill a dike extending to the surface, and that when eruptions occurred, the dike geometry and magma flow rate were such that the magma did not cool excessively while traveling to the surface. This was checked by evaluating the minimum rise speed, U_{min}, to avoid significant cooling given by Wilson and Head (1981) as

$$U_{\mathrm{min}} = 5\ \kappa\ Z\ /\ W_{\mathrm{av}}^2 \qquad (25)$$

where κ is the thermal diffusivity of the magma, ~7×10^{-7} m^2 s^{-1}. In all cases U_{i} was found to be much greater than U_{min}, so that cooling was never a problem.

The simplest result of this analysis can be illustrated by setting the vertical extent of the mantle melting zone, *E*, to a very small value, essentially zero. In that case an eruption will occur if the magma source is at a depth below the surface greater than a critical value Z_{crit} such that

$$g\ \rho_{\mathrm{l}}\ Z_{\mathrm{crit}} = g\ \rho_{\mathrm{c}}\ C + g\ (Z_{\mathrm{crit}} - C)\ \rho_{\mathrm{m}} \qquad (26)$$

Using C = 30 km on the lunar nearside and 50 km on the farside we find that if the magma density is 2900 kg m^{-3}, Z_{crit} for the nearside is 59.2 km and the value for the farside is 98.6 km. For a magma density of 3010 kg m^{-3}, Z_{crit} is 85.2 km for the nearside and 142.0 km for the farside. Thus if the tops of melt zones feeding dikes connected continuously to the surface had been at depths greater than a critical value in the range ~99 to ~140 km, eruptions should have taken place on the farside. If the vertical extent of the partial melting zone is increased to a finite value greater than zero, an excess pressure is generated at the dike inlet by the positive buoyancy of the magma below this level and it is possible for a dike to reach the surface from a source region having its top at a greater depth than the critical values given above.

To illustrate this we first set the top of the mantle partial melting zone to be at a rheological boundary at an absolute depth of 50 km below the surface everywhere on the Moon, putting it at a depth of 20 km below the nearside crust, and at the exact base of the farside crust. We assign the same depth on both the near and far sides to the top of the diapir because the rheological boundary defining its location will probably be controlled more by the temperature than the pressure distribution in the lithosphere. We then explore the consequences of increasing the extent of the zone of partial melting, *E*, from zero to at least many tens of km based on the arguments in Section 2. Table 3 shows the results for a magma density of 2900 kg m^{-3}. First compare parts (a) and (b) of the table. For all vertical extents of the partial melt zone greater than ~5 km there is a great enough net buoyancy to ensure that eruptions must occur on the lunar nearside. In contrast, only if the vertical extent of partial melting within the diapir is greater than ~45 km is it possible for eruptions to occur on the farside; all smaller extents of melting lead to intrusions stalled at depths up to ~6 km below the surface. Thus a simple explanation for the paucity of mare basalt eruptions on the lunar farside is that the vertical extent of melting in very shallow mantle melt zones was less than 45 km. If the assumed depth to the top of the melt source zone is increased, for example to 60 km below the surface, eruptions now take place on the nearside for all extents of mantle melting, and the effective density contrast driving eruptions is somewhat increased because of the greater contribution from magma buoyancy in the mantle.

However, now eruptions can only occur on the farside if the vertical extent of the melting zone is at least ~35 km. Thus the range of melt-zone depths dictating the distinction between common eruptions on the nearside and rare eruptions on the farside decreases as the depth to the top of the melting zone increases. If the depth to the top of the melt source zone is increased further, to 70 km, eruptions on the nearside again occur for all source extents whereas eruptions on the farside require source sizes greater than ~25 km. The other important trend show by Table 3 is that as both the depth and the vertical extent of the partial melt zone increase, the magma rise speeds (all turbulent) and the erupted volume fluxes also increase. Many of the largest values in the table are greater than any inferred in the literature for actual eruptions on the Moon. This strongly suggests that if partial melt zones existed in the shallow mantle in early lunar history, they did not have great vertical extents.

The above analysis was repeated for a magma density of 3260 kg m^{-3}. The trends (not shown) are the same as those in Table 3 but the greater magma density leads to some systematic differences. Greater vertical extents of partial melt zones are needed to ensure that eruptions occur, on both the near- and farsides. Intruded dike widths are less by a factor of 2 to 3, magma rise speeds (still turbulent) are smaller by a factor of ~2, and eruption volume fluxes are less by up to an order of magnitude than the values for the lower density melt. None of these differences change the major conclusion that shallow partial melt zones must not have had great vertical extents.

3.F Dike intrusions and sills

Examples of dikes from deep sources whose tops intrude a distance A_u into the crust are shown in Table 2. The allowed range of values of A_u, assuming that melt zone extents can range up to tens of km, is so large that the tops of those dikes that do not erupt could be located at any depth below the surface, in both the nearside and farside crusts. The widths of dikes stalling at a few km depth would be ~35 m on the nearside and ~50 m on the farside. In contrast, Table 2 shows the properties of dikes from sources at shallow depths in the upper mantle, and indicates that the range of values of depths of dike tops, when eruptions do not occur, is much more restricted, especially on the lunar nearside. For partial melt zones with their tops at 50 km, intruded dikes should have widths up to ~40 m and have their tops at up to ~1 km below the surface.

Dikes intruding to shallow depths have the potential to induce surface graben if they generate stresses causing major fractures in the overlying crust (Head and Wilson, 1994; Petrycki et al., 2004; Klimczak, 2013). Petrycki et al. (2004) assessed the morphologies and measured the geometries of 248 lunar graben and found that 72 of them had associated minor volcanic features. The widths of these graben averaged 1.2 ± 0.6 km. Assuming that these graben were produced in response to the stresses associated with dike intrusion, the depths to the dike tops were inferred to lie in the range 0.5-1.6 km. An additional 176 graben not having easily recognized volcanic associations averaged 1.8 ± 0.8 km in width, implying possible dike top depths of 0.9-2.3 km. The depths of the graben with associated volcanic features were systematically greater than the depths of those without such associations, and the difference was inferred to imply a mean dike width of ~50 m, with a few examples implying greater widths in excess of ~150 m (Head and Wilson, 1994). The results presented here seem entirely consistent with these inferences.

The low mean flux of lunar magma (Head and Wilson, 1992a), the small percentage of the lunar crust formed of mare basaltic magma (Head, 1976), and the consequent infrequency of dike emplacement events, all conspire to limit large shallow magma reservoirs and large Hawaii-like shield volcanoes on the Moon (Head and Wilson, 1991). Repeated intrusions of dikes over more extended geologic time, however, will have increased the bulk density of the crust, somewhat reducing the negative buoyancy of magmas. Intrusions will also have reinforced the trend, controlled by global cooling (Solomon and Head, 1980), of increasing compressive stress in the crust with time. This in turn will have led to the least compressive stress becoming vertical, thus favoring the formation of sills if opportunities exist. The clear example of such opportunities is present in the form of the breccia lenses beneath impact craters. Several authors have proposed magma injection as a possible origin of distinctive impact craters in which the floor is uplifted and fractured (Brennan, 1975; Schultz, 1976b; Wichman and Schultz, 1995; Jozwiak et al., 2012, 2015) (Figure 8). The diameters of craters with floors modified in this way range from ~10 to ~300 km, so that the breccia lenses beneath them may have extended to depths of order two to a few tens of kilometers.

Tables 2 and 3 show that there are a wide range of circumstances that can lead to dikes ceasing to propagate upward when their tops reach depths of ~2-4 km. If one of these dikes encounters a breccia lens before it has reached its equilibrium height, it will initially invade the fractures between crustal blocks. This branching of the magma transport system will lead to magma cooling and reduce the chances of continued magma rise. Instead, the low density of the crustal material relative to the magma will create a tendency for a sill to form at the base of the brecciated zone. This sill will in principle be inflated until the top of the sill lies at the level that the magma would have reached if the crater were not present, so that sill thicknesses, and extents of crater floor uplift, may be at least of order a few km. Jozwiak et al. (2012, 2015) measured uplifts of up to 2 km in the small sample of floor-fractured craters that they examined in detail. The progressive enlargement of the growing intrusive body at the base of the breccia lens must have much in common with the growth of a laccolith as modeled by Michaut (2011), implying that small floor-fractured craters might display a domical uplift, largest in the crater center, whereas the largest diameter craters should have intrusions of more nearly uniform thickness and flatter floors (Jozwiak et al., 2012, 2015).

A second potentially attractive location for sills to form is at the density discontinuity at the base of the crust. However, two criteria must be satisfied for such intrusions to form when dikes arrive at the density boundary: the state of stress in the lithosphere must be such that the least principle stress is vertical and the excess pressure at the upper tip of the dike must be greater than the weight of the overlying crust. Favorable circumstances for this configuration would include (i) a dike generated by a very vertically extensive partial melt zone in the mantle, (ii) the dike arriving under a part of the crust that had been thinned by a basin-forming event, or (iii) the event taking place in the second half of lunar history when planetary cooling had induced a global horizontal compressive stress in the lithosphere. The weight of a 30 km thick crust thinned by a 3 km deep basin is ~112 MPa. Table 1 gives the excess pressures at the base, P_d, and the middle, P_0, of dikes from deep sources. The excess pressure at the top of such a dike is ($2 P_0 - P_d$) and the table therefore implies that a dike from a source of vertical extent ~46 km or greater would have the potential to form a sill as its upper tip arrived at the base of the crust. The magma volume involved in a single event could be as great at 5000 km^3, forming, for example, a ~40 km radius sill of thickness 1 km. Without more detailed models of mantle melting and better information on the history of the stress state of the lithosphere it is hard to comment on the likely frequency of such events.

We now turn to the consequences of dikes breaching the surface to cause eruptions. Since all lunar magmas contained some, albeit small, amounts of volatiles and were erupted into what is essentially the interplanetary vacuum, some element of explosive activity should always have been involved. In such cases we need to distinguish three phases: a first phase when the dike is in the process of growing from its source but has not yet reached the surface; a second phase when the dike tip has broken through the surface but the pressure distribution in the dike magma has not yet reached an equilibrium configuration; and a final phase when the pressure distribution has stabilized to one that maximizes the magma discharge rate. The amounts and the release conditions of volatiles and the consequent styles of explosive activity can be very different in these three phases. They can also differ significantly from the consequences of the accumulation of gas at the shallow top of a dike that has initially failed to erupt at the surface, or at the top of a shallow sill growing from such a dike. In these cases both explosive eruptions of juvenile magma and simple surface collapse due to gas release can occur. We first consider the transient processes associated with dike propagation to the surface.

4. Transient eruptions associated with dike emplacement

4.A Conditions in a dike propagating toward the surface

While a dike is still propagating, the pressure distribution within it adjusts to maximize the flow rate (Lister and Kerr, 1991; Rubin, 1993, 1995; Detournay et al., 2003). The pressure at the base of the dike is fixed by the pressure in the magma source zone, and so the pressure at the propagating upper tip must decrease to the lowest possible value. Lister and Kerr (1991) and Rubin (1993) suggested that this minimum value should be the pressure at which the most soluble magmatic volatile present (commonly water on Earth) is just saturated, but did not consider the dynamics of volatile exsolution into small gas bubbles and the growth and eventual bursting of these bubbles to transfer free gas into the narrow, elongate tip cavity. Wilson and Head (2003a) suggested that beneath the gas-filled tip cavity there must be a zone of magmatic foam, with the pressure at the base of the foam layer being the saturation pressure at which gas exsolution starts.

The pressure at the base of the foam layer is controlled by the first appearance of exsolved magmatic volatiles. Hauri et al. (2011, 2015) showed that at least some lunar magmas may have contained small amounts (up to 1000 ppm) of water, with small amounts of sulfur and chlorine also present. The solubility of water in terrestrial mafic magmas can be approximated by $n_d = 6.8 \times 10^{-8} P^{0.7}$ where n_d is given as a mass fraction and the ambient pressure P is expressed in Pascals (Dixon, 1997), so 1000 ppm water would saturate at a pressure of 0.9 MPa; detailed solubility data for S and Cl are not available but their vapor pressures in lunar magmas are expected to be much less than 0.1 MPa (Sato, 1976). However, pressure at the onset of gas release in a lunar dike is expected to be much greater than any of these values. This is because the dominant lunar volatile is expected to be a mixture of CO and CO_2 (with CO comprising ~90% of the mixture) produced in amounts up to ~2000 ppm by a smelting reaction between elemental carbon (graphite) and various metal oxides (Sato, 1976; Fogel and Rutherford, 1995; Nicholis & Rutherford, 2006; Wetzel et al., 2015). Gas production will begin when the ambient pressure in the magma decreases below P_{sm} = ~40 MPa (Fogel and Rutherford, 1995) and we take this to be the pressure at the base of the foam layer. Nicholis and Rutherford (2006) show that the smelting reaction proceeds very rapidly with decreasing pressure, at a rate of ~0.43 MPa change per 1000 ppm of CO produced for typical lunar magmas. Thus the production of ~2000 ppm of CO-dominated gas will be complete when the pressure has decreased from ~40 MPa to

~39 MPa. The vertical extent, ΔZ, of the foam layer, over which the pressure decreases from the ~40 MPa level of onset of CO production at the base to ~0.5 MPa at the top, can be estimated from the fact that the average pressure gradient, dP/dz, in the magma as the dike top nears the surface must be approximately equal to the average gradient of the lithostatic load in the host rocks, i.e.

$$dP/dz = \rho_c g \tag{27}$$

A pressure decrease of (40 - 0.5 =) 39.5 MPa then implies that the foam layer extends vertically for ΔZ = ~9.6 km.

The pressure at the top of the foam layer, P_i, marking the interface between the foam and free gas, will be controlled by the mechanism determining the stability of the foam. The pressure at the point of foam disruption can be found from either a critical gas bubble volume fraction criterion (Sparks, 1978) or a critical strain rate criterion (Papale, 1999). Rutherford and Papale (2009) found that, for mafic magmas, adopting the strain rate criterion did not predict eruption conditions very different from the bubble volume fraction criterion. We therefore adopt the simplest possible criterion, that the pressure at the interface between foam and free gas is the pressure at which the gas bubble volume fraction reaches a critical value at which the foam becomes unstable. Jaupart and Vergniolle (1989) suggest a critical value of 0.85, a little larger than the ~0.75 value suggested by Sparks (1978). Approximating the gas properties by the perfect gas law, the partial volumes of gas, v_g, and liquid, v_l, in the foam are

$$v_g = (n\, Q_u\, T_m) / (m\, P) \tag{28}$$

$$v_l = (1 - n) / \rho_l \tag{29}$$

Here m is the molecular mass of the volatile, n the mass fraction of the volatile exsolved from the magma, Q_u the universal gas constant (8.314 kJ kmol^{-1} K^{-1}), T_m the (assumed constant) temperature of the magma and ρ the density of the magmatic liquid. Thus the criterion $[v_g / (v_g + v_l)] = 0.85$ implies that the magma disruption pressure P_i is given by

$$P_i = (0.15\, n\, Q_u\, T\, \rho_l) / [0.85\, (1 - n)\, m] \tag{30}$$

Assuming a 90% CO, 10% CO_2 mixture with m = 29.6 kg kmol^{-1}, T_m = 1623 K (i.e. the 1350 ºC liquidus of the Apollo 17 orange glass magma) and ρ_l = 2900 kg m^{-3}, Figure 9 shows how P_i varies with the total amount of released gas, n. This pressure must also be the pressure in the gas in the tip cavity above the interface. Values are less than 1 MPa for likely volatile amounts.

The vertical extent of the free gas cavity cannot be found analytically because, as discussed by Lister and Kerr (1991), Rubin (1993, 1995) and Detournay et al. (2003), it depends on the detailed motion of the magma in the region between the onset of gas generation and bubble bursting. For dikes in the Earth's crust estimates are of order hundreds of meters (Lister and Kerr, 1991). We approach the problem as follows. Magma rising through the foam layer toward the dike tip moves most quickly along the center-line of the dike and migrates to the dike walls where it stagnates (a no-slip boundary condition requires the magma speed to be zero at the wall). If gas bubbles nucleate at the base of the foam layer with diameters of ~20 microns (Sparks, 1978; Larsen and Gardner, 2004; Yamada et al., 2005, 2008; Bai et al., 2008) and decompress from the 40 MPa pressure at nucleation to the gas pressure in the dike tip as they are carried up by the magma flow, they will have expanded isothermally to the sizes shown in Figure 9, of order 100 microns. The rise speed of bubbles of these sizes in the closely packed foam will be very small. The bulk viscosity of the foam will be much greater than that of the liquid magma alone. Jaupart and Vergniolle (1989) suggest that the effective viscosity increase is by a factor of $(1 - \varepsilon)^{5/2}$ where ε is the bubble volume fraction, 0.85; with a melt viscosity of 1 Pa s this suggests a foam viscosity of 115 Pa s. Equating the buoyancy to the viscous drag shows that the rise speed of a 100 micron diameter bubble in lunar magma will be ~30 nm s^{-1}. During the 5×10^3 to 5×10^4 s needed for a magma to rise from a depth of 50 to 500 km at ~10 m s^{-1}, bubbles at the top of the foam will have migrated at most 50 to 1500 microns, no more than 15 bubble diameters. Thus gas addition to the tip cavity by this mechanism is minimal.

More important will be the shearing of gas bubbles as magma approaches the dike walls. If we assume that a single layer of bubbles collapses and delivers gas to the cavity as it migrates to the wall, we can track numerically the amount of gas delivered as the dike tip propagates upward by multiplying the current width of the gas/foam interface, initially assumed to be vanishingly small, by the ~100 micron diameter of the bubbles. The detailed shape of the cavity depends on the stress distribution around the dike tip. The width/length aspect ratios of dikes are essentially equal to the ratio of the shear modulus of the host rocks (~4 GPa, *Rubin*, 1995) to the dike inlet pressure. In the case of the dikes illustrated in Tables 1 and 3 the ratio would be ~(4 GPa/10 MPa), i.e. 400, and using this value implies the gas cavity heights and widths shown in Figure 10 for a range of dike source depths encompassing mare basalts and deep-sourced picrites. If multiple layers of bubbles shear at the wall the values in Figure 10 would increase. The relationship involves the square root of the number of bubble layers; thus if 100 layers of bubbles collapsed near the dike wall the heights and widths in Figure 10 would increase by a factor of 10. Thus it seems likely that the vertical extents of dike tip gas cavities associated with the eruptions of mare basalts will have been a few tens to a few hundreds of meters. Deep-sourced picritic dikes may have had gas cavities extending for as much as 1 to 2 km.

4.B Transient eruption phenomena as dikes first breach the surface

4.B.1 Release of gas from the dike tip cavity

The first consequence of a dike breaking through to the surface will be the very rapid release of the gas that has accumulated in the cavity in the dike tip. Given the likely vertical length of the cavity, at least tens to hundreds of meters, this gas should contain almost no entrained magma droplets from the disrupting gas-magma interface below it. The gas may, however, entrain regolith clasts as it emerges, and may also have entrained rock fragments from the walls of the dike. The latter is likely because the decompression of the gas causes inward stresses across the dike walls that may exceed the tensile strength of the crustal rocks if the gas cavity is more than several hundred meters deep. We therefore define the gas to represent a mass fraction N of the expelled gas-clast mixture and expect N to range from 1.0 (no entrained clasts) to perhaps 0.5 if a great deal of dike wall disruption occurs. The gas will probably be at a temperature close to that of the magma from which it has been released, though heat loss to the cavity walls may be non-trivial if the cavity is very long. The ultimate velocity U_u reached by a parcel of gas in expanding into the vacuum above the lunar surface from a depth z and pressure P_i is given by

$$0.5\, U_u^2 = [\gamma / (\gamma - 1)]\, [(N\, Q_u\, T_m) / m] + [(1 - N) / \rho_l]\, P_i - g\, z \qquad (31)$$

where γ is the ratio of the specific heats of the gas at constant pressure and constant volume, very close to 1.3 for dominantly CO, and it is assumed that the gas receives no additional heat from the underlying magma during its very rapid expansion. Insertion of P_i = ~0.5 MPa, the value found in Section 4.A for a magma producing 2000 ppm of CO, and values of z as large as 10 km, we find that the last two terms in equation (31) are very small compared with the first term, and using T_m = 1623 K for a picritic melt we have U_u = 2.0 km s^{-1} when N = 1.0 and U_u = 1.4 km s^{-1} when N = 0.5. These values are less than the 2.38 km s^{-1} escape velocity from the Moon, but lead to extremely wide dispersal of all ejected clasts small enough to acquire an appreciable fraction of the gas speed. The distance D_u measured along the surface of a planet radius R traveled by a clast ejected at speed U_u and at an elevation angle from the horizontal θ is

$$D_u = 2\, R \tan^{-1}[(U_u^2 \sin\theta \cos\theta)/(R\, g - U_u^2 \cos^2\theta)] \qquad (32)$$

The maximum distance is not in general given by θ = 45°, the maximum range on a horizontal surface, and is most simply found by trial and error. For U_u = 1.4 km s^{-1} the maximum travel distance is ~1950 km when θ = ~30°, and for U_u = 2 km s^{-1} it is ~5210 km (almost to the middle of the opposite hemisphere) when θ = ~35°. Thus while this kind of event might qualify as the lunar equivalent of a terrestrial ultraplinian eruption, it would produce a deposit of very limited volume that was so widespread that it would almost certainly never be recognizable. The duration of such an event would be determined by the passage of an expansion wave through the trapped gas; with a typical wave speed of order half of the 765 m s^{-1} speed of sound in CO at magmatic temperature, gas cavities with lengths of 200 m and 2 km would be emptied on time scales of 0.25 and 2.5 seconds, respectively. A likely consequence of this gas release process would be the severe disturbance of the fine-grained regolith in the immediate vicinity of the vent.

4.B.2 Release of gas and magma from the foam beneath the dike tip

After all of the gas trapped in the dike tip cavity has been released, the expansion wave continues to propagate, now into the underlying foam. A simplifying characteristic of the foam layer is that, although the pressure within it will increase with depth, all of the magma within it will have passed through the ~40 MPa pressure level at which the smelting reaction occurs and so will contain the same amount of released dominantly CO gas. Section 4.A showed that the most likely vertical extent of the foam layer is ΔZ = 9.6 km. Section 4.B.1 provided a range of estimates of the vertical length of the gas cavity from which 300 m can be selected as typical. Thus a plausible scenario is one where the pressure P_{foam} in the foam layer varies from P_i = 0.5 MPa at 0.3 km depth to P_{sm} = ~40 MPa at 9.6 km depth. As the expansion wave passes down the foam layer the foam disaggregates into a mixture of gas and pyroclasts which expands to a pressure P_f at which the clasts and gas decouple as the system reaches the Knusden regime where the mean free path of the gas molecules exceeds the typical pyroclast size, d. The pressure at which this takes place is given by Wilson and Keil (2010) as

$$P_f = (2^{1/2}\, Q_u\, T)/(3\, \pi\, \phi^2\, N_a\, d) \qquad (33)$$

where ϕ is the effective diameter of the gas molecules, 3.4×10^{-10} m for CO, and N_a is Avogadro's number, 6.0225×10^{26} kmol^{-1}. For typical d = 300 μm sized pyroclasts, P_f is ~90 Pa.

The speed U_m reached by the mixture of gas and pyroclasts as it decompresses from the pressure P_{foam} at depth z to its final pressure P_f = 90 Pa, is

$$0.5\ U_m^2 = [(n\ Q_u\ T)/m]\ \ln(P_{foam}/P_f) + [(1 - n)/\rho_l]\ (P_{foam} - P_f) - g\ z \qquad (34)$$

Table 4 then shows how the eruption speed U_m changes as the foam layer is progressively erupted to the surface and also gives the corresponding maximum pyroclast ranges R_m. The maximum range increases from ~6 to ~10 km as the foam is discharged. Adding the effects of the exsolution of 1000 ppm H_2O from a very water-rich lunar magma would approximately double these dispersal distances to ~12 to ~20 km.

4.C Dikes that approach the surface but do not erupt large magma volumes

An upward-propagating dike may fail to reach the surface for a number of reasons, e.g., insufficient magma volume and pressure in the source region or inappropriate combinations of lithosphere and magma density. If such a dike has a small width or stops with its upper tip sufficiently far below the surface, there will never be any surface indication of its presence (Figure 8), though it might be detectable by geophysical techniques and it will contribute to increasing the mean density of the crust - see calculations in Head and Wilson (1992a). However, if the dikes induce stresses that allow fractures to form between the dike tip and the surface, graben formation is possible (Figure 8), as discussed in Section 3.F, and minor eruption of juvenile material or surface collapse due to gas release may take place, on both short and long time scales.

4.C.1 Short-term effects of near-surface dikes

As the top of a dike approaches its final configuration (Figure 8), the component of the vertical pressure gradient driving magma upward must decrease smoothly to zero. This implies that the absolute pressures in the gas in the dike tip cavity and in the underlying foam layer will be significantly greater than their values during most of the vertical rise of the dike. If the pressure in the gas becomes greater than ~10 MPa, the stresses on the crustal rocks overlying the dike top may exceed their tensile strength and fractures may open to the surface allowing the gas to vent. Given that the pressure prior to this adjustment was probably ~0.5 MPa, an approximately (10/0.5 =) 20-fold compression of the gas would occur during the build-up to this gas release, reducing the vertical extent of the gas cavity by a similar factor and bringing the underlying foam layer closer to the surface. There is clearly the potential for the propagation of an expansion wave into the foam, causing a restricted but energetic pyroclastic eruption through the crustal fractures until the foam is exhausted. All of the magma immediately beneath the foam layer will have passed through the critical 40 MPa pressure level during the emplacement of the dike and so will have produced all of the CO that it is capable of producing by the smelting reaction, but if the fractures to the surface remain open, exposure of the magma at the top of the melt column to the essentially zero pressure above the surface may cause some exsolution of dissolved species like water and sulphur, increasing the total volatile budget. A calculation using equation (34) but now allowing for the compaction of the foam layer and hence the reduction in z implies ranges for CO-dominated but also water-rich magma pyroclasts of up to ~25 km.

4.C.2 Longer-term effects of near-surface dikes

For the widest dikes likely to be emplaced with their tops near the surface, formation of collapse craters, as well as graben, is a possible consequence of gas accumulation and subsequent venting to the surface. However, features like these are rare on the Moon and only two cases have been described and analyzed. Head et al. (2002) showed that an ~75 km radius dark pyroclastic deposit superposed on the southern part of the Orientale basin interior could have been the consequence of gas accumulation at the top of an unusually wide (~500 m) dike with eventual surface collapse producing a 7.5 km by 16 km depression. Wilson et al. (2011) found that the ~30 km radius pyroclastic deposit surrounding the Hyginus crater complex could be explained by smaller amounts of gas accumulation at the top of a ~240 m wide dike that also intruded a small sill at shallow depth and produced Hyginus crater and the graben and associated minor collapse pits of Rima Hyginus. In both of these cases, convective overturn of the magma in the cooling dike was invoked to enhance the amount of gas accumulation at the top of the intrusion. Clearly this process is only likely to have been important for a few unusually wide dikes where the long dike cooling time allows for many cycles of convective overturn and upward gas segregation.

5. Steady eruptions from dikes erupting at the surface

Section 3 provided estimates of magma rise speeds up to tens of m s^{-1} and erupted volume fluxes mainly in the range 10^4 to 10^6 m^3 s^{-1} through dikes feeding surface eruptions, and Section 4 introduced the concept of volatile release from lunar magmas, implying that explosive activity was common on the Moon. We now show how the resulting pyroclastic deposits are related to the fire fountains produced by steady explosive eruptions.

5.A Near-surface processes of gas release in steady explosive eruptions

Local and regional dark mantle deposits (DMD) interpreted to be of pyroclastic origin have long been recognized on the Moon (Wilhelms and McCauley, 1971), generally in association with irregular depressions and sinuous rilles (Head, 1974, Head and Wilson, 1980; Wilson and Head, 1980, Gaddis et al., 1985, 2003; Hawke et al., 1989; Weitz et al., 1998; Weitz and Head, 1999; Gustafson et al., 2012). Regional deposits are the most extensive (equivalent radii mostly in the range 20-40 km) and are commonly located on uplands adjacent to younger mare deposits (e.g., Head, 1974; Weitz et al., 1998; Gaddis et al., 2003). Localized deposits, in contrast, are smaller in extent and more widely distributed across the lunar surface (Head 1976; Hawke et al., 1989; Coombs et al., 1990; Gaddis et al., 2003), and we consider these first.

Shortly after the upper tip of a dike breaches the surface, the pressure distribution with depth in the magma develops into whatever pattern maximizes the volume flux flowing through the system. This adjustment takes place via the passage of pressure waves through the dike system at speeds comparable to the speed of sound in the magma, ~ 1 km s^{-1}. The time needed for such a wave to propagate from a magma source at 400 km depth in the mantle would be 400 s and so even if the adjustment required the passage of waves back and forth between the source and surface several times the process would be complete in less than an hour. This is a very small fraction of the durations that we shall infer later for many lunar eruptions.

Numerous models of the key aspects of explosive volcanic processes on the terrestrial planets have been published (McGetchin and Ulrich, 1973; Wilson, 1980; Wilson and Head, 1981; Valentine and Wohletz, 1989; Giberti and Wilson, 1990; Dobran et al., 1993; Papale and Dobran, 1993; Wilson and Keil, 1997; Kaminski and Jaupart, 1998; Neri et al., 1998, 2003; Papale et al., 1999; Wilson, 1999; Cataldo et al., 2002; Wilson and Head, 2001, 2003; Mitchell, 2005; Wilson and Head, 2007b; Rutherford and Papale, 2009). In the simplest possible scenario, the equilibrium pressure in the magma emerging through the surface vent is equal to the local atmospheric pressure. However, when the atmospheric pressure is essentially zero, as on the Moon, this implies an infinitely wide vent, clearly physically impossible. In practice, the presence of even extremely small amounts of volatiles intervenes to dictate a finite pressure in the vent. Volatiles dissolved in the magma, or produced by pressure-dependent chemical processes, will be released as the magma ascends and the pressure decreases toward the surface in the shallow part of the conduit system. Whatever the source, the volatiles form gas bubbles in the liquid melt, and expansion of the bubbles as the magma rises and the pressure decreases accelerates the magma. The bubble volume fraction may become large enough that, combined with the strain rates to which the liquid-bubble foam is subjected, the liquid is disrupted into a free gas phase entraining pyroclasts. However, such disruption does not necessarily take place below the surface in all cases on the Moon (*Rutherford and Papale*, 2009); when it does not occur, magma disruption must occur immediately above the vent at the base of the system of shocks that decompresses the gas phase into the vacuum.

The speed of sound in a 2-phase (3-phase if crystals are also present) fluid, whether liquid plus bubbles or gas plus pyroclasts, is much less than the speed of sound in a single-phase liquid (Kieffer, 1977). Thus as magma approaches the surface it is possible for the steadily increasing magma rise speed to become equal to the rapidly decreasing sound speed. If this condition is reached in a parallel-sided or converging conduit system, there can be little further acceleration; the magma speed stays equal to the sound speed and the system is said to be choked. There may in fact be some change in speed, because if the pressure decreases and more volatiles exsolve, the sound speed will change and hence so will the flow speed; however, the Mach number must stay equal to unity. As shown by Giberti and Wilson (1990) and Mitchell (2005), the total mass flux through the volcanic system is maximized when the sonic condition is reached exactly at the surface vent, and it is likely that the system will rapidly adjust to this condition. Decompression to atmospheric pressure, zero pressure in the case of the Moon, and acceleration to supersonic speeds, is then accomplished immediately above the vent through a system of shocks (Kieffer, 1982, 1989).

The only way that a subsonic to supersonic transition can occur beneath the surface is for the conduit system to flare outward toward the surface by more than a critical amount. The combinations of conduit shapes and volatile contents of both mafic and silicic magmas on Earth ensure that both choked flows, where the vent pressure is greater than atmospheric, and supersonic flows, where the vent pressure is equal to the atmospheric pressure, may occur in eruptions. Wilson and Head (1981) showed that to ensure that the vent pressure can be equal to the atmospheric pressure in mafic eruptions on Earth it is typically necessary for the conduit to increase in width by a factor of 2 to 3 over the uppermost ~100 m of the conduit system. The equivalent expansion factor for the Moon, where the atmospheric pressure is essentially zero, was shown to be in the range 10 to 30. It is not likely that the stresses inducing dike propagation, even if there were large near-surface tensile stresses in the lithosphere, would lead to dikes with these near-surface shapes. Thus whereas some but not all explosive eruptions on Earth may be choked, all explosive eruptions on the Moon are expected to be choked. This is true even though lunar magma volatile amounts are much less than typical terrestrial values.

The vent pressure implied by imposing choked flow can be found by evaluating the rise speed, U, of the magma and the sound speed, S, within it as a function of pressure, P. This is particularly straightforward for lunar magmas where the dominant volatile is the CO-dominated mixture generated by smelting (Fogel and Rutherford, 1995), because formation of gas bubbles in the magma will have been completed very quickly as the pressure in the magma fell below 40 MPa (Nicholis and Rutherford, 2005), in contrast to conditions in terrestrial magmas where pressure-dependent gas release will in general still be ongoing. Wilson and Head (1981) showed that for the ranges of pressures and volatile contents relevant to volcanic systems the formula

$$S = P\,[m / (n\,Q_u\,T_m)]^{1/2}\,\{[(n\,Q_u\,T_m) / (m\,P)] + [(1 - n) / \rho_l]\} \qquad (35)$$

gives values of the sound speed within a few percent of those obtained from more complex treatments (e.g. Hsieh and Plesset, 1961; Soo, 1961, 1967; Kliegel, 1963; Rudinger, 1964; Cole et al., 1970; Kieffer, 1977; Pai et al., 1978). To illustrate likely values for mafic melts we adopt a density of 2900 kg m^{-3} and a temperature of 1500 K. On Earth mafic magma volatiles are dominated by H_2O (m = 18 kg $kmol^{-1}$) and CO_2 (m = 44 kg $kmol^{-1}$) in roughly equal proportions whereas lunar magmas mainly produced a 90% CO, 10% CO_2 mixture with m = 29.6 via a smelting reaction (Fogel and Rutherford, 1995) and exsolved smaller amounts of H_2O (Hauri et al., 2011) and traces of S_2 (m = 64 kg $kmol^{-1}$) (Saal et al., 2008). In both cases, therefore, a value of m = ~30 kg $kmol^{-1}$ seems an adequate approximation for comparisons.

The variation with pressure of the eruption speed though the vent in an explosive eruption is not easy to evaluate, choked or otherwise. When significant amounts of volatiles are exsolved it is generally the case (e.g. see examples in Wilson and Head, 1981) that the magma rise speed before exsolution starts is very much less than the eruption speed, and so can be neglected. Also, the motion after the onset of volatile release but prior to magma disruption into pyroclasts is limited by friction between the magmatic liquid and the conduit walls and so the speed increase is not large. It is after magma disruption into a continuous gas phase with entrained pyroclasts that most of the acceleration occurs. If the pressure at the point of disruption is P_{dis}, and the magma accelerates to reach speed U when the pressure is some smaller value P, then to a good approximation (Wilson, 1980)

$$0.5\,U^2 = [(n\,Q_u\,T) / m] \ln(P_{dis} / P) + [(1 - n) / \rho_l]\,(P_{dis} - P) - g\,Z_{diff} \qquad (36)$$

where Z_{diff} is the distance over which the pressure change occurs, estimated by assuming that the pressure in the erupting magma is close to lithostatic, so that $Z_{diff} = (P_{dis} - P) / (g\,\rho_c)$. Two energy terms have been neglected here, the initial kinetic energy of the rising magma before the smelting reaction begins and the work done against wall friction; detailed numerical simulations like those in Wilson and Head (1981) show that both of these terms are small compared with the terms listed in equation (36) and, being of opposite signs, they partially compensate for one another.

The pressure, P_{dis}, at which magma disruption takes place is controlled by the same foam stability criterion discussed in the previous section, and so P_{dis} is the equivalent in a steady eruption of P_i given by equation (30). Substitution of equation (30) into equation (36) allows U to be found as a function of P, and equation (35) gives S as a function of P. Thus the pressure P_{ch} at which the choked sonic condition $U = S$ exists at the vent will be the pressure simultaneously satisfying the expressions for U and S from equations (35) and (36), given by

$$[(n\,Q_u\,T_m) / m] \ln(P_{dis} / P_{ch}) + [(1 - n) / \rho_l]\,(P_{dis} - P_{ch}) =$$
$$P_{ch}^2\,[m / (2\,n\,Q_u\,T_m)]\,\{[(n\,Q_u\,T_m) / (m\,P_{ch})] + [(1 - n) / \rho_l]\}^2 \qquad (37)$$

This equation involves P_{ch} in both logarithmic and algebraic terms, so there is no analytical solution and the value of P_{ch} must be found by an iterative method. For equations of this kind we can calculate a new approximation to P, P_{new}, from an older approximation, P_{old}, using

$$[(n\,Q_u\,T_m) / m] \ln(P_{dis} / P_{new}) + [(1 - n) / \rho_l] (P_{dis} - P_{old}) = P_{old}^2\,[m / (2\,n\,Q_u\,T_m)]\,\{[(n\,Q_u\,T_m) / (m\,P_{old})] + [(1 - n) / \rho_l]\}^2 \quad (38)$$

which can, of course, be solved analytically; if the value ($0.5\,P_{dis}$) is used as the first value of P_{old} the solution converges to better than 1% after 4 iterations and better than 1 part in 10^6 after 12 iterations.

Figure 11 gives the values of P_{dis} and P_{ch} found in this way for a wide range of value of n for m = 30 kg kmol^{-1}. In all cases P_{dis} is greater than P_{ch}, i.e. magma is disrupted into pyroclasts before emerging from the vent. For the Moon, with total released amounts of CO probably in the range 250-2000 ppm (Fogel and Rutherford, 1995; Saal et al., 2008) and up to ~1000 ppm H_2O (Hauri et al., 2011), P_{ch} is predicted to be in the range 0.04-0.4 MPa. For comparison on Earth, mafic magmas commonly exsolve from 0.2 to 1.0 mass % total volatiles (Wallace and Anderson, 2000) implying that P_{ch} is at least ~1 MPa for eruptions where the vent shape does not become wide enough to prevent choking. For the Moon, a key issue is what these combinations of P_{ch} and n imply about the ranges of pyroclasts in steady eruptions. As discussed by Wilson and Head (1981), the dispersion of pyroclasts into a vacuum is determined mainly by the speed with which the pyroclasts emerge from the vent and in part by the size distribution of the liquid droplets into which the magma is disrupted. The pyroclastic glass beads returned by the Apollo missions generally have sizes in the 100-1000 micrometer range (Weitz et al., 1998); if these are typical of all lunar pyroclasts then almost all of the pyroclasts in any of the eruptions modeled here would stay locked to the expanding and accelerating gas cloud for long enough that they acquired a very large fraction of the ultimate gas speed. However, we have no direct evidence of how far from their source vents the Apollo sample pyroclasts were collected, and it is possible that larger, unsampled clasts may have been produced.

The speed with which gas and small pyroclasts emerge through the vent into a lunar fire-fountain-like eruption, U_v, is obtained by substituting the value of P_{ch} for P in equation (36). Next, the gas-pyroclast mixture is allowed to expand above the vent to the final pressure P_f at which gas and clasts decouple, which we saw earlier is ~90 Pa. In the simplest case, therefore, where all of the pyroclastic droplets stay locked to the expanding gas until this decoupling pressure is reached, this allows their final common velocity U_b to be found from

$$0.5\,U_b^2 = 0.5\,U_v^2 + [(n\,Q_u\,T_m) / m] \ln(P_{ch} / P_f) + [(1 - n) / \rho_l] (P_{ch} - P_f) \quad (39)$$

Figure 12 shows the resulting values of U_b for a range of values of n, and also the implied maximum ranges R_f that pyroclasts would reach assuming ballistic trajectories. For total magmatic CO and H_2O contents up to ~3000 ppm, maximum dispersal distances of sub-mm sized pyroclasts from their vents will be up to ~10 km.

It is extremely important to consider the structure of the fire fountain that forms over a lunar vent. Some combination of limited range, small pyroclast size and large volume flux can lead to conditions in which the fire fountain is optically dense, in the sense that pyroclasts in the interior of the fountain cannot radiate heat into space because they are shielded by other pyroclasts. The result is that essentially all of the pyroclasts reach the ground at magmatic temperature and coalesce into a lava pond, which in turn feeds a lava flow. Treatments of this issue have been given by Wilson and Keil (1997), Wilson and Head (2001) and Wilson and Keil (2012) who found that significant heat can only be lost from within an outer shell extending inward from the edge of the fountain by a critical distance X, which may be termed the opacity depth. All of these treatments assumed that pyroclasts were distributed uniformly in the fire fountains, and we have now extended the analysis by relaxing this assumption. The detailed distribution is found by numerically following the paths of a large number of pyroclasts ejected at a given speed and over a given range of elevation angles for a great enough time that all of the pyroclast reach the surface. The space around the vent is divided radially into 5000 discrete, equal-sized cells and a record is kept of the cell in which each pyroclast is located at each of 1000 finite time intervals during its flight. We find that for a 2-dimensional fountain produced by an elongate fissure vent the mean number of pyroclasts per unit volume in the outer part of the fountain is about double the mean value. The situation is quite different for a point-source vent producing a circularly-symmetric fountain because pyroclasts are distributed into ever-larger annular zones as their horizontal distance from the vent increases. This causes the mean number of pyroclasts per unit volume in the outer part of the fountain to be about one fifth of the mean value for the entire fountain. With these geometric corrections to the treatment of Wilson and Keil (2012) we find that for a point-source vent forming a circularly-symmetric fountain

$$X = (6.17\, d\, g^{1/2}\, R_f^{5/2}) / F_e \qquad (40)$$

where F_e is the total erupted volume flux, and for a fissure vent erupting actively for a distance L_e along strike

$$X = (0.52\, d\, g^{1/2}\, R_f^{3/2}\, L_e) / F_e \qquad (41)$$

We now combine these results with the data in Figure 12 to show how the fraction of pyroclasts falling back to the surface at magmatic temperatures is related to the volume flux and volatile content of the magma. We treat the more conservative case of point-source vent feeding a circularly-symmetric fire fountain. The fraction of pyroclasts landing hot to form a lava pond is then $F = [(R_f - X) / R_f]^2$. This quantity is shown as a percentage in Table 5 as a function of magma CO content n for a range of values of magma volume flux F_e. Wilson and Head (1980) suggested that lava ponds of this kind formed around vents feeding high effusion rate eruptions of turbulent lavas that thermally eroded their substrates to erode sinuous rilles (Hulme, 1973; Carr, 1974). Wilson and Head (1981) showed that the motion of the lava in the ponds would also be turbulent, so that the pond floors should also be eroded. Head and Wilson (1980) measured the radii and smaller half-widths of several sinuous rille source depressions, finding values between 1.1 and 2.4 km, entirely consistent with the present predicted pyroclast ranges, especially for the smaller values of n.

A final issue deserves attention for steady explosive eruptions. We have assumed in Figure 12 that all pyroclasts are small enough to stay locked to the gas phase during its expansion and thus to acquire most of the gas speed. We have no pyroclast samples from the Moon that are known to be collected very close a vent, and so we cannot rule out the possibility that coalescence of gas bubbles, perhaps encouraged by shearing forces at the edge of the conduit, may sometimes lead to magmas being erupted with a wider range of clast sizes, including clasts significantly coarser than the ~1 mm typical of the Apollo samples. In Figure 13 we simulate an eruption in which a large fraction, in this case 80%, of the clasts are so coarse that they acquire only 50% of the gas speed and fall out of the ejecta cloud near the vent. This implies that the effective gas mass fraction accelerating the remaining 20% consisting of small clasts is increased by a factor of (80/20 =) 4, causing their incremental speeds to increase by a factor of up to 2 and their ranges by a factor of up to 4. Figure 13 gives the ranges of the largest, R_{coarse}, and smallest, R_{fine}, clasts predicted by this simple model for the same values of n as Figure 12 and compares these ranges with the range R_{mono} of the monodisperse size distribution listed in Figure 12. Consider the case for n = 2000 ppm. Whereas Figure 12 would have predicted that pyroclasts would reach the surface fairly uniformly distributed over an area having a radius of 6.5 km, we now expect 80% of the erupted mass to fall within a radius of 1.6 km, covering an area $(5.1/1.6)^2$ = 10 times smaller and thus forming a layer (0.8×10 =) 8 times deeper than before. This layer could, of course, take the form of a cinder- or spatter-cone around the vent, detectable using Lunar Orbiter Laser Altimeter (LOLA) data (Head and Wilson, 2015). The remaining 20% of the pyroclasts are distributed out to a radius of 19.3 km, covering an area 14.3 times larger than before, and forming a layer (14.3/0.2 =) ~72 times thinner than before. Thus some small cinder or spatter cones might be expected to be surrounded by a 10-30 km radius aureole of thinly spread pyroclasts (Head and Wilson, 1994), no doubt at least partly disguised by regolith gardening, but possibly detectable using multispectral data (see Head and Wilson, 2015).

5.B Consequences of steady magma eruption (1): lava flows

Although some element of explosive activity is expected to have been present in all lunar basaltic eruptions, lava ponds formed by the accumulation of hot pyroclasts will have been common and will have drained down-slope to feed lava flows. The speed U_{f} of a lava flow of density ρ and thickness D_{f} will depend on whether the lava motion is laminar or turbulent. In laminar flow the speed is given by

$$U_{\mathrm{f}} = (\rho\, g\, D_{\mathrm{f}}^{2} \sin \alpha_{\mathrm{f}}) / (3\, \eta) \tag{42}$$

where η is the bulk viscosity and in turbulent flow by

$$U_{\mathrm{f}} = [(8\, g\, D_{\mathrm{f}} \sin \alpha_{\mathrm{f}}) / \lambda\,]^{1/2} \tag{43}$$

where a convenient formulation of the friction factor λ in terms of the Reynolds number Re_{f} is

$$\lambda = [0.79 \ln Re_{\mathrm{f}} - 1.64]^{-2} \tag{44}$$

and Re_{f} is defined by

$$Re_{\mathrm{f}} = (4\, U_{\mathrm{f}}\, D_{\mathrm{f}}\, \rho) / \eta \tag{45}$$

The dependence of Re_{f} on U_{f} and the presence of the ($\ln Re_{\mathrm{f}}$) term in the definition of λ mean that in turbulent flow U_{f} must be obtained from equation (43) by a recursive method from an initial estimate. Further, the decision as to whether the flow motion is laminar or turbulent must also be made retrospectively after evaluating U_{f} from both of equations (42) and (43); the relative dependencies of friction on Reynolds number in laminar and turbulent flow are such that taking the smaller value of U_f is always the correct solution (Wilson and Head, 1981). These operations are readily programmed as a spreadsheet.

Although the boundaries of many mare lava flows have been blurred by regolith formation after their emplacement, it is possible to measure the lengths and thicknesses of a few of the flows in Mare Imbrium (Schaber, 1973; Bugiolacchi and Guest, 2008; Campbell et al., 2009) and to estimate the topographic slopes of the surfaces on which they flowed (Rosenburg et al., 2011; Kreslavsky et al., 2013). We take as representative measured values a thickness D_f of 20 m, a width W_f of 20 km, and a slope α_f such that $\sin \alpha_f = 1 \times 10^{-3}$. The largest flow length X_f described by Schaber (1973) was 1200 km. With a plausible mare lava viscosity of 1 Pa s we find $U_f = 4.8$ m s^{-1}; the flow motion is fully turbulent with $Re_f = 1.15 \times 10^6$. A flow length of X_f = 1200 km would require an emplacement time, t_f, of ~69 hours and the volume flux feeding a W_{flow} = 20 km wide flow would be $F_f = (U_f\, W_{flow}\, D_f) = 1.9 \times 10^6$ m^3 s^{-1}. Increasing the viscosity by a factor of 10 to 10 Pa s decreases the implied speed to 3.75 m s^{-1}; the volume flux decreases to 1.5×10^6 m^3 s^{-1} and the emplacement time increases to ~89 hours. The most recent Lunar Reconnaissance Orbiter images show outcrops on steep slopes of what may be lava flows having thicknesses of 3-14 m (Ashley et al., 2012). These are comparable to flow thickness estimates of 10-20 m for outcrops in the walls of Rima Hadley (Howard and Head, 1972; Spudis et al., 1988). To illustrate the conditions that may have produced these deposits we show in Table 13 the flow speeds, Reynolds numbers, emplacement times and volume fluxes for 20 km wide flows with viscosity 1 Pa s emplaced on a slope of $\sin \alpha_f = 1 \times 10^{-3}$ with thicknesses between 1 and 30 m. The emplacement times assume a more conservative flow length of 600 km. All of these flows are fully turbulent.

We have explored the possibility that these large volume fluxes are overestimates. Thus it is possible that isostatic subsidence of the centers of mare basins has caused present-day slopes to be greater than those at the time of eruptive activity; also large-volume lava flows on Earth often exhibit inflation (Hon et al., 1994; Self et al., 1996, 1998; Thordarson and Self, 1998). To explore the consequence of such changes we reduce α_f by a factor of 3 in the example given above so that $\sin \alpha_f = 0.3 \times 10^{-3}$ and we decrease D_f by a factor of ~3 from 20 m to 7 m. The result is $U_f = 0.89$ m s^{-1}; the flow motion is still fully turbulent with $Re_f = 7.5 \times 10^3$ and the volume flux feeding a 20 km wide flow is 1.25×10^5 m^3 s^{-1}. It is thus very difficult to avoid the conclusion that mare lava flows having thicknesses of at least ~10 m were emplaced in eruptions having volume eruption rates of at least 10^4 and more commonly 10^5 to 10^6 m^3 s^{-1}. We note that this result, along with all of the cases shown in Table 13, is entirely consistent with our conclusions in Section 3 regarding the range of volume eruption rates expected for a magma rising from great depths in the Moon.

It is of interest to explore whether the sizes of mare lava flows were typically limited by the available volume of magma in the deep source zone or by the environmental conditions - specifically were they volume-limited or cooling-limited. By definition a volume-limited flow stops advancing when the source region can no longer supply magma to the vent. A cooling-limited flow, in contrast, stops advancing when cooling at the margins of the flow penetrates far enough into the interior. Pinkerton and Wilson (1994) showed that cooling limited flows stop when the Grätz number for the flow, G_z, defined by

$$G_z = [(16\, D_f^2)/(\kappa\, t_f)] \qquad (46)$$

decreases from an initially large value to a critical limiting value, G_{zc}, equal to ~300. Here κ = ~7 $\times 10^{-7}$ m^2 s^{-1} is the thermal diffusivity of silicate lava and t_f is the time after which lava motion ceases. Eliminating t_f by assuming a constant flow speed U_f, so that $t_f = (X_f / U_f)$, and writing U_f in terms of the volume flux $F_f = (U_f\ W_f\ D_f)$ we can re-order equation (U) in terms of F_f and measurable quantities as

$$F_f = (18.75\ \kappa\ X_f\ W_f) / D_f \qquad (47)$$

which with X_f = 1200 km, W_f = 20 km and D_f = 20 m yields $F_f = 1.6 \times 10^4$ m^3 s^{-1}. Thus only if the volume flux feeding this flow had been this small would the flow unit have stopped growing due to cooling. All volume fluxes larger than this value (which the cooling constraint on magma rise from the mantle suggests should be common) feeding a lava flow with this thickness and width would have been capable of generating a flow unit longer than 1200 km. The clear inference is that the typical lava flow units observed on the Moon, which are shorter than 1200 km, were limited in their extents by the volumes of magma available for eruption and not by cooling. Given that a flow 300 km long, 20 km wide and 20 m thick has a volume of ~120 km^3, this suggests that magma batches with volumes of a few hundred km^3 were commonly generated in and extracted from the mantle. This result, combined with the data in Table 1, suggests that the vertical extents of deep mantle partial melt zones were of order 20 to 25 km.

5.C Consequences of steady magma eruption (2): sinuous rilles

Hulme (1973) proposed that lunar sinuous rilles were the products of surface erosion by turbulent flowing lava and Carr (1974) estimated erosion rates that supported this idea. Subsequently Hulme and Fielder (1977), using Hulme's (1974) model of non-Newtonian lava rheology, suggested that the low viscosity of lunar lavas, combined with the shallow slopes of pre-existing lava surfaces within mare basins, meant that small differences in slope or effusion rate could determine whether lava flows were turbulent or laminar, and hence more or less likely to erode sinuous rilles. The efficiency of thermal erosion was discussed by Hulme (1982) and Fagents and Greeley (2001). Detailed models of thermal erosion using explicit thermal and mechanical properties of volcanic rocks known or inferred to be present on planetary surfaces were developed for eruptions on Earth (Williams et al., 1998, 1999), Io (Williams et al., 2000a), the Moon (Williams et al., 2000b) and Mars (Williams et al., 2005) and have been applied specifically to the formation of the major Rima Prinz rille on the Moon (Hurwitz et al., 2012). These newer models concur with the earlier work in requiring eruptions lasting typically a few months to explain the observed depths of the rille channels.

Our focus is on relating sinuous rille formation to lava eruption rates. We therefore use arguments developed by Head and Wilson (1980, 1981) and Wilson and Head (1980) that utilize the observed widths of sinuous rille channels, W_r, and the geometries of the source depressions that feed the rilles. In the case of a rille, let the volume flow rate of lava in the channel be F_r; the depth of flowing lava (which in general will not fill the channel) is D_r and the speed is U_r; then by definition

$$F_r = (U_r\ D_r\ W_r) \qquad (48)$$

The Reynolds number for the flow motion is

$$Re_r = (4\ U_r\ D_r\ \rho) / \eta \qquad (49)$$

and eliminating the product ($U_r\ D_r$) between the equations gives

$$F_r = (W_r\ Re_r\ \eta) / (4\ \rho) \qquad (50)$$

We postulate that for efficient thermal erosion the motion must be fully turbulent, so that Re_r must be at least ~2000; this implies that the minimum volume flow rate through the rille channel must be F_{min} given by

$$F_{min} = (500\ W_r\ \eta) / \rho \qquad (51)$$

Typically rille channels have widths in the range 1000-3000 m (*Schubert et al*., 1970; Hurwitz et al, 2012; 2013) and so using D_r = 2000 m, η = 1 Pa s and ρ = 2900 kg m^{-3} we find F_{min} = ~300 $m^3\ s^{-1}$. More stringent limits can be set by considering the turbulent lava ponds that feed the rilles. Wilson and Head (1980) showed that the equivalent of equation (51) for such a pond is

$$F_{min} = (2000\ R_p\ \eta) / \rho \qquad (52)$$

where R_p is the pond radius. Measurements of the source ponds for the rilles Prinz, Vera, Ivan, Beethoven and Handel (Head and Wilson, 1980) give an average of R_p = 1860 m, implying F_{min} = ~1200 $m^3\ s^{-1}$.

Note, however, that both of these values of F_{min} are very much lower limits because we expect Re_r to be much greater than the limiting value of ~2000. Thus by applying Hulme's (1973) model of lava flow in rille channels to the rilles numbered 2, 3, 4, 5, 6, 7, and 18 in the catalog of Oberbeck et al. (1971), Head and Wilson (1981) found Reynolds number of order 10^5. Lava flow depths were inferred to be ~10 m in channels measured to be 100-300 m deep, flow speeds were within a factor of two of 6 m s^{-1}, channel floor erosion rates were within 50% of 1 meter per day, and eruption durations were 100-300 days. The implied volume eruption rates were in the range 10^4 to 10^6 $m^3\ s^{-1}$. The durations of the eruptions were found by dividing the rille channel depths by the thermal erosion rates, and multiplying the durations by the volume rates implied erupted volumes of ~100 to nearly 2000 km^3. Volumes this large would imply mantle partial melt source regions of up to ~35 km in vertical extent.

5.D Lava flows and sinuous rilles compared

In Section 5.B we found that the smallest volume flux likely to be associated with an eruption feeding a typical mare lava flow was ~10^4 $m^3\ s^{-1}$, and that typical flows were fed by eruption rates in the range 10^5 to 10^6 $m^3\ s^{-1}$ producing flow volumes of order 100 km^3. The analyses described in Section 5.C show that sinuous rille-forming eruptions have similar minimum and maximum magma discharge rates and minimum magma volumes. However, the rille-forming eruptions commonly involved greater magma volumes erupted over much longer periods of time. The longer durations, rather than any subtle topographic slope effects dictating laminar or turbulent flow, appear to be the key to the ability of these flows to erode rille channels.

Additional distinctive properties include narrower precursor lava flows erupted from vents with much smaller horizontal extents than those feeding the more common sheet-like flows. The greatest length of a fissure feeding a sinuous rille appears to be the ~14 km long major part of the source depression of Rima Hadley (Head and Wilson, 1981), but few other such fissures exceed ~6 km in length (Oberbeck et al., 1971). Indeed, where the sources of the rilles are circular depressions, it is not the actual vent geometry that defines the lava flow width but rather the size of the overflowing lava pond feeding the flow, which in turn is dictated by the explosivity of the eruption. Given that there is currently no available three-dimensional model of dike propagation through a planetary crust that takes detailed account of the stress changes associated with the dike reaching the surface, we cannot provide any detailed explanation of these observations in terms of crustal stresses.

There may, however, be an explanation in terms of the long durations of the eruptions. In long-lasting fissure eruptions on Earth it is common for activity to focus progressively toward the center of the active fissure, so that eventually just a short fissure segment or a single localized vent is active. This trend is ascribed in part to preferential magma chilling at the thin dike tips (Bruce and Huppert, 1987, 1990; Carrigan et al., 1992; Head and Wilson, 1992a). However, if flow in a fissure continues for long enough, the walls of the feeder dike are heated to the point where magma that has already chilled against the wall is re-melted and removed, and eventually the initial dike width increases as the wall rocks are thermally eroded. This change from narrowing to widening with time occurs preferentially at the widest part of the initial fissure, i.e., at or near its center. Magma transport then becomes concentrated in this central, widening part of the dike (Bruce and Huppert, 1987) and the eventual blocking of the distal ends takes place quickly. Bruce and Huppert (1990) provide examples of the behavior of mafic magma in dikes propagating vertically for distances of 2 and 5 km under similar pressure gradients to those inferred here for dikes penetrating the lunar crust. We have extrapolated these data to the ~30 km thickness of the nearside lunar crust. In the likely lunar case, where there is no pre-heating of the crustal rocks above lunar ambient temperatures by immediately-preceding regional volcanic activity, we find that, for a dike width in excess of ~2.5 m, which is a much smaller dike width than any we have found, there will be a negligible initial period of magma chilling against the dike walls in the widest part of the dike, and widening of this region, with consequent capture of most of the volume flux, begins almost immediately. The rate of dike wall erosion will be comparable to that found by Head and Wilson (1981) for the floors of sinuous rille channels, ~15 $\mu m\ s^{-1}$. For a range of eruption conditions, Table 7 shows how the magma rise speed at depth, below the levels where volatile release is important, increases by ~50% as a 1600 m long fissure vent evolves into the circular shape needed to accommodate the same volume flux. The time required for the change ranges for 66 to 108 days. Given the likely 100-500 day durations of the rille-forming eruptions (Hulme, 1973; Head and Wilson, 1981), it is not surprising, therefore, that they appear to be fed by relatively short fissures.

5.E Non-mare volcanism

The presence of the morphologically and spectroscopically (Head and McCord, 1978; Glotch et al., 2011; Kusuma et al., 2012; Ivanov et al., 2015) distinctive Gruithuisen and Mairan domes in N.E. Oceanus Procellarum and the domes between the craters Belkovich and Compton (Jolliff et al., 2011; Chauhan et al., 2015) implies the localized eruption of unusually viscous, probably rhyolitic, magma (Wilson and Head, 2003b), a very rare occurrence on the Moon. Wilson and Head (2003b) used the morphologies of the Gruithuisen and Mairan domes to infer the yield strengths and plastic viscosities of the magmas forming them assuming that they behaved as Bingham plastics and to deduce the magma volume eruption rates, ~tens of $m^3\ s^{-1}$, and durations, ~10-50 years. We have repeated the analysis, using the improved crustal density estimates from GRAIL, and relaxing some of the assumptions about the feeder dike geometry. Table 8 shows the original rheological parameters and the new estimates of dike width and magma rise speed. Also shown are the minimum magma rise speeds needed to offset excessive cooling during magma ascent from the base of the crust found using equation (25). In all cases the eruptions are thermally viable.

The origin of this highly silicic magma is uncertain; options include basal melting of the lunar crust by large volumes of under-plating basalt or differentiation during cooling of large-volume basaltic magma bodies, again most likely located at the crust-mantle boundary density trap. In section 3.F it was shown that substantial volumes, ~5000 km^3, of basaltic magma could be emplaced as intrusions at the base of the crust under suitable circumstances. Such intrusions are easiest to understand late in lunar history when horizontal compressive stresses in the lithosphere make it likely that the least principle stress will have been vertical. However, the silicic domes are inferred to have been formed ~ 3.8 Ga ago, and so crustal thinning and stress modification due to basin-forming impacts in the early period before warming of the lunar interior generated extensional stresses in the lithosphere are the more likely source of the required stress conditions. The volumes of the larger domes are ~300-500 km^3, (Wilson and Head, 2003b), an order of magnitude smaller than a possible 5000 km^3 basalt intrusion, and so both partial melting of overlying crust and fractional crystallization of sill magma are viable sources of the silicic melt on thermal grounds.

If fractional crystallization were the source mechanism, concentration of volatiles into residual melt could have enriched the melt in water, perhaps by a factor of ~10 over the ~1000 ppm found in some lunar samples by Hauri et al. (2011). The treatment of section 5.A shows that the eruption of silicic melt with ~10,000 ppm, i.e. ~1 mass %, of water could have ejected pyroclastic material in explosive phases of the eruptions to distances of ~30 km.

5.F Late-stage lunar volcanism

The thermal models of Solomon and Head (1982), Spohn et al. (2001) and Ziethe et al. (2009) all suggest that the zone within which partial melting can occur in the Moon's mantle must migrate deeper into the mantle with time and shrink in its vertical extent. The models differ in their predictions of when melting should have ceased, mainly as a result of differing assumptions about the solidification of the initial magma ocean. It is inevitable that the progressive decay of radioactive heat sources must cause the rate of melt generation to decrease with time. The rate of percolation of melt within partial melt zones is linked to the melt volume fraction and melt viscosity. If melting is occurring at all, the melt viscosity will not change significantly, but the percolation speed will decrease because the melt volume fraction will decrease as the melt production rate decreases. Thus it will take longer for a given dike to grow upward from a diapiric partial melt zone, and the vertical extent, and hence volume, of the dike that eventually detaches from the melt zone will be less as a function of time because the vertical extent of the melt zone decreases.

These trends suggest that late in lunar volcanic history both the volumes of batches of melt arriving at the crust-mantle boundary and the frequency with which they arrived will have been less than in earlier times. Given that the horizontal compressive stress in the lithosphere will have been increasing with time in late lunar history, it is difficult to anticipate with confidence how these changes will have influenced the ability of magma to penetrate the crust. However, the likely expectation is that large volumes of basaltic melt must have accumulated in sills at the base of the crust before conditions allowed dikes to penetrate the crust as a result of excess pressures in the sills. When eruptions finally occurred, they would have involved larger volumes of magma than in earlier times, with the intervals between eruptions being much greater than before. The final stages of such activity might have involved dikes that penetrated part way through the crust but did not erupt magma. Volatiles in the accumulation zones at the tops of these dikes might, however, have made their way to the surface. It is tempting to speculate that morphologically (Garry et al., 2012) and spectroscopically (Braden et al., 2014) enigmatic features like Ina, which may have formed relatively recently (Schultz et al., 2006), may be linked to this very late stage activity (Figure 8) (Head and Wilson, 2015).

6. Summary and Conclusions

6.A General Setting for Mare Volcanism

Secondary planetary crusts are those derived from partial melting of the mantle, and the consequent collection, ascent and eruption of the resulting magmas. The geologic record of these plutonic and volcanic products represents the history of planetary crustal and thermal evolution, and reflects the dominant mode of planetary lithospheric configuration and heat transfer. Lunar mare volcanism is the primary manifestation of secondary crustal formation on the Moon and provides key insights into lunar thermal evolution. We used new data on the density and thickness of the crust, the petrologic properties and the geologic record of mare basalt volcanism to assess: 1) the range of magma source depths, 2) modes of magma generation, ascent and eruption, 3) the volumes and volume fluxes of magma, 4) the partitioning into intrusive and extrusive deposits, 5) the role of primary lunar crustal formation and configuration in modulating intrusion and eruption style, 6) the role of thermal evolution in controlling the source depths and eruption frequencies, styles and fluxes, 7) the predicted relationship of these properties to observed landforms and deposits, 8) the relationship of magmatic volatile production to predicted explosive eruption style, and landform/deposit characteristics, 9) the causes of patterns of mare basalt areal distribution (e.g., nearside/farside asymmetry) and styles (e.g., long lava flows, sinuous rilles), and 10) the likelihood of recent and current mare basalt plutonic and volcanic activity on the Moon. We use this basic setting and the following considerations to assess the lunar geological record for consistency with these predictions (Head and Wilson, 2015).

6.B Basic Configuration of Lunar Mare Basalt Genesis and Eruption

We find that the basic configuration of lunar mare magmatism is fundamentally controlled by 1) the formation of the low-density anorthositic primary crust, 2) the consequences of its formation and aftermath for the nature of the mantle and the distribution of heat sources, and 3) the resulting one-plate-planet tectonic structure characterized by conduction-dominated lithospheric heat transfer, and a lithosphere that progressively thickened with time. The formation of large multi-ringed basins, some of which date to the early lunar mare volcanism era, regionally thinned the crust and introduced short-term perturbations in the thickness of the lithosphere. These basic factors provided a density barrier (the low-density anorthositic crust) fixed early in lunar history, and a mechanical barrier (the base of the lithosphere) that progressively deepened with time. The thermal evolution of the Moon, characterized by the evolving ratio of accretional heat and radiogenic heat sources, and continual lithospheric heat loss to space, resulted in a change in the net state of stress in the lithosphere from extensional to contractional in early-middle lunar history. This change was a key factor in the mare basalt surface volcanic flux and eruption style, progressively inhibiting the ascent and eruption of magma, and changing eruption styles toward extremely voluminous individual eruptions, often with accompanying sinuous rilles.

6.C Modeling the Generation, Ascent and Eruption of Magma

In modeling the generation, ascent and eruption of magma, we used new estimates of the vertical extent of partial melting (up to ~150 km) in lunar mantle diapirs and of the depths of density/rheological traps, and include excess magma source pressures as well as magma buoyancy. We find that excess pressures in shallower magma reservoirs and buoyancy traps are about an order of magnitude smaller than those in deep partial melt zones. Rates of melt removal from the mantle source regions should be much lower on the Moon than Earth; lunar mantle convection rates are lower by about an order of magnitude due to lunar gravity, so reservoir overpressurization and melt extraction should be at much lower rates, implying that only a very small amount of magma can be extracted rapidly from a deep lunar mantle source, and, consequently, that large mantle source regions, of the order 10^5 to 10^6 km^3, are required.

6.D Lunar Mare Basalt Magma Transport in Dikes

Transport of magma toward the surface is by brittle fracture in rocks overlying the melt source and the consequent propagation of a dike. A dike containing magma everywhere buoyant relative to its host rock would inevitably reach the surface and erupt until the magma supply is exhausted. If magma is not positively buoyant at all depths, excess pressure in the source region can assist in the vertical growth of a dike. Dikes can cease to grow due to: 1) lack of sufficient buoyancy/overpressure, 2) excessive cooling, 3) lack of sufficient dike tip stress intensity, or 4) exhaustion of magma supply in the source region. Unlike Earth, the great depth of lunar magma source regions generally limits the role of volatiles in assisting magma ascent.

Mare basalt magma dikes intruding into the anorthositic crust should be everywhere negatively buoyant, and if the horizontal stress in the lithosphere is sufficiently compressive are predicted to extend laterally to underplate and create secondary reservoirs at the crust-mantle boundary. If the positive excess pressure of the portion of the dike in the mantle is great enough, however, dikes containing magma that is negatively buoyant relative to the crust can still penetrate into the crust and reach the surface to erupt. In the first quarter of lunar history, with abundant mantle heating and mild global expansion inducing an extensional state of stress in the lithosphere, such dike intrusions through the crust and consequent eruptions should have been common. In later lunar history, when global cooling thickened the lithosphere and induced lithospheric compressional stresses, eruptions should have been inhibited and crustal underplating is predicted to be favored.

With sufficiently deep melt source regions and slow growth, dikes can disconnect from their source regions and rise as discrete blade-shaped diapirs of fixed volume. We find that from source depths greater than about 500 km, it is implausible that continuous dike pathways can exist between the deep mantle source regions and the surface. Volumes of magma in these pinched-off dikes are of the order of a few thousand km^3 (a fraction of which will reach the surface) and dike widths are so large that magma motion is predicted to be turbulent and not controlled by viscosity or influenced by heat loss to the host rocks; typical rates of ascent are 30 m s^{-1}, requiring only ~4.6 hours to reach the surface.

For isolated dikes encountering the basal crustal density trap, what are the conditions by which they reach the surface? The tops of typical intrusions (up to ~43 km) in thicker farside crust is much deeper than those in the thinner nearside crust (up to ~13 km), and the range of values for the nearside indicates that nearside eruptions should be heavily favored over farside eruptions. The predominance of lunar nearside eruptions (thinner crust) also implies that the vertical extents of mantle diapiric source regions that could produce eruptions lie in the range of 17-36 km. When dike tips reach the surface, the volume of magma erupted is a function of the magnitude of the horizontal extensional stresses and can range from a small percentage of, to the vast majority of, the total dike volume (i.e., tens of km^3 to more than 1600 km^3). The implied eruption volume fluxes are huge, ranging from 10^5 to 10^6 m^3 s^{-1}.

Dikes that remain connected to their melt source zones are generally required to be sourced from the shallower mantle, and would be favored in the earlier period of mare history under several global thermal evolution models, with shallow partial melt zones being limited in vertical extent relative to their deeper counterparts. We show that a simple explanation for the paucity of eruptions on the lunar farside is that the vertical extent of melting in relatively shallow mantle melt zones was less than ~45 km.

Dikes from deep mantle source regions could extrude to the surface or intrude to any depth in the lunar crust and are predicted to have widths of 35-50 m, with rise speeds during emplacement indicating turbulent flow behavior. Dikes from shallow mantle sources are more restricted in the range of the depth to the top of the dike when eruptions do not occur. A 50 km deep mantle source (ponded near the base of the crust) is predicted to produce ~50 m wide dikes, with the tops of dike intrusion within ~1 km of the surface.

6.E Range of Behavior of Dikes Intruding the Crust

Dikes intruding into the lunar crust can have several fates and consequences (Figure 8): 1) those intruded to more than 10-20 km below the surface will solidify; 2) those reaching shallower depths will undergo gas exsolution and gas accumulation and potentially vent gasses to the surface; 3) those reaching the upper several kilometers of the crust and stalling can produce near-surface stress fields and graben; 4) those reaching near-surface very low density regions (brecciated crater lenses) can intrude laterally and produce sills and floor-fractured craters; 5) those that just reach the surface can extrude small amounts of lava and produce small shield volcanoes and pyroclastic venting; and 6) those that reach and have the potential to overshoot the surface can produce high-flux and high-volume effusive volcanic eruptions, creating long lava flows and sinuous rilles.

6.F Explosive Activity Accompanying Mare Basalt Eruptions

Dikes that breach the surface and erupt should all be accompanied by some level of explosive activity due to the presence of small amounts of mainly CO from the smelting reaction that occurs in the upper few kilometers, and the venting of this gas into the vacuum. There are three phases of gas production during dike ascent and eruption, each with consequences for pyroclastic activity: 1) gas is generated in the low-pressure dike-tip during dike propagation from the source toward the surface, and accumulates into gas-filled cavities with vertical extents of tens to hundreds of meters, overlying a magmatic foam layer of up to 10 kilometers vertical extent above the rising magma); 2) there is a very short period (tens of seconds) after the dike tip breaks the surface during which the gas in the pure gas cavity vents to the surface at very high velocity with few magmatic particles but some entrained regolith/wall rock fragments; this is a lunar equivalent of a terrestrial ultraplinian eruption phase with a pyroclast dispersal maximum approaching 2000 km); 3) the pressure distribution in the dike now evolves to maximize the magma discharge rate; an expansion wave initially propagates into the underlying foam, disrupting it into gas and pyroclasts which are dispersed to a maximum range of 6-20 km from the vent; complete stability and steady eruption conditions are reached after the passage of pressure waves down and back up the dike, taking ~1 hour. Unusually wide dikes (250-500 m) that stalled near the surface without initially erupting could experience further gas accumulation at the top of the magma column due to convection in the underlying magma, eventually causing a gas-rich eruption.

Dikes producing steady effusive eruptions to the surface should be accompanied by steady pyroclastic activity. Volatiles form gas bubbles in the rising melt and these undergo expansion, increasing the speed of the rising magma, and ultimately disrupting it into a free gas phase entraining pyroclasts. On Earth, two types of conditions in the conduit can evolve at this point: choked flow (where the vent pressure is greater than atmospheric) and supersonic flow (where the vent pressure is equal to the atmospheric pressure). All lunar explosive eruption are predicted to be choked. The ensuing dispersal of pyroclasts into the vacuum above the vent is controlled by the exit speed from the vent and the size distribution of the liquid droplets into which the magma is disrupted. Liquid droplets similar in size to the pyroclastic beads collected on the Moon (100-1000 micrometers) will stay locked to the expanding and accelerating gas cloud sufficiently long to be accelerated to significant speeds, ensuring widespread dispersal away from the vent up to about 10 km. Larger particles that are produced will be accelerated much less efficiently and will collect nearer the vent, with the largest ones potentially forming cinder or spatter cones.

Despite the very rapid acceleration of magma droplets by the gas cloud expanding out into the surface vacuum, combinations of factors (limited range, small pyroclast size and large volume flux) can lead to parts of the fire fountain being optically dense, with some specific consequences for deposits and landforms. A high optical density means that particles cannot radiate heat efficiently, due to shielding by other particles, and they fall to the ground at magmatic temperatures and coalesce into a lava pond, which typically feeds a lava flow. Large volume flux eruptions are typically predicted to be surrounded by such a lava pond, in which the flow is turbulent, and to have formed the source depressions surrounding many sinuous rilles by thermal erosion. For lower volume fluxes and larger clast sizes (larger than the ~1 mm glass beads collected by the Apollo astronauts), acceleration by the expanding gas cloud is much less efficient, and pyroclasts will fall out of the cloud within a range typically less than about 2 km from the vent to produce cinder and spatter cones. When the large particles fall out of the cloud, the effective gas mass fraction is increased, and this can cause increased acceleration of the finer droplets, propelling them to several tens of km.

6.G Effusive Activity Accompanying Mare Basalt Eruptions

The typical fate of dikes reaching the close vicinity of the surface is to penetrate to the surface and form effusive eruptions. Dikes with magmatic pressures just sufficient to penetrate the surface will form low effusion rate, low-volume eruptions, and produce small shield volcanoes situated on or along the top of the dike. The spectrum of overpressurization values required to propagate a dike to the vicinity of the lunar surface means that a portion of the dike population will be characterized by sufficiently high values to "overshoot" the surface; these dikes will be characterized by very high effusion rates and the magma they erupt will drain downslope from the vent to feed extensive lava flows. The velocity of erupting lava flows will control whether the motion in the flow is laminar or turbulent. Lava flow thicknesses of a few to

~30 m have been reported, and for typical slopes and flow widths, and lengths of ~600 km, all flows are fully turbulent. Discrete lava flows with thicknesses in excess of ~10 m were characterized by eruptions having volume eruption rates of at least 10^4, and more likely, 10^5 to 10^6 m^3 s^{-1}, comparable to our predictions for magma rising from significant depths in the lunar interior.

Lava flows generally have one of two fates: the flows can stop due to sufficient cooling of the lavas so that the flow front can no longer advance (cooling-limited flows; reaching a limiting Gratz number of ~300), or alternatively, the source region no longer supplies magma to the vent, and the advancing flow stops due to lack of new magma (volume-limited flows). Analysis of the fluxes and cooling behavior of lunar lava flows strongly implies that typical lava flows shorter than ~1200 km would be supply-limited, not cooling-limited. This, in turn, suggests that magma batches with volumes of a few hundred km^3 were commonly generated in the mantle and extracted through dike and lava flow emplacement.

How are sinuous rilles, interpreted to be caused by thermal erosion, related to lava flows? Flow in sinuous rilles, like that in long lava flows, is shown to be fully turbulent. Analysis of sinuous rille morphologies suggests that typical sinuous rille eruptions were characterized by volume eruption rates of 10^4 to 10^6 m^3 s^{-1}, eruptions volumes of 100-2000 km^3, eruption durations of 100-300 days, and thermal erosion rates of ~1 meter per day. Thus, eruptions producing typical lunar lava flows (volume eruption rates >10^4 to 10^6 m^3 s^{-1}, typically 10^5 to 10^6 m^3 s^{-1}; eruptions volumes of ~100 km^3) overlap on the lower end of, and have similar characteristics to, those producing sinuous rilles. The major difference between lava flow-producing eruptions and those producing sinuous rilles is the longer durations of the eruptions and the generally greater volumes of lava erupted, both factors enhancing the role of thermal erosion in creating the rille channels. A further distinction between lunar lava flows and sinuous rilles is the nature of the typical source regions. Lava flows often emerge from linear fissures, but sinuous rille sources are commonly circular or slightly elongate depressions less than a few kilometers in diameter. These sinuous rille vent shapes strongly suggest that due to the high magma flux and duration of sinuous rille eruptions, thermal erosion of the widest parts of fissure vent walls together with cooling of magma in the thinnest parts of the underlying dikes acts to centralize the effusion to a pipe-like conduit; the result is the capture of most of the mass flux in the central pipe, more rapid cooling of the rest of the dike walls, and an increase of magma rise speeds by ~50%. Thus, sinuous rilles appear to differ from lava flows due to thermal erosion of both the vent region and the substrate below the vent.

6.H Mare Basalt Lunar Resurfacing

The fate of erupted lavas fed by both flows and sinuous rilles depends on local and regional slopes and the nature of the range of topographic features existing prior to eruptions. Mare lava flows in early lunar history are predicted to be focused in the interiors of impact craters and basins. Later lava flows will spread out over larger areas, or down regional slopes related to loading and flexure by the earlier lava emplacement and basin filling. Repeated dike intrusions over the course of mare basalt magmatism will also increase the density of the crust, somewhat reducing the negative buoyancy of the magmas. The trend in global cooling will increase compressive stress in the lithosphere with time, a trend reinforced by the progressive intrusion of dikes in the crust.

In summary, in this contribution we make specific predictions about the nature and distribution of the spectrum of lunar mare volcanic landforms and deposits. These predictions and guidelines are analyzed and tested using the comprehensive array of data obtained by the Lunar Reconnaissance Orbiter (LRO) and other missions (*Head and Wilson*, 2015).

Acknowledgments: We gratefully acknowledge financial support from the NASA Solar System Exploration Research Virtual Institute (SSERVI) grant for Evolution and Environment of Exploration Destinations under cooperative agreement number NNA14AB01A at Brown University, the NASA Lunar Reconnaissance Orbiter (LRO) Mission, Lunar Orbiter Laser Altimeter (LOLA) Experiment Team (Grants NNX11AK29G and NNX13AO77G), and the NASA Gravity Recovery and Interior Laboratory (GRAIL) Mission Guest Scientist Program (Grant NNX12AL07G). We thank *Icarus* Guest Editor Lisa Gaddis and two reviewers, Peter Mouginis-Mark and an anonymous reviewer, for helpful comments that improved the manuscript. We thank Anne Côté for help in drafting and manuscript preparation.

References

Andrews-Hanna, J.C. and 18 others, 2013. Ancient igneous intrusions and early expansion of the Moon revealed by GRAIL gravity gradiometry. Science 339, 675-678, doi: 10.1126/science.1231753.

Ashley, J.W., Robinson, M.S., Boyd, A.K., Wagner, R.V., Speyerer, E.J., Hawke, B.R., Hiesinger, H., van der Bogert, C.H., Burns, K., Sato H., 2012. LROC Imaging of Thin Layering in Lunar Mare Deposits. Lunar Planet. Sci. Conf. 42, abstract 2115.

Bai, L.-P., Baker, D.R., Rivers, M., 2008. Experimental study of bubble growth in Stromboli basalt melts at 1 atm. Earth Planet. Sci. Lett. 267, 533–547, doi: 10.1016/j.epsl.2007.11.063.

Baldwin, R.B., 1963. *The Measure of the Moon*, Univ. of Chicago Press, Chicago, Ill., 488 pp.

Beck, A.R., Morgan, Z.T., Liang, Y., Hess, P.C., 2006. Dunite channels as viable pathways for mare basalt transport in the deep lunar mantle. Geophys. Res. Lett. 33, L01202, doi: 10.1029/2005GL024008.

Bieniawski, Z.T., 1984. *Rock Mechanics Design in Mining and Tunneling*. Balkema, Boston, 272 pp.

Blake, S., 1981. Volcanism and the dynamics of open magma chambers. Nature 289, 783-785.

Bouilhol, P., Connolly, J.A.D., Burg, J.-P., 2011. Geological evidence and modeling of melt migration by porosity waves in the sub-arc mantle of Kohistan (Pakistan). Geology 39 (12), 1091-1094, doi: 10.1130/G32219.1.

Bugiolacchi, R., Guest, J.E., 2008. Compositional and temporal investigation of exposed lunar basalts in the Mare Imbrium region. Icarus 197, 1–18.

Braden, S.E., Stopar, J.D., Robinson, M.S., Lawrence, S J., van der Bogert, C.H., Hiesinger, H., 2014. Evidence for basaltic volcanism on the Moon within the past 100 million years. Nature Geosci. 7, 787-791.

Brown, M., 2004. The mechanisms of melt extraction from lower continental crust of orogens: Is it a self-organized critical phenomenon? Transactions of the Royal Society of Edinburgh, Earth Sciences 95, 35–48, doi: 10.1017/S0263593300000900

Bruce, P.M., Huppert, H.E., 1987. Thermal control of basaltic fissure eruptions. Nature 342, 665-667.

BVSP (Basaltic Volcanism Study Project), 1981. *Basaltic Volcanism on the Terrestrial Planets*, Pergamon Press.

Campbell, B. A., B. R. Hawke, L. M. Carter, R. R. Ghent, and D. B. Campbell, 2009. Rugged lava flows on the Moon revealed by Earth-based radar. Geophys. Res. Letters 36, L22201, doi:10.1029/2009GL041087.

Carrigan, C.R., Schubert, G., Eichelberger, J.C., 1992. Thermal and dynamical regimes of single and two-phase magmatic flow in dikes. J. Geophys. Res. 97, 17,377- 17,392.

Carslaw, H. S., Jaeger, J.C., 1947. *Conduction of Heat in Solids*. Clarendon Press, Oxford, 386 pp.

Cataldo, E., Wilson, L., Lane, S., Gilbert, J., 2002. A model for large-scale volcanic plumes on Io: Implications for eruption rates and interactions between magmas and near-surface volatiles. J. Geophys. Res. 107 (E11), 5109, 10.1029/2001JE001513.

Chauhan, M., Bhattacharya, S., Saran, S., Chauhan, P., Dagar, A., 2015. Compton-Belkovich volcanic complex (CBVC): An ash flow caldera on the Moon. Icarus 253, 115-129.

Chen, Z., Jin, Z.-H., Johnson, S.E., 2007. A perturbation solution for dike propagation in an elastic medium with graded density. Geophys. J. Int. 169, 348–356.

Chen, Z., Jin, Z.-H., Johnson, S.E., 2011. Transient dike propagation and arrest near the level of neutral buoyancy. J. Volcanol. Geotherm. Res. 203, 81-86.

Coombs C.R., Hawke, B.R., Peterson, C.A., Zisk, S.H., 1990. Regional pyroclastic deposits in the north-central portion of the lunar nearside. Lunar Planet Sci Conf. 41, 228-229.

Crawford, G.D., Stevenson, D.J., 1988. Gas-driven water volcanism and the resurfacing of Europa. Icarus 73 (1), 66-79.

Crowley, J.W., O'Connell, R.J., 2012. An analytical model of convection in a system with layered viscosity and plates. Geophys. J. Int. 188, 61-78, doi: 10.1111/j.1365-246X.2011.05254.x

Dahm, T., 2000a. Numerical simulations of the propagation and arrest of fluid-filled fractures in the Earth. Geophys. J. Int. 141, 623–638.

Dahm, T., 2000b. On the shape and velocity of fluid-filled fractures in the Earth. Geophys. J. Int. 142, 181–192.

Delano, J.W., 1990. Pristine mare glasses and mare basalts: Evidence for a general dichotomy of source regions. In: Workshop on Lunar Volcanic Glasses: Scientific and Resource Potential, LPI Tech Rpt 90-02, Lunar an Planetary Institute, 30-31.

Detournay, E., Mastin, L.G., Pearson, J.R.A., Rubin, A.M., Spera, F.J., 2003. Final Report of the Igneous Consequences Peer Review Panel, With Appendices. ML20031014.0097 and ML20030730.0163, Las Vegas, Nevada: Bechtel SAIC Company, LLC.

Dixon, J.E., 1997. Degassing of alkali basalts. American Mineralogist 82, 368-378.

Dobran, F., Neri, A., Macedonio, G., 1993. Numerical simulations of collapsing volcanic columns. J. Geophys. Res. 98, 4231-4259.

Fagents, S.A., Greeley, R., 2001. Factors influencing lava-substrate heat transfer and implications for thermomechanical erosion. Bull. Volcanol. 62, 519– 532.

Farnetani, C.G., Hofmann, A.W., 2010. Dynamics and internal structure of the Hawaiian plume. Earth Planet. Sci. Lett. 295 (1-2), 231-240.

Fielder, G., 1961. *Structure of the Moon's Surface*, Pergamon, London.

Fogel, R., Rutherford, M., 1995. Magmatic volatiles in primitive lunar glasses, I, FTIR and EPMA analyses of Apollo 15 green and yellow glasses and revision of the volatile-assisted fire-fountain theory. Geochim. Cosmochim. Acta 59, 201-215.

Gaddis L.R., Pieters, C.M., Hawke, B.R., 1985. Remote sensing of lunar pyroclastic mantling deposits. Icarus 61, 461-489.

Gaddis, L.R., Staid, M.I., Tyburczy, J.A., Hawke, B.R., Petro, N.E., 2003. Compositional analyses of lunar pyroclastic deposits. Icarus 161, 262-280.

Garry, W.B., Robinson, M.S., Zimbelman, J.R., Bleacher, J.E., Hawke, B.R., Crumpler, L.S., Braden, S.E., Sato, H., 2012. The origin of Ina: Evidence for inflated lava flows on the Moon. J. Geophys. Res. 117, E00H31, doi: 10.1029/2011JE003981.

Giberti, G., Wilson, L., 1990. The influence of geometry on the ascent of magma in open fissures, Bulletin of Volcanology 52, 515-521.

Glotch, T.D., Hagerty, J.J., Lucey, P.G., Hawke, B.R., Giguere, T.A., Arnold, J.A., Williams, J.P., Jolliff, B.L., Paige, D.A., 2011. The Mairan domes: Silicic volcanic constructs on the Moon. Geophys. Res. Lett. 38, L21204, doi: 10.1029/2011GL049548.

Guest, J.E., Murray, J.B., 1976. Volcanic features of the nearside equatorial lunar maria. J. Geol. Soc. Lond. 132, 251-258.

Gustafson, J.O., Bell III, J.F., Gaddis, L.R., Hawke, B.R., Giguere, T.A., 2012. Characterization of previously unidentified lunar pyroclastic deposits using Lunar Reconnaissance Orbiter

Camera data. J. Geophys. Res. 117, E00H25, doi: 10.1029/2011JE003893.

Hauri, E.H., Weinreich, T., Saal, A.E., Rutherford, M.C., Van Orman, J.A., 2011. High pre-eruptive water contents preserved in lunar melt inclusions. Science 333, 213–215.

Hauri, E.H., Saal, A.E., Rutherford, M.J., Van Orman, J.A., 2015. Water in the Moon's interior: Truth and consequences. Earth Planet. Sci. Lett. 409, 252-264.

Havlin, C., Parmentier, E.M., Hirth, G., 2013. Dike propagation driven by melt accumulation at the lithosphere–asthenosphere boundary. Earth Planet. Sci. Lett. 376, 20-28.

Hawke, B.R., Coombs, C.R., Gaddis, L.R., Lucey, P.G., Owensby, P.D., 1989. Remote sensing and geologic studies of localized dark mantle deposits on the Moon. Proc. Lunar Planet. Sci. Conf. 19, 255-268.

Head, J.W., 1974. Lunar dark-mantle deposits: Possible clues to the distribution of early mare deposits. Proc. Lunar Sci. Conf. 5, 207-222.

Head, J.W., 1976. Lunar volcanism in space and time. Reviews of Geophysics and Space Physics 14, 265-300.

Head, J.W., McCord, T.B., 1978. Imbrian-age highland volcanism on Moon - Gruithuisen and Mairan domes. Science 199, 1433-1436.

Head, J.W., Wilson, L., 1980. The formation of eroded depressions around the sources of lunar sinuous rilles: Observations. Lunar Planet. Sci. 11, 426-428.

Head, J.W., Wilson, L., 1981. Lunar sinuous rille formation by thermal erosion: Eruption conditions, rates and durations. Lunar Planet. Sci. 12, 427-429.

Head, J.W., Wilson, L., 1991. Absence of large shield volcanoes and calderas on the Moon: Consequences of magma transport phenomena? Geophys. Res. Lett. 18, 2121-2124.

Head, J.W., Wilson, L., 1992a. Lunar mare volcanism: Stratigraphy, eruption conditions, and the evolution of secondary crusts. Geochim. Cosmochim. Acta 56, 2155-2175.

Head, J. W., Wilson, L. 1992b. Magma reservoirs and neutral buoyancy zones on Venus: Implications for the formation and evolution of volcanic landforms. J. Geophys. Res. 97 (E3), 3877-3903.

Head, J.W., Wilson, L., 1994. Lunar graben formation due to near-surface deformation accompanying dike emplacement. Planetary Space Sci. 41, 719-727.

Head, J.W., Wilson, L., 2015. Generation, ascent and eruption of magma on the Moon: New insights into source depths, magma supply, intrusions and effusive/explosive eruptions (Part 2: Observations). Submitted to *Icarus* Special issue on Lunar Reconnaissance Orbiter.

Head, J.W., Wilson, L., Weitz, C.M., 2002. Dark ring in southwestern Orientale Basin: Origin as a single pyroclastic eruption. J. Geophys. Res. 107 (E1), doi: 10.1029/2000JE001438.

Hess, P.C., 1991. Diapirism and the origin of high TiO_2 mare glasses. Geophys. Res. Lett. 18 (11), 2069-2072.

Hess, P.C., 2000. On the source regions for mare picrite glasses . J. Geophys. Res. 105 (E2), 4347-4360.

Hess, P.C., Parmentier, E.M., 1995. A model for the thermal and chemical evolution of the Moon's interior: Implications for the onset of mare volcanism. Earth Planet. Sci. Lett. 134, 501-514, doi: 10.1016/0012-821X(95)00138-3.

Hess, P.C., Parmentier, E.M., 2001. Thermal evolution of a thicker KREEP liquid layer. J. Geophys. Res. 106 (E11), 28,023–28,032, doi: 10.1029/2000JE001416.

Hiesinger, H., Jaumann, R., Neukum, G., Head, J.W., 2000. Ages of mare basalts on the lunar nearside. J. Geophys. Res. 105, 29,259-29,275.

Hiesinger, H., Head, J.W., Wolf, U., Jaumann, R., Neukum, G., 2003. Ages and stratigraphy of mare basalts in Oceanus Procellarum, Mare Nubium, Mare Cognitum, and Mare Insularum. J. Geophys. Res. 108, doi: 10.1029/2002JE001985.

Hiesinger, H., Head, J.W., Wolf, U., Jaumann, R., Neukum, G., 2011. Ages and stratigraphy of lunar mare basalts: A synthesis. In: *Recent Advances and Current Research Issues in Lunar Stratigraphy*, edited by W. A. Ambrose and D. A. Williams, pp. 1-51, Geological Society of America Special Paper 477.

Hikida, H., Wieczorek, M.A., 2007. Crustal thickness of the Moon: New constraints from gravity inversions using polyhedral shape models. Icarus 192, 150-166, doi: 10.1016/j.icarus.2007.06.015.

Hon, K., Kauahikaua, J., Delinger, R., Mackay, K., 1994. Emplacement and inflation of pahoehoe sheet flows: Observations and measurements of active lava flows on Kilauea Volcano, Hawaii. Geol. Soc. Am. Bull. 106, 351–370.

Howard, K.A., Head, J.W., 1972. Regional geology of Hadley Rille, Apollo 15 Preliminary Science Report, NASA, Special Publication, NASA SP-289, pp. 25-53-25-58.

Hulme, G., 1973. Turbulent Lava Flow and the Formation of Lunar Sinuous Rilles. Modern Geology 4, 107-117.

Hulme, G., 1974. The interpretation of lava flow morphology. Journal of the Royal Astronomical Society 39, 361-383.

Hulme, G., Fielder, G., 1977. Effusion rates and rheology of lunar lavas. Phil. Trans. Roy. Soc. London A285, 227-234.

Hulme, G., 1982. A review of lava flow processes related to the formation of lunar sinuous rilles. Surveys in Geophysics 5 (3), 245-279.

Hurwitz, D.M., Head III, J.W., Wilson, L., Hiesinger, H., 2012. Origin of lunar sinuous rilles: Modeling effects of gravity, surface slope, and lava composition on erosion rates during the formation of Rima Prinz. J. Geophys. Res. 117, E00H14, doi: 10.1029/2011JE004000.

Hurwitz, D.M., Head III, J.W., Hiesinger, H., 2013. Lunar sinuous rilles: Distribution, characteristics, and implications for their origin. Planet. Space Sci. 79-80, 1-38, doi: 10.1016/j.pss.2012.10.019.

Ivanov, M.A., Head, J.W., Bystrov, A., 2015. The lunar Gruithuisen silicic extrusive domes: Topographic configuration, morphology, ages, and internal structure. Submitted to the Icarus special issue on Lunar Reconnaissance Orbiter.

Jaupart, C., Vergniolle, S., 1989. The generation and collapse of a foam layer at the roof of a basaltic magma chamber. J. Fluid Mech. 203, 347-380.

Jolliff, B.L., Wiseman, S.A., Lawrence, S.J., Tran, T.N., Robinson, M.S., Sato, H., Hawke, B.R., Scholten, F., Oberst, J., Hiesinger, H., van der Bogert, C.H., Greenhagen, B.T., Glotch, T.D., Paige, D.A., 2011. Non-mare silicic volcanism on the lunar farside at Compton-Belkovich. Nature Geosci. 4, 566-571.

Jozwiak, L.M., Head III, J.W., Zuber, M.T., Smith, D.E., Neumann, G.A., 2012. Lunar floor-fractured craters: Classification, distribution, origin and implications for magmatism and shallow crustal structure. J. Geophys. Res. 117, E11005, doi: 10.1029/2012JE004134.

Jozwiak, L.M., Head III, J.W., Wilson, L., 2015. Lunar floor-fractured craters as magmatic intrusions: Geometry, modes of emplacement, associated tectonic and volcanic features, and implications for gravity anomalies. Icarus 248, 424-447, doi: 10.1016/j.icarus.2014.10.052.

Kaminski, E., Jaupart, C., 1998. The size distribution of pyroclasts and the fragmentation sequence in explosive volcanic eruptions. J. Geophys. Res. 103 (B12), 29,759-29,779.

Kiefer, W.S., Macke, R.J., Britt, D.T., Irving, A.J., Consolmagno, G.J., 2012. The density and porosity of lunar rocks. Geophys. Res. Lett. 39, L07201, doi: 10.1029/2012GL051319.

Kieffer, S.W., 1977. Sound speed in liquid-gas mixtures: water-air and water-steam. J. Geophys. Res. 82, 2895-2904.

Kieffer, S.W., 1982. Dynamics and thermodynamics of volcanic eruptions: Implications for the plumes on Io. In: *Satellites of Jupiter*, ed. D. Morrison, Univ. of Arizona Press, Tucson, pp. 647-723.

Kieffer, S.W., 1989. Geologic nozzles. Rev. Geophys. 27, 3-38.

Klimczak, C., 2013. Igneous dikes on the Moon: Evidence from Lunar Orbiter Laser Altimeter topography. Lunar Planet. Sci. 44, 1391.

Kreslavsky, M.A., Head III, J.W., Neumann, G.A., Rosenburg, M.A., Aharonson, O., Smith, D.E., Zuber, M.T., 2013. Lunar topographic roughness maps from Lunar Orbiter Laser Altimeter (LOLA) data: Scale dependence and correlation with geologic features and units. Icarus 226, 52-66, doi: 10.1016/j.icarus.2013.04.027.

Kusuma, K.N., Sebastian, N., Murty, S.V.S., 2012. Geochemical and mineralogical analysis of Gruithuisen region on Moon using M^3 and DIVINER images. Planet. Space Sci. 67, 46-56.

Larsen, J.F., Gardner, J.E., 2004. Experimental study of water degassing from phonolite melts: implications for volatile oversaturation during magmatic ascent. J. Volcanol. Geotherm. Res. 134, 109-124.

Lister, J.R., 1991. Steady solutions for feeder dykes in a density-stratified lithosphere. Earth Planet. Sci. Lett. 107 (2), 233-242.

Lister, J.R., 1990a. Buoyancy-driven fluid fracture - the effects of material toughness and of low-viscosity precursors. J. Fluid. Mech. 210, 263-280.

Lister, J. R. (1990b) Buoyancy-driven fluid fracture - similarity solutions for the horizontal and vertical propagation of fluid-filled cracks. J. Fluid. Mech. 217, 213-239.

Lister, J.R., Kerr, R.C., 1991. Fluid-mechanical models of crack-propagation and their application to magma transport in dykes. J. Geophys. Res. 96 (B6), 10,049-10,077.

Maaløe, S., 2005. Extraction of melt from veined mantle source regions during eruptions. J. Volcanol. Geotherm. Res. 147, 377-390.

Maccaferri, F., Bonafede, M., Rivalta, E., 2011. A quantitative study of the mechanisms governing dike propagation, dike arrest and sill formation. J. Volcanol. Geotherm. Res. 208, 39-50.

McGetchin, T.R., Ulrich, G.W., 1973. Zenoliths in maars and diatremes with inferences for the Moon, Mars and Venus. J. Geophys. Res. 78, 1832-1853.

Menand, T., Tait, S.R., 2002. The propagation of a buoyant liquid-filled fissure from a source under constant pressure: an experimental approach. J. Geophys. Res. 107, 2306, doi: 10.1029/2001JB000589.

Mériaux, C., Jaupart, C., 1998. Dike propagation through an elastic plate. J. Geophys. Res. 103 (B8), 18,295-18,314.

Michaut, C., 2011. Dynamics of magmatic intrusions in the upper crust: Theory and applications to laccoliths on Earth and the Moon. J. Geophys. Res. 116, B05205.

Mitchell, K.L., 2005. Coupled conduit flow and shape in explosive volcanic eruptions. J. Volcanol. Geotherm. Res. 143, 187-203.

Moore, H.J., Shaber, G.G., 1975. An estimate of the yield strength of the Imbrium flows. Proc.

Lunar Sci. Conf. 6th, 101-118.

Muller, O.H., Muller, M.R., 1980. Near surface magma movement. Proc. Lunar Planet Sci. Conf. 11th, pp. 1979-1985. Pergamon Press, New York.

Neri, A., Papale, P., Macedonio, G., 1998. The role of magma composition and water content in explosive eruptions: 2. Pyroclastic dispersion dynamics. J. Volcanol. Geotherm. Res. 87 (1-4), 95-115.

Neri, A., Papale, P., Del Seppia, D., Santacroce, R., 2003. Coupled conduit and atmospheric dispersal dynamics of the AD 79 Plinian eruption of Vesuvius. J. Volcanol. Geotherm. Res. 120 (1-2), 141-160.

Nicholis, M.G. Rutherford, M.J., 2006. Vapor/melt partitioning behavior of S and Cl in a C-O gas mixture. Lunar Planet. Sci. 37, abstract 2061.

Nicholis, M.G., Rutherford, M.J., 2009. Graphite oxidation in the Apollo 17 orange glass magma: Implications for the generation of a lunar volcanic gas phase. Geochim. Cosmochim. Acta 73, 5905–5917.

Oberbeck, V.R., Greeley, R., Morgan, R.B., Lovas, M.J., 1971. Lunar rilles - a catalog and method of classification. NASA Technical Memorandum TM X-62,088.

Papale, P., 1999. Strain-induced magma fragmentation in explosive eruptions. Nature 397, 425-428.

Papale, P., Dobran, F., 1993. Modeling of the ascent of magma during the plinian eruption of Vesuvius in AD 79. J. Volcanol. Geotherm. Res. 58 (1-4), 101-132.

Papale, P., Neri, A., Macedonio, G., 1999. The role of water content and magma composition on explosive eruption dynamics. Physics and Chemistry of the Earth Part A. Solid Earth and Geodesy 24 (11-12), 969-975.

Petrycki, J.A., Wilson, L., Head, J.W., 2004. The significance of the geometries of linear graben for the widths of shallow dike intrusions on the Moon. Lunar Planet. Sci. 35, abstract 1123.

Pieters, C.M., Boardman, J., Buratti, B.J., Chatterjee, A., Clark, R., Glavich, T., Green, R., Head, J.W., Isaacson, P.J., Malaret, E., McCord, T.B., Mustard, J.F., Petro, N. E., Runyon, C., Staid, M., Sunshine, J., Taylor, L., Tompkins, S., Varanasi, P., White, M., 2009. The Moon Mineralogy Mapper (M^3) on Chandrayaan-1. Current Science 96, 500-505.

Pinkerton, H., Wilson, L., 1994. Factors controlling the lengths of channel-fed lava flows. Bull. Volcanol. 56, 108-120.

Pollard, D.D., 1988. Elementary fracture mechanics applied to the structural interpretation of dykes. In: *Mafic Dyke Swarms*, edited by H. C. Halls and W. F. Fahrig, Spec. Pap. Geol. Assoc. Can. 34, 5-24.

Richter, F.M, McKenzie, D., 1984. Dynamical models for melt segregation from a deformable matrix. Journal of Geology 92, 729-740, doi:10.1086/628908.

Rivalta, E., Dahm, T., 2006. Acceleration of buoyancy-driven fractures and magmatic dikes beneath the free surface. Geophys. J. Int. 166, 1424–1439.

Robinson, M.S., Brylow, S.M., Tschimmel, M., Humm, D., Lawrence, S.J., Thomas, P.C., Denevi, B.W., Bowman-Cisneros, E., Zerr, J., Ravine, M.A., Caplinger, M.A., Ghaemi, F.T., Schaffner, J.A., Malin, M.C., Mahanti, P., Bartels, A., Anderson, J., Tran, T.N., Eliason, E.M., McEwen, A.S., Turtle, E., Jolliff, B.L., Hiesinger, H., 2010. Lunar Reconnaissance Orbiter Camera (LROC) instrument overview. Space Sci Rev 150, 81–124, doi: 10.1007/s11214-010-9634-2.

Roper, S.M., Lister, J.R., 2005. Buoyancy-driven crack propagation from an over-pressured source. J. Fluid Mech. 536, 79–98.

Roper, S.M., Lister, J.R., 2007. Buoyancy-driven crack propagation: The limit of large fracture toughness. J. Fluid Mech. 580, 359–380.

Rosenburg, M.A., Aharonson, O., Head, J.W., Kreslavsky, M.A., Mazarico, E., Neumann, G.A., Smith, D.E., Torrence, M.H., Zuber, M.T., 2011. Global surface slopes and roughness of the Moon from the Lunar Orbiter Laser Altimeter. J. Geophys. Res. 116, doi: 10.1029/2010je003716.

Rubin, A.M., 1990. A comparison of rift-zone tectonics in Iceland and Hawaii. Bull. Volcanol. 52, 302-319.

Rubin, A.M., 1993. Dikes vs. diapirs in viscoelastic rock. Earth Planet. Sci. Lett. 119, 641-659.

Rubin, A.M., 1995. Propagation of magma-filled cracks. Annual Review of Earth and Planetary Sciences 23, 287-336.

Rubin, A.M., Pollard, D.D., 1987. Origins of blade-like dikes in volcanic rift zones. In: *Volcanism in Hawaii*, edited by R. W. Decker, T. L. Wright, and P. H. Stauffer, U.S. Geol. Surv. Prof. Pap. 1350, 1449-1470.

Rutherford, M.J., Papale, P., 2009. Origin of basalt fire-fountain eruptions on Earth versus the Moon. Geology 37 (3) 219-222.

Saal, A.E., Hauri, E.H., Lo Cascio, M., Van Orman, J.A., Rutherford, M.C., Cooper, R.F., 2008. Volatile content of lunar volcanic glasses and the presence of water in the Moon's interior. Nature 454 (7201), 192-195.

Sato, M., 1976. Oxygen fugacity and other thermochemical parameters of Apollo 17 high-Ti basalts and their implications on the reduction mechanism. Proc. Lunar Sci. Conf. 7, 1323–1344.

Sato, M., 1979. The driving mechanism of lunar pyroclastic eruptions inferred from the oxygen fugacity behavior of Apollo 17 orange glass. Proc. Lunar Sci. Conf. 10, 311–325.

Schaber, G.G., 1973. Lava flows in Mare Imbrium: Geologic evaluation from Apollo orbital photography. Proc. Lunar Planet. Sci. Conf. 4th, 73–92.

Schmeling, H., 2006. A model of episodic melt extraction for plumes. J. Geophys. Res. 111, B03202, doi: 10.1029/2004JB003423.

Schubert, G., Lingenfelter, R.E., Peale, S.J., 1970. The morphology, distribution and origin of lunar sinuous rilles. Rev. Geophys. Space Phys. 8, 199-224.

Schultz, P.H., 1976a. Moon Morphology, University of Texas Press, Austin, TX, 604 pp.

Schultz P.H., 1976b. Floor-fractured lunar craters. The Moon 15. 241-273.

Schultz, P.H., Staid, M.I., Pieters, C.M., 2006. Lunar activity from recent gas release. Nature 444, 184-186.

Self, S., Keszthelyi, L., Thordarson, Th., 1998. The importance of pahoehoe. Am. Rev. Earth Planet. Sci. 26, 81–110.

Self, S., Thordarson, T. Keszthelyi, L., Walker, G.P.L., Hon, K., Murphy, M.T., Lond, P., Finnemore, S., 1996. A new model for the emplacement of Columbia River Basalts as large, inflated pahoehoe lava flow fields. Geophys. Res. Lett. 23, 2689–2692.

Shearer, C.K. and 15 others, 2006. Thermal and magmatic evolution of the Moon. In: New Views of the Moon, Reviews in Mineralogy & Geochemistry 60, 365-518.

Sleep, N.H., 1988. Tapping of melt by veins and dikes. J. Geophys. Res. 93, 10,255-10,272.

Smith, D.E., Zuber, M.T., Neumann, G.A., Lemoine, F.G., Mazarico, E., Torrence, M.H., McGarry, J.F., Rowlands, D.D., Head III, J.W., Duxbury, T.H., Aharonson, O., Lucey, P.G., Robinson, M.S., Barnouin, O.S., Cavanaugh, J.F., Sun, X., Liiva, P., Mao, D., Smith, J.C., Bartels, A.E., 2010, Initial observations from the Lunar Orbiter Laser Altimeter (LOLA). Geophys. Res. Lett. 37, L18204, doi: 10.1029/2010GL043751.

Solomon, S.C., 1975. Mare volcanism and lunar crustal structure. Proc. Lunar Planet. Sci. Conf. 6, 1021-1042.

Solomon, S.C., 1978. On volcanism and thermal tectonics on one-plate planets. Geophys. Res. Lett. 5, 461-464.

Solomon, S.C., Head, J.W., 1980. Lunar mascon basins: Lava filling, tectonics, and evolution of the lithosphere. Rev. Geophys. Space Phys. 18, 107-141.

Solomon, S.C., Head, J.W., 1982. Mechanisms for lithospheric heat transport on Venus: Implications for tectonic style and volcanism. J. Geophys. Res. 87, 9236-9246.

Sparks, R.S.J., 1978. The dynamics of bubble formation and growth in magmas: A review and analysis. J. Volcanol. Geotherm. Res. 3, 1-37.

Spence, D.A., Sharp, P., Turcotte, D.L., 1987. Buoyancy-driven crack propagation: A mechanism for magma migration. J. Fluid Mech. 174, 135–153.

Spera, F.J., 1980. Aspects of magma transport. In: Hargraves, R.B. (Ed.), *Physics of Magmatic Processes*. Princeton University Press, pp. 232–265.

Spera, F.J., 1992. Lunar magma transport phenomena. Geochim. Cosmochim. Acta 56, 2253-2266.

Spohn, T.,Konrad, W., Breuer, D., Ziethe, R., 2001. The longevity of lunar volcanism: Implications of thermal evolution calculations with 2D and 3D mantle convection models. Icarus 149, 54-65.

Spudis, P.D., Swann, G.A., Greeley, R., 1988. The formation of Hadley Rille and implications for the geology of the Apollo 15 region. Proc. Lunar Planet. Sci. Conf. 18, 243-254.

Stevenson, D.J., 2003. Styles of mantle convection and their influence on planetary evolution. Comptes Rendus Geosci. 335, 99-111, doi:10.1016/S1631-0713(03)00009-9.

Taisne, B., Tait, S., Jaupart, C., 2011. Conditions for the arrest of a vertical propagating dyke. Bull. Volcanol. 73, 191-204.

Tait, S.R., Jaupart, C., Vergniolle, S., 1989. Pressure, gas content and eruptive periodicity of a shallow crystallising magma chamber. Earth and Planetary Science Letters 92, 107-123.

Taylor, S.R., 1982. *Planetary Science: A Lunar Perspective*, Lunar and Planet. Inst., Houston, Tex., 481 pp.

Taylor, S.R., 1989. Growth of planetary crusts. Tectonophysics 161, 147-156, doi: 10.1016/0040-1951(89)90151-0.

Thordarson, Th., Self, S., 1998. The Roza Member, Columbia River Basalt Group: A gigantic pahoehoe lava flow formed by endogenous processes. J. Geophys. Res. 103, 27,411–27,445.

Toksöz, M.N., Dainty, A.M., Solomon, S.C., Anderson, K.R., 1974. Structure of the Moon. Rev. Geophys. 12, 539-567.

Turcotte, D.L., Schubert, G., 2002. *Geodynamics*. Cambridge Univ. Press, 275 pp.

Valentine, G., Wohletz, K., 1989. Numerical models of plinian eruption columns and pyroclastic flows. J. Geophys. Res. 94, 1867-1887.

Wagner, T.P., Grove, T.L., 1997. Experimental constraints on the origin of lunar high-Ti ultramafic glasses. Geochim. Cosmochim. Acta 61, 1315-1328.

Wallace, P., Anderson, A.T., 2000. Volatiles in magmas. In: *Encyclopedia of Volcanoes*, H. Sigurdsson, Ed. in Chief, Academic Press, San Diego, 149-170.

Weertman, J., 1971. Theory of water-filled crevasses in glaciers applied to vertical magma transport beneath oceanic ridges. J. Geophys. Res. 76, 1171-1183.

Weinberg, R.F., Regenauer-Lieb, K., 2010. Ductile fractures and magma migration from source, Geology 38, 363-366, doi: 10.1130/G30482.1.

Weitz, C., Head, J.W., 1999. Spectral properties of the Marius Hills volcanic complex and implications for the formation of lunar domes and cones. J. Geophys. Res. 104, 18,933-18,956.

Weitz, C.M., Head, J.W., Pieters, C.M., 1998. Lunar regional dark mantle deposits: Geologic, multispectral, and modeling studies. J. Geophys. Res.103, 22,725–22,759.

Wetzel, D. T., Hauri, E. H., Saal, A. E., and Rutherford, M. J., 2015, Carbon content and degassing history of the lunar volcanic glasses. Nature Geosci. 8, 755–758, doi:10.1038/ngeo2511.

Whitten, J., Head III, J.W., Staid, M.I., Pieters, C.M., Mustard, J.F., Clark, R., Nettles, J.W., Klima, R.L., Taylor, L.A., 2011. Lunar mare deposits associated with the Orientale impact basin: New insights into mineralogy, history, mode of emplacement, and relation to Orientale Basin evolution from Moon Mineralogy Mapper (M^3) data from Chandrayaan- 1. J. Geophys. Res. 116, doi: 10.1029/2010JE003736.

Whitten, J.L., Head III, J.W., 2015a. Lunar cryptomaria: Physical characteristics, distribution, and implications for ancient volcanism. Icarus 247, 150-171, doi: 10.1016/j.icarus.2014.09.031.

Whitten, J.L., Head III, J.W., 2015b. Lunar cryptomaria: Mineralogy and composition of ancient volcanic deposits. Planet. Space Sci. 106, 67-81, doi: 10.1016/j.pss.2014.11.027.

Wichman, R.W., Schultz, P.H., 1995. Floor-fractured craters in Mare Smythii and west of Oceanus Procellarum: Implications of crater modification by viscous relaxation and igneous intrusion models. J. Geophys. Res. 100(E10), 21,201-21,218.

Wieczorek, M.A., Phillips, R.J., 1998. Potential anomalies on a sphere: Application to the thickness of the lunar crust. J. Geophys. Res. 103 (E1) 1715-1724.

Wieczorek, M.A., Zuber, M.T., 2001. The composition and origin of the lunar crust: Constraints from central peaks and crustal thickness modeling. Geophys. Res. Lett. 28, 4023-4026.

Wieczorek, M.A., Zuber, M.T. Phillips, R.J., 2001. The role of magma buoyancy on the eruption of lunar basalts. Earth Planet. Sci. Lett. 185, 71-83, doi: 10.1016/S0012-821X(00)00355-1.

Wieczorek, M.A., Neumann, G.A., Nimmo, F., Kiefer, W.S., Taylor, G.J., Melosh, H.J., Phillips, R.J., Solomon, S.C., Andrews-Hanna, J.C., Asmar, S.W., Konopliv, A.S., Lemoine, F.G., Smith, D.E., Watkins, M.M., Williams, J.G., Zuber, M.T., 2013. The crust of the Moon as seen on GRAIL. Science 339, 671-675, doi: 10.1126/science.1231530.

Wilhelms, D.E., 1987. *The geologic history of the Moon*. U.S. Geol. Surv., Prof. Paper 134.

Wilhelms, D.E., McCauley, J., 1971. Geological map of the near side of the Moon. Map I-703, Misc. Investigations Ser. US Geological Survey, Denver, Colo.

Williams, D.A., Kerr, R.C., Lesher, C.M., 1998. Emplacement and erosion by Archean komatiite lava flows at Kambalda: Revisited. J. Geophys. Res. 103, 27,533– 27,550.

Williams, D.A., Kerr, R.C., Lesher, C.M., 1999. Thermal and fluid dynamics of komatiitic lavas associated with magmatic Ni-Cu- (PGE) sulphide deposits. In: *Dynamic Processes in Magmatic Ore Deposits and Their Application in Mineral Exploration,* edited by R. R. Keays et al., Geol. Assoc. Can. Short Course, 13, pp. 367–412.

Williams, D.A., Wilson, A.H., Greeley, R., 2000a. A komatiite analog to potential ultramafic materials on Io. J. Geophys. Res. 105, 1671-1684.

Williams, D.A., Fagents, S.A., Greeley, R., 2000b. A reevaluation of the emplacement and erosional potential of turbulent, low-viscosity lavas on the Moon. J. Geophys. Res. 105, 20,189–20,206.

Williams, D.A., Greeley, R., Hauber, E., Gwinner, K., Neukum, G., 2005. Erosion by flowing Martian lava: New insights for Hecates Tholus from Mars Express and MER data. J. Geophys. Res. 110, E05006, doi: 10.1029/2004JE002377.

Wilson, L., 1980. Relationships between pressure, volatile content and ejecta velocity in three types of volcanic explosion. J. Volcanol. Geotherm. Res. 8, 297-313.

Wilson, L., 1999. Explosive Volcanic Eruptions - X. The influence of pyroclast size distributions and released magma gas contents on the eruption velocities of pyroclasts and gas in hawaiian and plinian eruptions. Geophys. J. Intern. 136, 609-619.

Wilson, L., Head, J.W., 1980. The formation of eroded depressions around the sources of lunar sinuous rilles: theory. Lunar Planet. Sci. 11, 1260-1262.

Wilson, L., Head, J.W., 1981. Ascent and eruption of basaltic magma on the Earth and Moon. J. Geophys. Res. 86, 2971-3001.

Wilson, L., Head, J.W., 2001. Lava fountains from the 1999 Tvashtar Catena fissure eruption on Io: Implications for dike emplacement mechanisms, eruption rates and crustal structure. J. Geophys. Res. 106 (E12), 32,997-33,004.

Wilson, L., Head, J.W., 2003a. Deep generation of magmatic gas on the Moon and implications for pyroclastic eruptions. Geophys. Res. Lett. 30 (12), 1605, doi: 10.1029/2002GL016082.)

Wilson, L., Head, J.W., 2003b. Lunar Gruithuisen and Mairan domes: Rheology and mode of emplacement. J. Geophys. Res. 108, doi 10.1029/2002JE001909.

Wilson, L., Head, J.W., 2007a. An integrated model of kimberlite ascent and eruption. Nature 447 (7140), 53-57, doi:10.1038/nature05692.)

Wilson, L., Head, J.W., 2007b. Explosive volcanic eruptions on Mars: Tephra and accretionary lapilli formation, dispersal and recognition in the geologic record. J. Volcanol. Geotherm. Res. 163, 83-97.

Wilson, L., Keil, K., 1997. The fate of pyroclasts produced in explosive eruptions on the asteroid 4 Vesta. Meteorit. Planet. Sci. 32, 813-823.

Wilson, L., Keil, K., 2012. Volcanic activity on differentiated asteroids: a review and analysis. Chemie der Erde 72 (4), 289-322, doi:/10.1016/j.chemer.2012.09.002

Wilson, L., Goodrich, C.A., Van Orman, J.A., 2008. Thermal evolution and physics of melt extraction on the Ureilite Parent Body. Geochim. Cosmochim. Acta 72 (24), 6154-6176, doi:10.1016/j.gca.2008.09.025.

Wilson, L., Keil, K., McCoy, T.J., 2010. Pyroclast loss or retention during explosive volcanism on asteroids: Influence of asteroid size and gas content of melt. Meteorit. Planet. Sci. 45 (8), 1284-1301, doi:10.1111/j.1945-5100.2010.01085.x.

Wilson, L., Hawke, B.R., Giguere, T.A., Petrycki, E.R., 2011. An igneous origin for Rima Hyginus and Hyginus crater on the Moon. Icarus 215, 584-595.

Yamada, K., Tanaka, H., Nakazawa, K., Emori, H., 2005. A new theory of bubble formation in magma. J. Geophys. Res. 110, B02203. doi:10.1029/2004JB003113.

Yamada, K., Emori, H., Nakazawa, K., 2008. Time-evolution of bubble formation in a viscous liquid. Earth Planets Space 60, 661–679.

Yingst, R.A., Head, J.W., 1997. Volumes of lunar lava ponds in South Pole-Aitken and Orientale basins: Implications for eruption conditions, transport mechanisms and magma source regions. J. Geophys. Res. 102, 10,909-10,931.
Yingst, R.A., Head, J.W., 1998. Characteristics of lunar mare deposits in Smythii and Marginis basins: Implications for magma transport mechanisms. J. Geophys. Res. 103, 11,135-11,158.
Zuber, M.T., Smith, D.E., Zellar, R.S., Neumann, G.A., Sun, X., Katz, R.B., Kleyner, I., Matuszeski, A., McGarry, J.F., Ott, M.N., Ramos-Izquierdo, L.A. Rowlands, D.D., Torrence, M.H., Zagwodzki, T.W., 2010. The Lunar Reconnaissance Orbiter Laser Ranging Investigation. Space Sci. Rev. 150, 63–80, doi: 10.1007/s11214-009-9511-z.
Zuber, M.T., Smith, D.E., Watkins, M.M., Asmar, S.W., Konopliv, A.S., Lemoine, F.G., Melosh, H.J., Neumann, G.A., Phillips, R.J., Solomon, S.C., Wieczorek, M.A., Williams, J.G., Goossens, S.J., Kruizinga, G., Mazarico, E., Park, R.S., Yuan, D.-N., 2013. Gravity field of the Moon from the Gravity Recovery and Interior Laboratory (GRAIL) mission. Science 339, doi: 10.1126/science.1231507.
Ziethe, R., Seiferlin, K., Hiesinger, H., 2009. Duration and extent of lunar volcanism: Comparison of 3D convection models to mare basalt ages. Planet. Space Sci. 57, 784-796.

Notation

Symbol	Definition and Units
A_d	total vertical extent of dike, m
A_l	vertical extent of dike below base of crust, m
A_{lf}	vertical extent of lower part of dike that reaches the surface, m
A_u	vertical extent of dike above base of crust, m
C	thickness of planetary crust, m
D_f	thickness of lava flow, m
D_r	depth of flowing lava in sinuous rille channel, m
D_u	distance along planetary surface traveled by pyroclast, m
E	vertical extent of shallow mantle partial melt zone, m
E_d	vertical extent of deep mantle partial melt zone, m
F	dimensionless fraction of pyroclasts landing hot to form lava pond
F_d	volume flux of viscous magma forming domes, $m^3\ s^{-1}$
F_e	erupted magma volume flux from fissure vent, $m^3\ s^{-1}$
F_f	volume flux of lava in lava flow, $m^3\ s^{-1}$
F_i	initial erupted volume flux from fissure, $m^3\ s^{-1}$
F_{min}	minimum volume flux in sinuous rille lava for channel erosion, , $m^3\ s^{-1}$
F_r	volume flux of lava in sinuous rille channel, $m^3\ s^{-1}$
Gz	dimensionless Grätz number for lava flow
H	depth below surface of intruded dike top, m
K_{base}	stress intensity at lower tip of dike at crust-mantle boundary, Pa $m^{1/2}$
K_{crit}	fracture toughness of host rocks, Pa $m^{1/2}$
K_l	stress intensity at lower tip of deep mantle dike, Pa $m^{1/2}$
K_{top}	stress intensity at upper tip of dike at crust-mantle boundary, Pa $m^{1/2}$
K_u	stress intensity at upper tip of deep mantle dike, Pa $m^{1/2}$
L	vertical extent of dike growing from deep mantle melt zone, m
L_d	horizontal extent of surface fissure vent forming dome, m
L_e	horizontal extent of surface fissure vent, m
L_m	critical length at which dike disconnects from melt source, m
N	mass fraction of gas in mixture of gas and entrained wall rocks
N_a	Avogadro's number, equal to 6.0225×10^{26} $kmol^{-1}$
P	ambient pressure, Pa
P_b	pressure at base of dike, Pa
P_c	pressure due to the weight of the crust, Pa
P_{ch}	pressure when gas-pyroclast flow speed is choked at sonic speed, Pa
P_d	driving pressure at inlet at base of dike, Pa
P_{dis}	pressure at which magmatic foam disrupts, Pa
P_f	pressure at which gas and clasts decouple in Knudsen regime, Pa
P_{foam}	pressure in magmatic foam layer, Pa
P_i	initial pressure of explosively erupting gas-pyroclast mixture, Pa
P_m	pressure due to the weight of a magma column, Pa
P_n	driving pressure at center of dike at base of crust, Pa
P_{sm}	pressure below which smelting reaction occurs, Pa
P_w	pressure due to weight of magma in dike, Pa

P_0	driving pressure at center of deep mantle dike, Pa
Q_u	universal gas constant, equal to 8.314 kJ kmol^{-1} K^{-1}
R	radius of planetary body, m
R_{coarse}	range of large pyroclasts in polydisperse mixture, m
R_f	maximum range of ballistic pyroclasts, m
R_{fine}	range of small pyroclasts in polydisperse mixture, m
R_{mono}	range of ballistic pyroclasts in monodisperse mixture, m
R_p	radius of lava pond fed by opaque fire fountain, m
Re_f	dimensionless Reynolds number for surface lava flow
Re_r	dimensionless Reynolds number for lava in sinuous rille
S	speed of sound in gas-pyroclast mixture, m s^{-1}
T	horizontal tension, relative to hydrostatic stresses, in lithosphere, Pa
T_m	magma temperature, equal to 1623 K
U	flow speed of magma in deep mantle dike, m s^{-1}
U_b	eruption speed of pyroclasts entering fire fountain, m s^{-1}
U_d	rise speed of viscous magma forming domes, m s^{-1}
U_e	rise speed of erupting basaltic magma at depth, m s^{-1}
U_f	mean speed of lava flow, m s^{-1}
U_i	initial rise speed of erupting magma from shallow source, m s^{-1}
U_{lam}	laminar flow speed of magma, m s^{-1}
U_m	final eruption speed of pyroclasts locked to gas motion, m s^{-1}
U_{min}	minimum rise speed of erupting magma to avoid cooling, m s^{-1}
U_{turb}	turbulent flow speed of magma, m s^{-1}
U_u	ultimate velocity of gas expanding to a vacuum, m s^{-1}
U_v	speed at which gas and small pyroclasts emerge through vent m s^{-1}
V	volume of magma in deep mantle dike, m^3
V_e	volume of magma erupted from dike, m^3
V_f	volume of magma remaining in dike after eruption, m^3
V_i	initial volume flux of erupting magma from shallow source, m^3 s^{-1}
W	mean thickness of deep mantle dike, m
W_{av}	mean thickness of dike reaching surface from shallow depth, m
W_d	mean thickness of dike feeding dome-forming eruption, m
W_f	mean thickness of dike reaching surface from great depth, m
W_{flow}	width of lava flow, m
W_n	mean thickness of dike at crust-mantle boundary, m
W_r	width of sinuous rille channel, m
X	opacity depth of fire fountain, m
X_f	length of lava flow, m
Z	depth to top of melt zone in shallow mantle, m
Z_{crit}	minimum depth to top of melt zone in mantle to ensure eruption, m
Z_{diff}	distance over which pressure decreases in erupting material, m
d	average diameter of molecules in magmatic gas, equal to ~300 μm
dP/dz	pressure gradient driving magma flow, Pa m^{-1}
f	dimensionless friction factor at dike wall, equal to 0.02
g	acceleration due to gravity, equal to 1.62 m s^{-2}
m	average molecular mass of released magmatic volatiles, kg kmol^{-1}

n	mass fraction of volatiles released from magma
n_d	solubility of water in terrestrial mafic magma, as mass fraction
t_f	time to emplace lava flow, s
v_g	dimensionless partial volume of gas in magmatic foam
v_l	dimensionless partial volume of liquid in magmatic foam
z	depth from which gas-pyroclast mixture erupts explosively, m
ΔZ	vertical extent of foam layer near top of propagating dike, m
$\Delta\rho$	density difference between host mantle and magma, kg m^{-3}
α_f	slope of ground on which lava flows
γ	ratio of specific heats of gas at constant pressure and constant volume
ε	dimensionless bubble volume fraction in magmatic foam, 0.85
η	basaltic magma viscosity, equal to 1 Pa s
η_d	plastic viscosity of magma in viscous domes, m
θ	elevation angle from horizontal at which pyroclast is ejected
κ	thermal diffusivity of magma, equal to 7×10^{-7} m^2 s^{-1}
λ	dimensionless basal friction factor for flow of lava on surface
μ	shear modulus of host rocks, Pa
ν	Poisson's ratio for host rocks, dimensionless
ρ	bulk density of lava flow, kg m^{-3}
$\rho_{\square}$	average mantle density, equal to 3260 kg m^{-3}
$\rho_{\square}$	average magma density, equal to 2900 or 3010 kg m^{-3}
$\rho_{\square}$	average crust density, equal to 2550 kg m^{-3}
τ_d	yield strength of magma in viscous domes
ϕ	effective diameter of gas molecules, equal to ~3.4×10^{-10} m
φ	diameter of largest bubbles in magmatic foam, m

Table 1. Variation with vertical extent, E_d, of mantle partial melt zone of the driving pressure at the dike base, P_d, the driving pressure at the dike center, P_0, the length, L_m, the mean width, W, and the volume, V, of a dike that disconnects from the source and migrates as a discrete magma body.

E_d /km	P_d /MPa	P_0 /MPa	L_m /km	W /m	V /km^3
5	2.9	7.5	15.7	4.5	0.9
10	5.8	15	31.4	18.0	13.9
15	8.7	22	47.1	40.5	71
20	12	30	62.8	71.9	223
25	15	37	78.5	112.4	545
30	17	45	94.2	161.9	1129
35	20	52	110.0	220.3	2092
40	23	60	125.7	287.8	3569
45	26	67	141.4	364.2	5718
50	29	75	157.1	449.7	8714
75	44	112	235.6	1011.8	44117
100	58	150	314.2	1798.7	139430

Table 2. Comparison of properties of isolated dikes as they disconnect from their mantle sources and after they are emplaced as stable intrusions at the crust-mantle boundary. Values at disconnection are: total vertical length, L_m; mean width, W; volume, V; and central driving pressure, P_0. Values after intrusion are: extent above crust-mantle boundary, A_u; extent below boundary, A_l; driving pressure at boundary, P_n; and mean width, W_n. Values in italics in the upper parts of the tables represent intrusions; values in the central parts of the tables represent eruptions on the near-side of the Moon; values in italics in the lower parts of the tables represent potential eruptions on the far-side, not observed.

(a) Values for magma density, ρ_l, = 2900 kg m^{-3}

E_d /km	L_m /km	W /m	V /km^3	P_0 /MPa	A_u /km	A_l /km	P_n /MPa	W_n /m
5	*15.7*	*4.5*	*0.9*	*7.5*	*7.3*	*9.7*	*3.7*	*3.9*
10	*31.4*	*18.0*	*13.9*	*15.0*	*17.3*	*18.7*	*7.0*	*13.8*
15	*47.1*	*40.5*	*70.6*	*22.5*	*27.0*	*27.8*	*10.3*	*29.9*
16.59	52.1	49.5	105.5	24.9	30.0	30.8	11.4	36.4
20	62.8	71.9	223.1	30.0	36.5	37.1	13.7	52.5
25	78.5	112.4	544.6	37.5	46.1	46.3	17.1	81.3
27.07	85.0	131.8	748.6	40.6	50.0	50.1	18.5	95.1
30	*94.2*	*161.9*	*1129.4*	*45.0*	*55.6*	*55.5*	*20.5*	*116.6*
35	*110.0*	*220.3*	*2092.3*	*52.5*	*65.0*	*64.7*	*24.0*	*158.1*
50	*157.1*	*449.7*	*8714.4*	*75.0*	*93.4*	*92.4*	*34.2*	*321.1*
100	*314.2*	*1798.7*	*139430.2*	*149.9*	*187.8*	*184.8*	*68.3*	*1278.7*

(b) Values for magma density, ρ_l, = 3010 kg m^{-3}

E_d /km	L_m /km	W /m	V /km^3	P_0 /MPa	A_u /km	A_l /km	P_n /MPa	W_n /m
5	*15.7*	*3.1*	*0.6*	*5.2*	*5.3*	*11.3*	*3.4*	*3.2*
10	*31.4*	*12.5*	*9.7*	*10.4*	*12.8*	*21.5*	*6.2*	*11.2*
15	*47.1*	*28.1*	*49.0*	*15.6*	*20.1*	*32.0*	*9.2*	*24.3*
20	*62.8*	*50.0*	*154.9*	*20.8*	*27.2*	*42.5*	*12.2*	*42.6*
21.93	68.9	60.1	223.8	22.8	30.0	46.6	13.3	51.0
25	78.5	78.1	378.2	26.0	34.4	53.1	15.2	66.0
30	94.2	112.4	784.3	31.2	41.5	63.6	18.2	94.5
35	110.0	153.0	1453.0	36.4	48.6	74.2	21.2	128.2
35.98	113.0	161.7	1623.0	37.5	50.0	76.3	21.8	135.5
50	*157.1*	*312.3*	*6051.7*	*52.1*	*69.9*	*105.9*	*30.3*	*260.3*
100	*314.2*	*1249.1*	*96826.5*	*104.1*	*140.5*	*211.7*	*60.4*	*1036.4*

Table 3. Parameters controlling whether eruptions or intrusions occur on the Moon from dikes connecting shallow mantle magma sources to the surface as a function of the vertical extent of the zone of partial melting, E. If an eruption occurs, values are given for the initial magma rise speed U_i and the volume flux F_i from a 1600 m long fissure. If no eruption can occur, the depth H of the top of an intruded dike is given. In all cases the mean dike width W_{av} is shown; Z is the depth of the top of the partial melt zone below the surface.

(a) nearside, Z = 50 km.

E /km	H /km	W_{av} /m	U_i /(m s^{-1})	F_i /(m^3 s^{-1})
0	1.1	38		
10		80	4	4.7×10^5
20		122	16	3.2×10^6
30		164	26	6.9×10^6
40		206	36	1.2×10^7
50		249	45	1.8×10^7

(b) farside, Z = 50 km.

E /km	H /km	W_{av} /m	U_i /(m s^{-1})	F_i /(m^3 s^{-1})
0	6.0			
10	4.8			
20	3.6	6		
30	2.3	79		
40	1.1	162		
50		251	8.4	3.4×10^6

(c) nearside, Z = 60 km.

E /km	H /km	W_{av} /m	U_i /(m s^{-1})	F_i /(m^3 s^{-1})
0		91	4	5.2×10^5
10		142	16	3.7×10^6
20		194	26	8.1×10^6
30		245	36	1.4×10^7
40		297	45	2.1×10^7
50		348	54	3.0×10^7

(d) farside, Z = 60 km.

E /km	H /km	W_{av} /m	U_i /(m s^{-1})	F_i /(m^3 s^{-1})
0	4.8			
10	3.6			
20	2.3	24		
30	1.1	62		
40		101	5	7.8×10^5
50		139	16	3.6×10^6

(e) nearside, Z = 70 km.

E /km	H /km	W_{av} /m	U_i /(m s^{-1})	F_i /(m^3 s^{-1})
0		149	15	3.6×10^6
10		208	25	8.3×10^6
20		268	34	1.5×10^7
30		327	44	2.3×10^7
40		387	53	3.3×10^7
50		446	62	4.5×10^7

(f) farside, Z = 70 km.

E /km	H /km	W_{av} /m	U_i /(m s^{-1})	F_i /(m^3 s^{-1})
0	3.6	6		
10	2.3	61		
20	1.1	115		
30		169	6	1.6×10^6
40		224	19	6.8×10^6
50		278	29	1.3×10^7

Table 4. Values of the eruption speeds U_m and resulting maximum ranges R_m of pyroclasts erupted from progressively greater depths below the surface and hence progressively greater pressures P_{foam} in a decompressing foam layer underlying the dike tip gas cavity in a dike that has just reached the surface.

depth below surface/km	P_{foam} /MPa	U_m /(m s^{-1})	R_m /km
0.3	0.5	96	5.7
1.0	3.7	113	7.9
3.0	12.8	122	9.1
5.0	21.8	125	9.6
7.0	30.9	126	9.8
9.6	40.0	127	10.0

Table 5. Values of opacity depth, X, and % of pyroclasts landing uncooled as a function of released magma volatile content n for each of a series of values of the erupting magma volume flux F_e. Maximum ranges, R_f, of pyroclasts are repeated for comparison with values of X.

		F_e/(m^3 s^{-1}) = 5 × 10^3		F_e/(m^3 s^{-1}) = 1 × 10^4		F_e/(m^3 s^{-1}) = 3 × 10^4		F_e/(m^3 s^{-1}) = 1 × 10^5		F_e/(m^3 s^{-1}) = 3 × 10^5		F_e/(m^3 s^{-1}) = 1 × 10^6	
n /ppm	R_f /km	X	% hot	X	% hot	X	% hot	X	% hot	X	% hot	X	% hot
250	0.8	8.5 m	97.9	4.3 m	98.9	1.4 m	99.6	0.4 m	99.9	0.1 m	100.0	40 mm	100.0
500	1.7	54 m	93.7	27 m	96.8	8.9 m	98.9	2.7 m	99.7	0.9 m	99.9	0.3 m	100.0
750	2.5	140 m	88.9	70 m	94.4	23 m	98.1	7.0 m	99.4	2.3 m	99.8	0.7 m	99.9
1000	3.2	292 m	83.0	146 m	91.3	49 m	97.1	15 m	99.1	4.9 m	99.7	1.5 m	99.9
1250	4.1	492 m	77.2	246 m	88.2	82 m	96.0	25 m	98.8	8.2 m	99.6	2.5 m	99.9
1500	4.9	788 m	70.4	394 m	84.5	131 m	94.7	39 m	98.4	13 m	99.5	3.9 m	99.8
2000	16.5	1.6 km	56.3	818 m	76.6	273 m	91.9	82 m	97.5	27 m	99.2	8.2 m	99.8
3000	9.8	4.5 km	29.5	2.2 km	59.5	747 m	85.3	224 m	95.5	75 m	98.5	22 m	99.5
5000	16.0	15.3 km	0.2	7.6 km	27.4	2.5 km	70.7	763 m	90.7	254 m	96.9	76 m	99.1
10000	32.7	90.8 km	0.0	45.4 km	15.2	15.1 km	28.8	4.5 km	74.1	1.5 km	91.0	454 m	97.2

Table 6. Flow parameters speed, U_f, Reynolds number, Re_f, emplacement time, t_f, and volume flux, F_f, for 20 km wide, 600 km long mare lava flows with viscosity 1 Pa s emplaced on a slope sin $\alpha_f = 1 \times 10^{-3}$ with thicknesses between 1 and 30 m.

D_f /m	U_f /(m s^{-1})	Re_f	t_f /days	F_f /(m^3 s^{-1})
1	0.6	7.4×10^3	11.6	1.2×10^4
2	1.0	2.5×10^4	6.9	4.1×10^4
5	1.9	1.2×10^5	3.7	1.9×10^5
10	3.1	3.7×10^5	2.2	6.1×10^5
20	4.8	1.2×10^6	1.4	1.9×10^6
30	6.2	2.2×10^6	1.1	3.7×10^6

Table 7. Comparison of magma rise conditions in a fissure and in a circular conduit carrying the same volume flux F_e. Values are for the range of eruption parameters shown in Table 2 for magmas of density 2900 kg m^{-3} erupting from mantle sources with the vertical extents E_d. The fissure is 1600 m long in each case. The average fissure width is W_n, the magma rise speed in the fissure is U_e, and the pressure gradient is dP/dz. Thermal erosion of the dike wall at a rate of 15 μm/s widens the central part of the fissure by a total horizontal amount Y and magma chilling pinches off the distal parts of the dike until magma is rising in a circular conduit of diameter D_c with speed U_c. t_Y is the time needed to accomplish this.

E_d /m	F_e /(m^3 s^{-1})	W_n /m	U_e /(m s^{-1})	dP/dz /(Pa m^{-1})	D_c /m	U_c /(m s^{-1})	Y /m	t_Y /days
16.59	1.80×10^5	36	3.1	15.3	209	5.2	173	66
20	6.61×10^5	52	7.9	68.6	260	12.4	208	81
25	1.76×10^6	81	13.5	130.8	339	19.5	257	99
27.07	2.41×10^6	95	15.8	152.4	372	22.1	277	108

Table 8. Parameters relating to eruption of Gruithuisen and Mairan domes. Magma yield strength, τ_d, plastic viscosity, η_d, volume eruption rate, F_d, and surface fissure length estimate, L_d, are from *Wilson and Head* (2003b). Dike width, W_d, magma rise speed, U_d, and minimum magma rise speed to avoid excessive cooling, U_{min}, are derived here.

Dome name	τ_d /Pa	η_d /(Pa s)	F_d /(m^3/s)	L_d /m	W_d /m	U_d /(m/s)	U_{min} /(m/s)
Gruithuisen γ	7.7×10^4	3.2×10^8	119	7500	173	9.2×10^{-5}	5.0×10^{-6}
Gruithuisen δ	1.3×10^5	1.2×10^9	48	13500	296	1.2×10^{-5}	1.7×10^{-6}
Gruithuisen NW	1.2×10^5	9.9×10^8	24	2500	276	3.5×10^{-5}	2.0×10^{-6}
Gruithuisen NW+γ	1.0×10^5	6.0×10^8	143	19000	224	3.4×10^{-5}	3.0×10^{-6}
Mairan T	1.3×10^5	1.2×10^9	24	1500	294	5.4×10^{-5}	1.7×10^{-6}
Mairan "middle"	6.9×10^4	2.5×10^8	52	2500	155	1.3×10^{-4}	6.3×10^{-6}
Mairan "south"	5.3×10^4	1.3×10^8	51	1000	119	4.3×10^{-4}	1.1×10^{-5}
Mairan "m"+"s"	6.1×10^4	1.8×10^8	52	9000	137	4.2×10^{-5}	8.0×10^{-6}

Figures and Captions

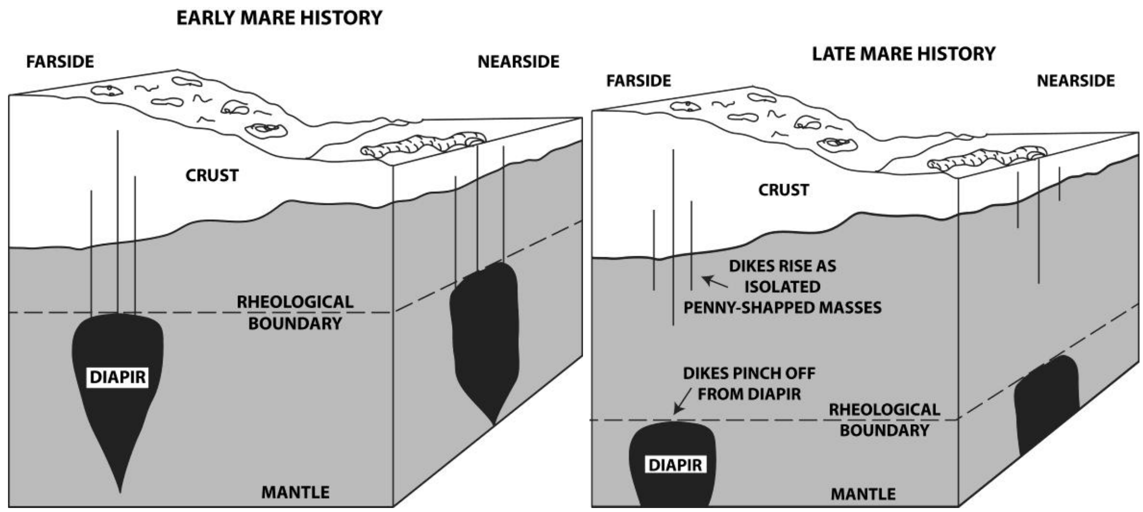

1a 1b

Figure 1. Block diagram perspective view of the lunar surface and interior showing the lunar anorthositic crust (white; thin nearside, thicker farside), the lunar mantle (gray), and basaltic source region diapirs (black) rising from deeper in the mantle. In the early history of mare volcanism (a), the lithosphere (thermal boundary layer) has thickened to greater than the thickness of the crust (compositional layer). Rising mantle diapirs rise, deforming plastically, and stall at the base of the lithosphere (rheological boundary; dashed line). Overpressurization causes the lithosphere to deform elastically and magma-filled cracks (dikes) are propagated toward the surface. For a typical range of overpressurization values, some dikes will reach the surface and form eruptions, while others will stall and solidify in the crust and mantle. The nearside-farside crustal thickness differences will favor eruptions on the lunar nearside, and intrusions on the farside. Later in mare history (b), the cooling of the Moon will thicken the lithosphere, driving the rheological boundary deeper into the interior. Diapir tops are so deep that magma supply is insufficient to permit dikes to be continuous from these depths to the surface; all dikes pinch off from their diapirs and rise buoyantly in the mantle as isolated penny-shaped entities. These dikes stall centered on the crust-mantle boundary; the largest dikes will cause surface eruptions, while others will solidify in the crust and upper mantle. Eventually, overall cooling of the Moon, decrease in sources of melting, thickening of the lithosphere, deepening of source regions, and increasingly contractional stresses in the lithosphere will all work to decrease magma generation, and minimize the likelihood of surface eruptions.

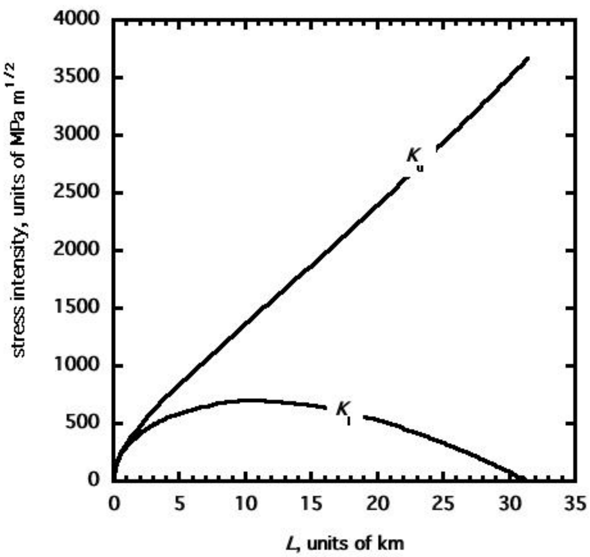

Figure 2. The variation with dike length, L, of K_u and K_l, the stress intensity at the upper and lower tips, respectively, of a growing vertical dike, when the driving pressure at the dike inlet, P_d = 5.8 MPa and the density difference between host mantle rocks and magma is $\Delta\rho$ = 360 kg m^{-3}.

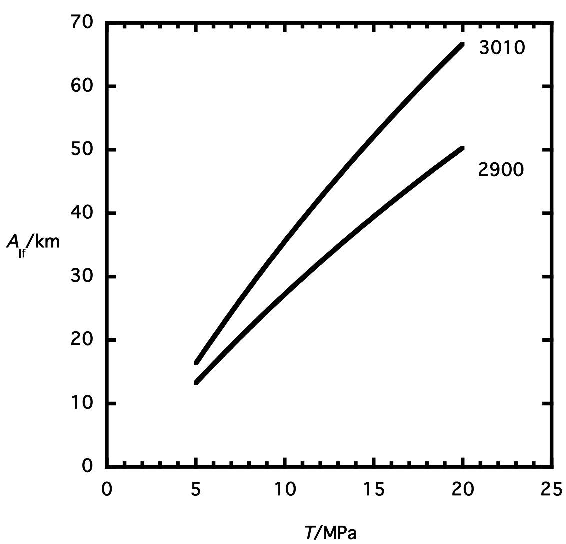

Figure 3. Variation of A_{lf}, the vertical extent into the mantle of a rising isolated dike that has penetrated through the crust and initiated an eruption, with T, the lithospheric tensional stress allowing the dike to exist as a stable structure, for two values of the dike magma density in kg m^{-3}.

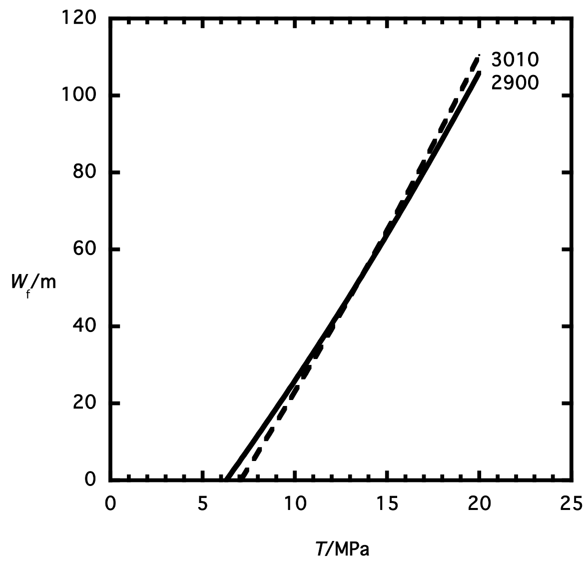

Figure 4. Variation of W_f, the mean width of a rising isolated dike that has penetrated through the crust and initiated an eruption, with T, the lithospheric tensional stress allowing the dike to exist as a stable structure, for two values of the dike magma density in kg m^{-3}. No stable residual intrusion can exist if T is less than 6-7 MPa.

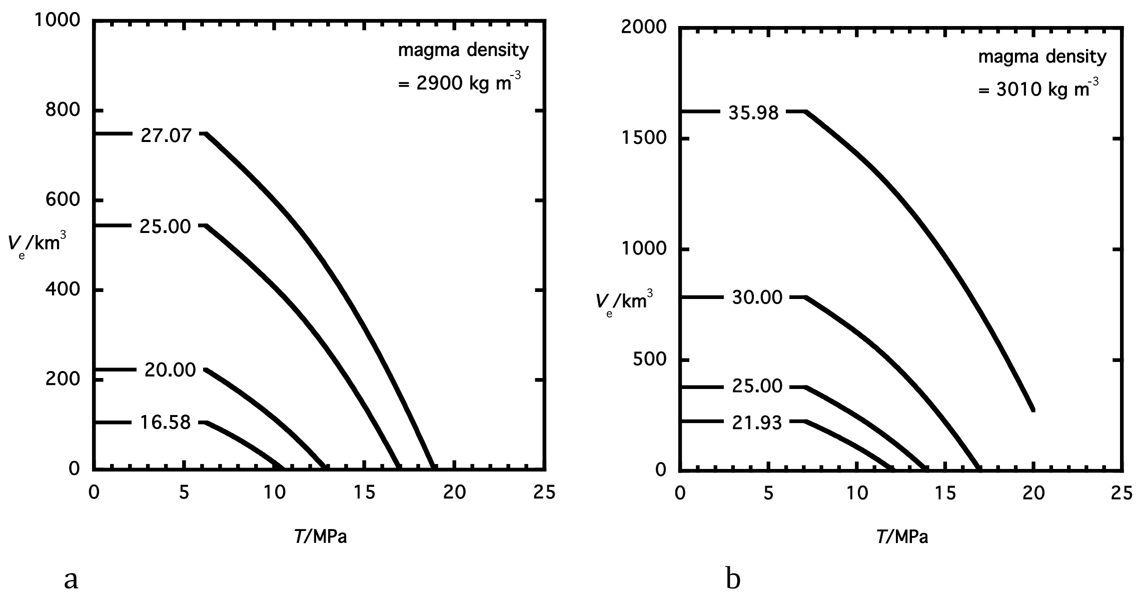

Figure 5. Variation of V_e, the volume of magma that is erupted, with T, the lithospheric tensional stress, after a dike with properties shown in Figs. 1 and 2 has reached its equilibrium configuration. Curves are labeled with the range of vertical extents of the deep mantle partial melt source region that can generate an erupting dike. Part (a), magma density 2900 kg m^{-3}. Part (b), magma density 3010 kg m^{-3}.

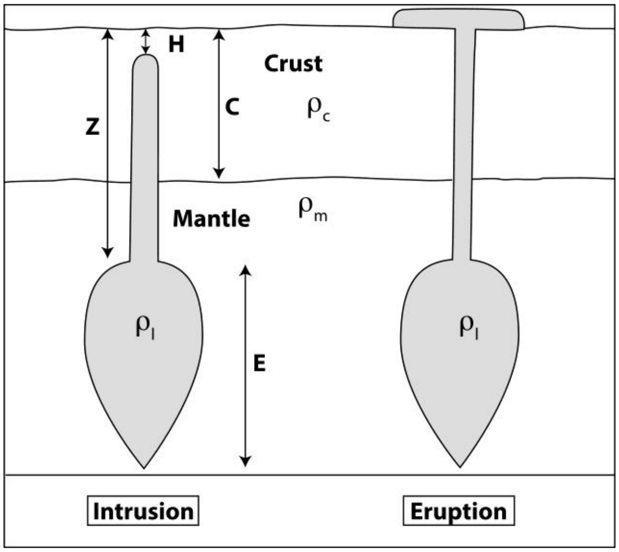

Figure 6. Intrusion and eruption of magma. Early mare basalts are generated by partial melting within a finite region in the upper mantle of vertical extent *E*, below a crust of thickness *C*. The level at which the stresses combine to initiate a dike is at a depth *Z* below the surface. The positive buoyancy of the magma in the mantle diapir leads to an excess pressure at the dike inlet, and this pressure is available to support the column of magma in the dike. If the excess pressure is great enough, the column of magma can be supported all the way to the surface and an eruption can occur. If the pressure is not great enough, the dike will stall with its top at some depth *H* below the surface. Density of the liquid magma, crust, and mantle are shown by ρ_l, ρ_c, ρ_m respectively.

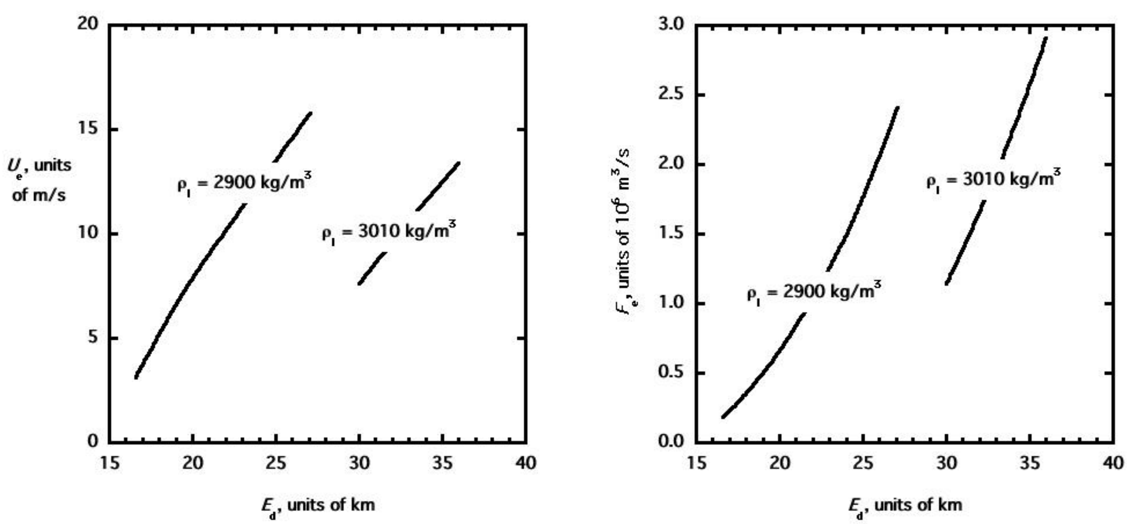

Figure 7. Parameters associated with the range of diapiric source zone extents E_d that allow the upper tips of isolated dikes to reach the surface and produce eruptions on the lunar near-side. (a) the rise speed, U_e, of magma erupting through the dike; (b) the erupted volume flux, F_e. In each case values are shown for magma densities, ρ_l, of 2900 and 3010 kg m^{-3}.

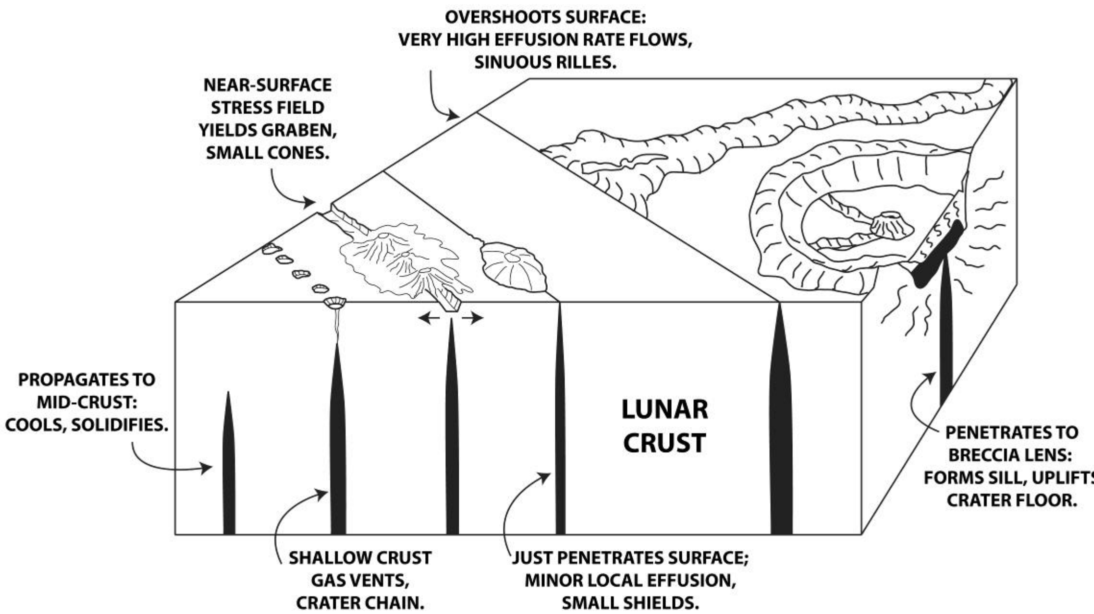

Figure 8. Perspective view block diagram illustrating the fate of dikes intruding into the crust to various levels. Left to right: Dikes propagating only to mid-crustal depths cool and solidify. Those nearing the surface, but not erupting, can vent gas to form a crater chain either abruptly (perhaps some pyroclasts and pulverized regolith), or passively (drainage). Those nearing the surface to form a near-surface extensional stress field will produce graben, and can vent gas and magma to produce an array of cones, domes and pyroclastic deposits. Dike just penetrating the surface, can produce small, low-volume eruptions that form small lava shields. Large dikes penetrating the surface will have very high effusion rates and form very long lava flows and if the eruption duration is sufficiently long to favor thermal erosion, sinuous rilles. Dikes approaching the surface, but encountering a low-density breccia lens below a crater floor, can intrude sills, uplifting the crater floor and forming floor-fractured craters.

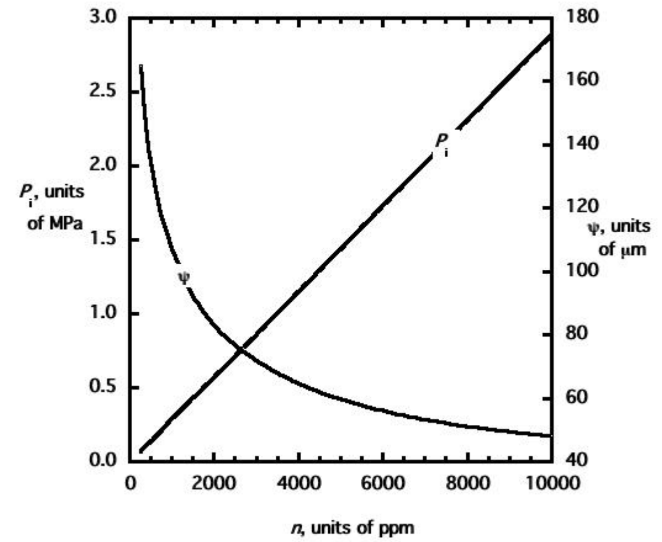

Figure 9. Variation of the pressure in the free gas at the top of the foam layer in a dike tip, P_i, and the diameters of the largest bubbles at the top of the foam, φ, as a function of the total amount of CO-dominated gas released from the magma, *n*.

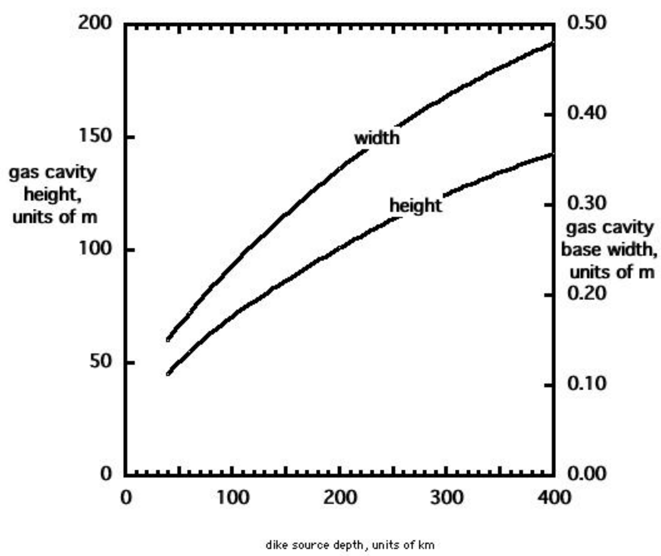

Figure 10. Minimum vertical extents and basal widths of gas cavities in the tips of dikes that have propagated from sources at the stated depths.

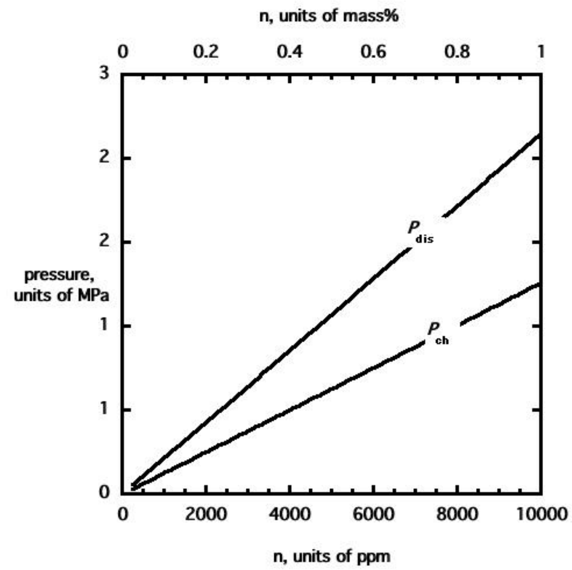

Figure 11. Values of pressure in magma at depth of disruption into pyroclasts, P_{dis}, and pressure in choked gas-pyroclast mixture exiting the vent, P_{ch}, for eruptions on the Moon and Earth as a function of released volatile contents *n*, given in both ppm and mass % for comparison with common usage. Values of *n* up to ~2000 ppm apply to most eruptions on the Moon and values greater than ~2000 ppm are relevant to most basaltic eruptions on Earth.

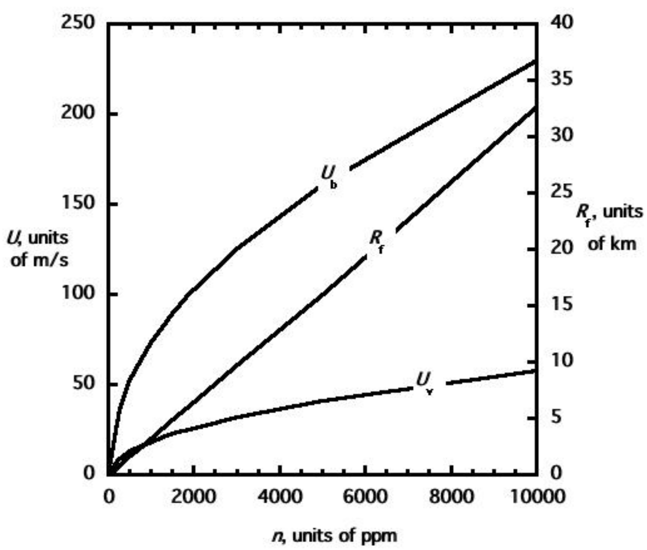

Figure 12. Implied speeds in the vent, U_v, speeds after decoupling from the gas expansion, U_b, and maximum ballistic ranges, R_f, of gas and 300 μm diameter pyroclasts in steady explosive eruptions as a function of the CO content, *n*, of the erupting magma.

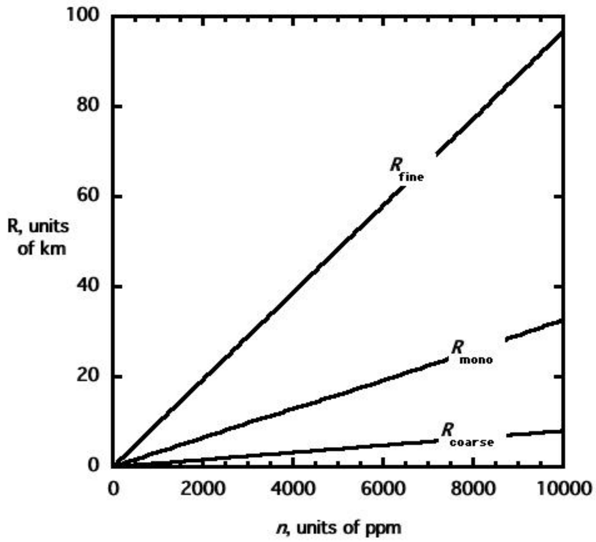

Figure 13. Pyroclast ranges R_{mono} in steady eruptions of monodisperse 300 m diameter pyroclasts compared with the maximum ranges of the coarse and fine size fractions of a distribution in which 80% of clasts are much larger than ~1 mm and decouple rapidly from the expanding gas phase.